Molecular organization of the actin cortex in apical constriction and epithelial folding

by

Jonathan S. Coravos
B.A., Bowdoin College (2011)

Submitted to the Department of Biology
in partial fulfillment of the requirements for the degree of

Doctor of Philosophy

at the

Massachusetts Institute of Technology

June 2017

Signature of author: _____
Department of Biology
February 3, 2017

Certified by: _____
Adam C. Martin
Associate Professor of Biology
Thesis Advisor

Accepted by: _____
Amy E. Keating
Professor of Biology
Chair, Biology of Graduate Committee

Molecular organization of the actin cortex in apical constriction and epithelial folding

by

Jonathan S. Coravos

Submitted to the Department of Biology on February 3, 2017 in Partial Fulfillment of the Requirements for the Degree of Doctor of Philosophy in Biology

Abstract

Actin and myosin generate contractile forces to change tissue and cell shape. These shape changes are essential for many biological functions, ranging from muscle contraction to tissue morphogenesis in development. While the spatial organization and composition of the actin and myosin contractile force generating machine is well known in muscle, it is less understood in nonmuscle epithelia, which change shape during development and form functional barriers on an organism's inner surfaces. Prevailing models for nonmuscle contractility suggest that the intrinsic ability of mixed polarity actin networks and uniformly distributed myosin to contract into asters drives nonmuscle contractility. Here, I provide insight into the mechanism of nonmuscle contraction by demonstrating that the apical actin cortex and associated proteins are spatially organized in epithelia. In addition, I demonstrate that this spatial organization forms a sarcomere-like actomyosin apparatus, which is essential for epithelial contractility. This updated model is likely to inform our understanding of a wide range of contractile force-generating systems, and may lead to advances in understanding of pathologies that involve defects in contractility, like cardiovascular disease and pulmonary fibrosis.

Thesis Supervisor: Adam C. Martin
Title: Associate Professor of Biology

Acknowledgments

To my advisor, Adam Martin, thank you. You have taught me to be a better critical thinker and writer, you have helped me cultivate perseverance in the face of hard problems, and you have given me constant freedom and support to follow my own path. You gave me room to make my own mistakes, and helped me learn from them, but you also reeled me when my excursions strayed into risky territory. You taught me how to construct narratives from data, and you supported me as I shared my work with the community. The students and scientists you have collected around yourself are a testament to your affability and your intellect, and I will always feel grateful to have been a part of your fold.

To past and present members of the Martin Lab, thank you for your rigorous critiques, your collegiality, and your encouragement to tackle the next question. A big reason I joined the Martin lab was the energy and friendliness of its then members, a quality that still fills the lab. Thank you for making lab a fun, and often hilarious, place. A special thanks to Soline for your company in the Jungle, to Frank for your coaching and pop culture inspiration, to Mimi for laughing at my worst jokes, to Claudia for always being on my team, and finally to Mike, for patiently and thanklessly making every single aspect of my life in lab easier.

To my thesis committee members, Iain Cheeseman, and Richard Hynes, thank you for your time, advice, and encouragement throughout my time at MIT. I am particularly grateful for your insistence on improving my original thesis proposal, which was the first step in becoming, I hope, a better scientific writer. Your critical feedback has made me a better thinker, and will follow me my whole life. Andrea McClatchey, thank you sharing your time with me and as you offered feedback on this thesis.

To my friends, thank you for being a constant source of renewal. To my friends in the program, thank you for the late-night beers after exhausting days in lab, for the persistent efforts to rip me away from the bench, and for being the only people in my world who can fully empathize with the ups and downs of doctoral student life. To my friends from other walks of life, thank you for being a constant source of laughter, for being part of my life, and keeping me a part of yours.

To my girlfriend, Laura, thank you for loving me. Thank you for being patient when I was absorbed in my work, and for sharing your full and wonderful life with me. You are an incredible person, full of energy, empathy, humor, and thoughtfulness. I've been lucky to be next to you, enjoying your total beauty, and learning from you. I've also been lucky to enter into your world, feeling the love and support of your friends and family. Thank you.

To my family—especially my grandparents, my parents, and my sister—thank you for being my most enduring supporters, and raising me surrounded with love and opportunity. Yiayia, Papu, Grandma, and Grandpa, thank you for laying the foundation of values, family, and love that created me. Everything I am is because of you. Catherine, you are the most wonderful sister I could hope for, and your affection has been a motivating and comforting energy over the past five years. Mom and Dad, thank you for raising me in a home full of love, for teaching me the value of hard work and education, and for giving me your full and unconditional support to pursue my path.

Table of Contents

Chapter 1: Introduction – Mechanisms and functions of actin and myosin contractility

Summary

All organisms are built and maintained using mechanical forces. In development, tissues change shape to produce the structures of an adult organism. After development, mechanical forces still play a role: they maintain tissue homeostasis, move an organism through its environment, pump blood and air through its body, regulate blood pressure, and propel cells through the body. Both muscle and nonmuscle tissues produce force with the core proteins actin and myosin II, referred to together as actomyosin. In this introduction, I will review what is known about *in vivo* contractile force production. I will go into further detail on contractile force production in a nonmuscle tissue type called epithelia, with a focus on the specific cellular contraction called apical constriction. I will also describe an epithelial system in *Drosophila* that has fueled much of the research in this field. This thesis focuses on two specific questions: (1) what is the spatial organization of molecular components of the contractile force-generating machinery in apical constriction, and (2) how does this spatial organization lead to contraction?

The actomyosin machine

The core components of the cellular contractile force-generating machine are actin filaments and myosin II motors. Actin filaments are composed of actin subunits strung together in a polarized chain with a “barbed” end and “pointed” end. The barbed end has faster polymerization and depolymerization kinetics than the pointed end. The motor protein, myosin II, is a hexameric protein complex containing two essential light chains, two regulatory light chains, and two heavy chains, which contain the motor

heads that bind and walk toward the barbed end of an actin filament, and a tail domain that allows myosin II to multimerize. Myosin II multimers are bipolar structures with many myosin molecules bundled together, and with motor heads at both ends of the bundled rod. These multimers are called thick filaments in muscle cells and minifilaments in nonmuscle cells. The myosin II motor head binds to an actin filament, and through the ATP hydrolysis cycle, produces a “power-stroke” that advances the motor along the actin filament. Bipolar myosin filaments can bind antiparallel actin filaments with outward-facing barbed ends, and then pull the actin filaments toward each other, generating a contraction. If the actin filament barbed ends are attached to a physical structure, for example a cell membrane or adhesive junction, myosin molecules will pull on that structure. This core actomyosin apparatus is used throughout contractile force-generating contexts, but is perhaps best known for its role in muscle sarcomere contraction.

Muscle sarcomere contractility

Striated muscle (skeletal and cardiac) is composed of bundles of parallel fibers called myofibrils, which contain a repeated contractile unit called a sarcomere. Striated muscles earn their name from the striking pattern of sarcomere banding in histological preparations or transmission electron microscopy. In addition to the core actomyosin machinery, sarcomeres require a collection of auxiliary proteins to function (Clark et al., 2002), and the spatial organization of these components is directly connected to their function. An individual sarcomere has two outer boundaries, called Z-disks (Luther,

2009). At Z-disks, α-actinin and nebulin anchor actin filament barbed ends through the barbed end binding protein, CapZ (Papa et al., 1999; Pappas et al., 2008) (Figure 1A).

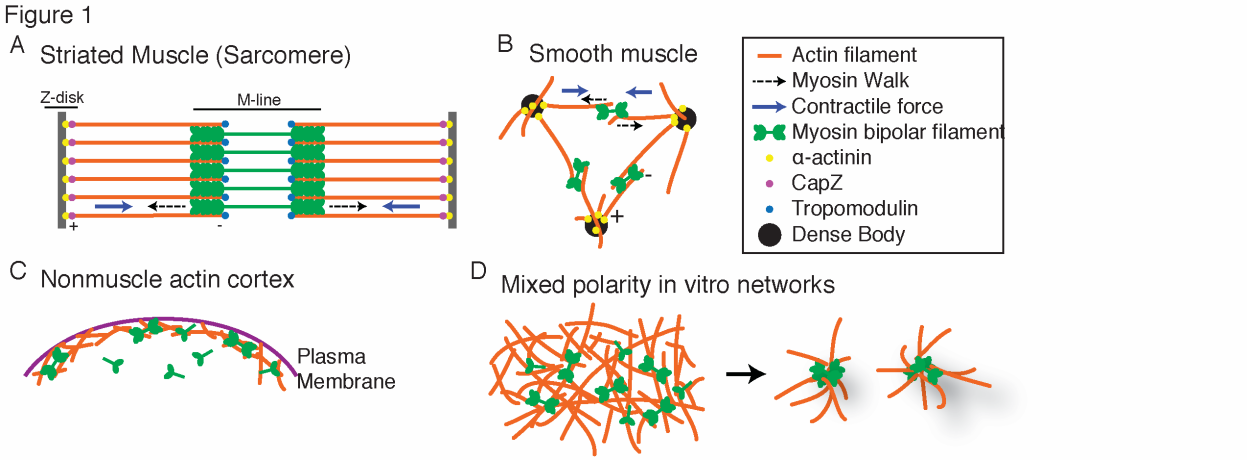

Figure 1. Models of actomyosin contractility in muscle and nonmuscle systems (A) Schematic of a sarcomere, the contractile apparatus in striated muscle. + and – correspond to actin filament barbed and pointed ends respectively. The sarcomere contracts when myosins walk outward toward the actin filament barbed ends, and both Z-disks therefore move inward toward the M-line. **(B)** Schematic of one hypothesis for organization of actin and myosin in smooth muscle. Actin filament barbed ends accumulate at dense bodies with α-actinin, and myosin bipolar filaments between dense bodies crosslink and contract actin filaments. **(C)** The actin cortex is a network of actin filaments under the membrane of nonmuscle cells. Bipolar myosin filaments can accumulate in the cortex and contract to generate forces. Inactive myosin disassembles into subunits. **(D)** Schematic of *in vitro* actomyosin network contracting to form a mixed polarity meshwork to asters. Not drawn to scale.

At the center of the sarcomere is the M-line, where the actin filament pointed ends face each other, and myosin II binds and bridges them across the gap. The actin filaments are coated with tropomyosin and troponins, which block myosin II from walking, until Ca^{2+} binds to troponin and causes a conformational shift in tropomyosin (Lehman, 2016). The entire apparatus is stabilized in part by titin, which connects the Z-disk to myosin bipolar filaments at the M-line and centers myosin in the sarcomere. Another important feature of the sarcomere is that actin filaments are polarized with barbed ends anchored at the Z-disk, and pointed ends, capped by Tropomodulin, localized in the center of the sarcomere. This entire apparatus contracts upon stimulation because the

bipolar myosin filaments walk outward toward both Z-disks, leading to a balance of forces across the M-line that produces a contraction.

In striated muscles the contractile apparatus is a stable feature of the tissue, and is stimulated by membrane depolarization that leads to increased cytosolic Ca^{2+}. In skeletal muscles, this depolarization is stimulated at the neuromuscular junction by a neurotransmitter that binds ion channels, leading to cell depolarization and a release of Ca^{2+} from the sarcoplasmic reticulum (Clark et al., 2002; Lieber, 2002). In cardiac muscle, membrane depolarization begins spontaneously in cardiac pacemaker cells, and a cardiac action potential then sweeps through gap junctions across the rest of the heart. This depolarization leads to Ca^{2+} ion release from the sarcoplasmic reticulum as in skeletal muscle, and then the increased concentration of cytoplasmic Ca^{2+} leads to further release of sarcoplasmic Ca^{2+} through Ca^{2+}-gated Ca^{2+} channels (Katz, 2010). In both cases, the increase in cytoplasmic Ca^{2+} leads to contraction.

Smooth muscle and nonmuscle contractility

Smooth muscles surround many organs, including the vasculature, the uterus, the bladder, and airways, where their contraction supports organ function (Horowitz et al., 1996). Contractile nonmuscle cells come in a wide range of types, including migrating immune cells and fibroblasts, and mechanically coupled sheets of cells called epithelia. I focus here on epithelia, which line the interior surfaces of many organs, and during development, change shape to sculpt the tissues of a developing organism.

One of the major differences between striated muscle and either smooth muscle or nonmuscle contraction is that in striated muscle, the sarcomere contractile apparatus

is a permanent feature of the tissue, whereas in nonmuscle tissues, and possibly smooth muscle, the contractile apparatus is assembled during contraction. The absence of a stable sarcomere structure makes it unclear how this assembly is regulated and organized. In smooth muscle, contractility might be assembled on dense bodies, at which actin filament barbed ends congregate (Bond and Somlyo, 1982; Fay et al., 1983; Tsukita et al., 1983). It is possible that myosin bipolar filaments crosslink and contract actin filaments emanating from periodically spaced dense bodies (Kargacin et al., 1989), which would provide a stable connection between force-generating components (Ali et al., 2011; Herrera et al., 2005; Zhang et al., 2010) (Figure 1B).

In nonmuscle cells, actin filaments are organized into a submembranous layer called the actin cortex, which imparts stiffness and shape to the fluid-like plasma membrane, and is also a medium for myosin II-based contractility (Salbreux et al., 2012) (Figure 1C). The mechanics and function of the actin cortex are influenced by many proteins. Some organization in the actin cortex and associated proteins has been observed at the subcellular scale. For example, “nodes”, in which formin-nucleated actin filaments extend outward from the node, might serve a function similar to dense bodies (Luo et al., 2016; Vavylonis et al., 2008). Another example is in the actin cortex of migratory cells: scanning electron micrographs of keratocytes (Svitkina et al., 1997), and fibroblasts (Verkhovsky and Borisy, 1993; Verkhovsky et al., 1995) revealed actin filament networks with mixed polarity and with some bundles of actin filaments, decorated throughout with myosin minifilaments. This mixed polarity is also evident in the actin cortex of some non-migratory cells (Fritzsche et al., 2016). It is not clear how an *in vivo* network of mixed polarity can contract, but interestingly, *in vitro* actin

networks of mixed polarity have been observed to contract spontaneously with the addition of muscle myosin II throughout the network (Backouche et al., 2006; Köster et al., 2016; Murrell and Gardel, 2012). This property of mixed polarity actin networks is thought to arise from the mechanical asymmetry of actin filaments, in which filaments withstand and transmit contractile forces, but bend and buckle easily under compressive stress, which dissipates compressive forces. This allows symmetry breaking in a network, where actin filaments contract into clusters, but do not expand (Murrell and Gardel, 2012; Silva et al., 2011) (Figure 1D). This intrinsic property of actomyosin networks might lead to the contraction of mixed polarity actin networks *in vivo* (Murrell et al., 2015).

Unlike striated muscle, where contractility is activated by relief of a steric block on myosin procession, smooth muscle and nonmuscle contractility is fundamentally regulated by the assembly of bipolar myosin filaments (Somlyo and Somlyo, 2003). Bipolar myosin filament assembly occurs through phosphorylation of the myosin II regulatory light chain, which assembles myosin into bipolar myosin filaments capable of contracting actin filaments. Phosphorylation can be achieved through Ca^{2+}-dependent and Ca^{2+}-independent mechanisms. Ca^{2+}-dependent activation occurs through an increase in cytoplasmic Ca^{2+}, which can occur as in striated muscle through membrane depolarization. Additional release is also stimulated by ligands signaling through G-protein coupled receptors (GPCRs) and $G\alpha_{q/11}$, which activates phospholipase C, producing IP_3 and DAG, leading respectively to sarcoplasmic Ca^{2+} release and PKC activation. Elevated cytoplasmic Ca^{2+} in smooth muscle stimulates contractility through Calmodulin (Cam). In the Ca^{2+}-bound state, Cam binds and activates Myosin Light

Chain Kinase (MLCK) (Hashimoto and Soderling, 1990). MLCK phosphorylates the myosin II regulatory light chain (MRLC), assembling myosin II into bipolar filaments, activating myosin motor activity, and producing an actomyosin contractile force (Brozovich et al., 2016). PKC also promotes contractility through phosphorylation of CPI-17, which when phosphorylated inhibits myosin phosphatase, a protein that, when uninhibited, binds and dephosphorylates myosin regulatory light chain through the myosin binding subunit (MBS) of the myosin phosphatase holoenzyme (Eto et al., 1995).

An alternative mode of myosin II regulation is Ca^{2+}-independent, and acts through GPCRs coupled to $G\alpha_{12/13}$ (Somlyo and Somlyo, 2000). $G\alpha_{12/13}$ activates the small GTPase, RhoA, through binding and activation of a guanine nucleotide exchange factor, RhoGEF. RhoGEF catalyzes the exchange of GDP for GTP, leading to a transiently active RhoA-GTP state that binds and activates Rho-associated, coiled-coil kinase (ROCK). ROCK indirectly promotes myosin phosphorylation by inhibiting myosin phosphatase, and also directly phosphorylates the myosin regulatory light chain (Fukata et al., 2001). This leads to a greater contractile force through an elevated number of myosins assembled as bipolar minifilaments. RhoA-GTP also binds and activates the formin Dia, which nucleates unbranched actin filaments (Goode and Eck, 2007). These two RhoA effectors provide a mechanism for RhoA to simultaneously assemble both components of the actomyosin contractile force-generating machinery.

Mechanisms of force transmission in nonmuscle

Nonmuscle tissues consist of individual cells connected by adhesive complexes. Therefore, force propagation across a nonmuscle tissue requires mechanical connections at cell-cell interfaces that can sustain and transmit contractile force. In this thesis, I focus on the specific case of epithelia, which are sheets of mechanically coupled cells with apical-basal and medial-junctional polarity (Figure 2A).

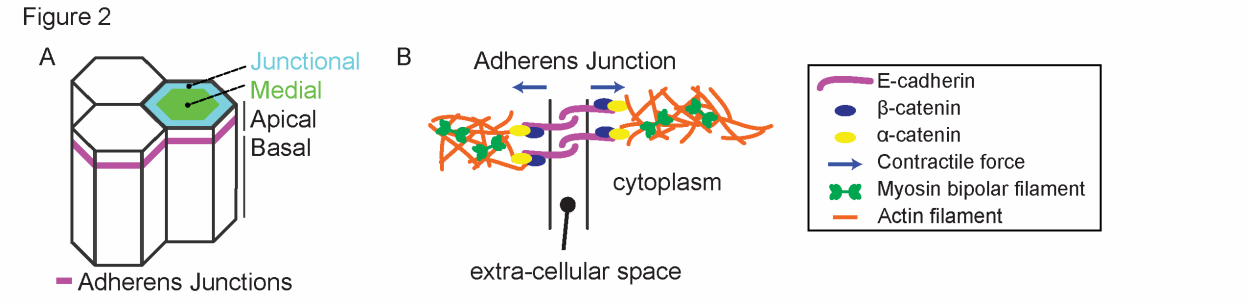

Figure 2. Schematics of epithelia and adherens junctions. (A) Epithelial cells have a top (apical) and bottom (basal) domain. The apical domain is split into medial and junctional areas. Adherens junctions mechanically link one epithelial cell to its neighbors, and are apical. **(B)** Adherens junctions are comprised of several proteins. The trans-membrane protein E-cadherin forms a homophilic adhesion in the extracellular space. On the cytoplasmic surface, E-cadherin binds α-catenin and β-catenin, which then form the link to actin filaments. Forces generated in the actin cortex are transmitted to adherens junctions and across the cell-cell junction. Not drawn to scale.

Epithelia form functional barriers on the interior surfaces of the body and also change shape during development to produce tissue structures. Epithelia use contractile force to accomplish their functions, and these forces propagate through cell-cell contacts known as adherens junctions (Figure 2B). Adherens junctions are analogous in function, but not in composition, to Z-disks and dense bodies because they are sites of actomyosin mechanical connection to force-transmitting structures. Adherens junctions contain a transmembrane homophilic adhesion protein, E-cadherin, and cytoplasmic adapters β-catenin and α-catenin. The catenins form the scaffold for attachment to the actin cytoskeleton (Nagafuchi, 2001) (Figure 2B).

While it is known that adherens junctions are required for the transmission of force across an epithelium (Martin et al., 2010), it is not completely clear how the actin cytoskeleton attaches to adherens junctions. *In vivo*, α-catenin is sufficient to bind adherens junctions to actin filaments (Desai et al., 2013), and this attachment appears to be stabilized by tension applied parallel to the plane of the membrane (Buckley et al., 2014). Adherens junctions are known sites of actin filament growth by both the branched actin nucleator, Arp2/3, and formin, and this growth stabilizes junctions and supports epithelial tension (Kobielak et al., 2003; Kovacs et al., 2002; 2011; Phng et al., 2015; Rao and Zaidel-Bar, 2016; Verma et al., 2012). While it is not clear how actin filaments transition from elongation/nucleation factors to stable adherens junction attachment, this attachment is essential for epithelial morphogenesis (Martin et al., 2010). Interestingly, despite the variations between Z-disks, dense bodies, adherens junctions, and focal adhesions, α-actinin is present in all these structures, where it is generally thought to play a role in linking actin filaments to the relevant structure (Fay et al., 1983; Goll et al., 1991; Knudsen et al., 1995; Luther, 2009; Mitra et al., 2005; Papa et al., 1999; Rajfur et al., 2002; Tang and Brieher, 2012). Determining the spatial organization of these components in the apical area will help explain how the contractile apical cortex is connected to adherens junctions.

Epithelial morphogenesis and apical constriction

Actomyosin contractility in epithelia plays a role in changing tissue shape during development, a process that leads to the acquisition of tissue structure. Forces are generated using the actin and myosin machinery, and then transmitted cell-to-cell

through adherens junctions. When coordinated across a field of cells, actomyosin contractility in epithelia can lead to tissue elongation/shortening, thickening/thinning, or folding. In this thesis, I focus on epithelial folding (Figure 3A).

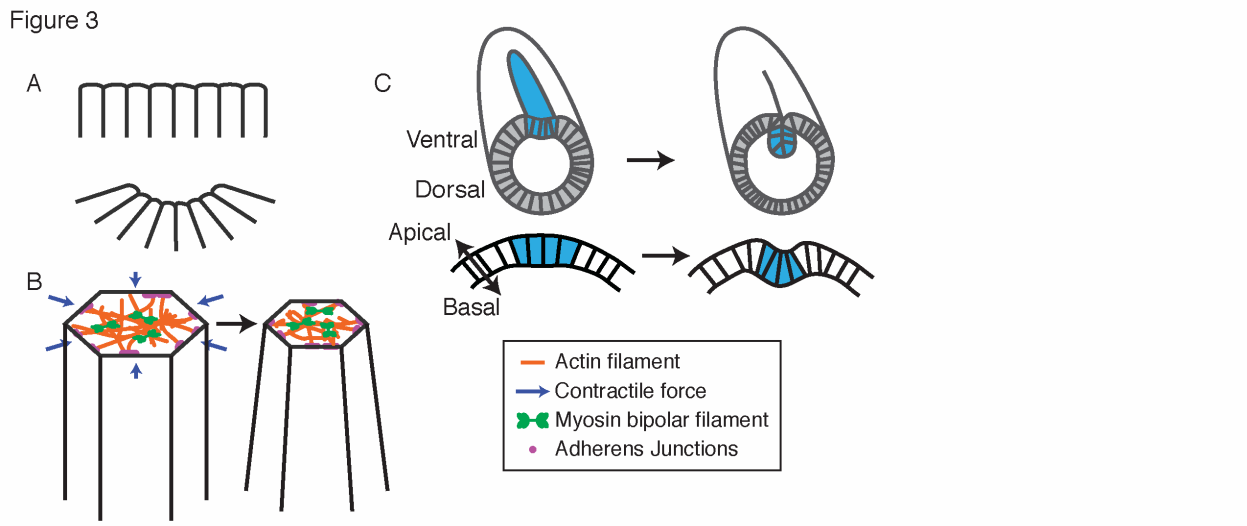

Figure 3. Epithelial folding and the *Drosophila* ventral furrow. (A) Epithelial folding involves the coordinated shape change of columnar epithelial cells from columns into wedges in a process known as apical constriction. Note the constricting apical (top) area that leads to wedge formation. **(B)** At the cellular level, apical constriction can occur through the contraction of an apical actin cortex spanning the surface. The organization of actin and myosin in this contraction is not known. **(C)** Cross sectional view of the *Drosophila* embryo at the point of ventral furrow formation. The *Drosophila* ventral furrow forms when the embryo is a columnar epithelium surrounding an interior yolk. Ventral cells (blue) undergo apical constriction, leading to invagination of the tissue into the embryo interior. Not drawn to scale.

An important example of epithelial folding is the formation of the neural tube, in large part because neural tube defects are one of the most common human birth defects (Copp et al., 2013; Wallingford et al., 2013). The neural tube forms from an epithelial sheet that folds to make a tube under the overlying epithelial sheet. This folding process occurs through bending at several hinge points that run along the length of the forming tube. These hinge points are the site of epithelial cells undergoing a shape change called apical constriction, which is an epithelial cell shape change that produces folds, like neural tube hinge points, or pits, like the optic cup (Martin and Goldstein, 2014).

In apical constriction, columnar epithelial cells contract their apical surface and change into a wedge or cone shape (Figure 3B). When this process is coordinated across a field of epithelial cells, a fold or a pit forms. While it was once thought that apical constriction was caused by a ring of actomyosin around the apical area, it is now known that apical constriction can be caused by an actomyosin cortex spanning the apical surface (Martin and Goldstein, 2014). However, it remains unclear how actin and myosin distributed across the apical surface produce a contraction.

Drosophila as a model system for studying actomyosin in epithelial folding

One of the challenges in determining the *in vivo* role of actomyosin in nonmuscle contexts has been the absence of a tractable model system for its study. Recent advances in microscopy, and the generation of powerful genetic and fluorescent tools, have made the *Drosophila* embryo an excellent model system for studying actomyosin spatial organization and dynamics. In this thesis, I focus on the *Drosophila* ventral furrow, which is a fold that forms as the first morphogenetic event of gastrulation in the early embryo, and produces the mesoderm tissue layer (Leptin and Grunewald, 1990; Sweeton et al., 1991). The early embryo is an ellipsoid (500 x 200 μm) comprised of a columnar epithelium of approximately 6,000 cells surrounding a yolk. The ventral furrow forms along the ventral surface of the embryo at this point, when approximately 1,000 cells invaginate into the center of the embryo (Figure 3C).

For several reasons, the ventral furrow is a useful system to dissect the molecular mechanism of epithelial morphogenesis. First, ventral furrow formation is a spontaneous and autonomous event; there is no need to induce cultured cells to recapitulate a biological phenomenon, which means that findings are likely to reflect

fundamental biology. Second, the furrow is optically accessible, allowing the acquisition of high resolution images and movies. Third, a century's worth of genetic tools, and decades of fluorescent probes, are easily available for creative and powerful experimentation.

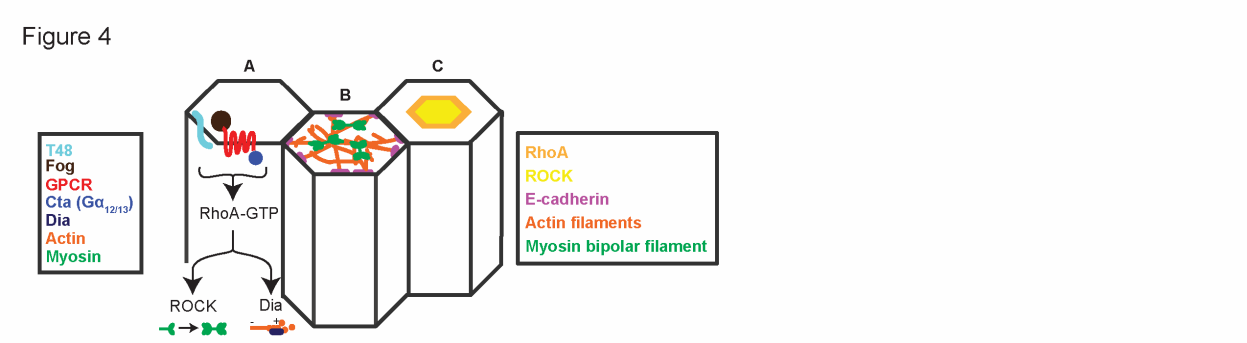

Figure 4. **Schematic of regulatory and actomyosin organization in *Drosophila* apical constriction.** **(A)** Components of the upstream signal transduction pathway. Fog binds and activates a GPCR that, along with T48, leads to $G\alpha_{12/13}$ activation and RhoA-GTP accumulation. RhoA-GTP activates both ROCK and Dia, which lead to myosin bipolar filament assembly and actin filament nucleation, respectively. **(B)** Actin and myosin form a network across the apical surface in apically constricting cells. The network as attached to adherens junctions to transmit forces to neighboring cells. **(C)** RhoA and ROCK are both localized the the medioapical area. Not drawn to scale.

Using the *Drosophila* ventral furrow, a number of important findings have emerged regarding the mechanism of apical constriction and epithelial folding. The ventral domain is genetically specified by the transcription factors Twist and Snail, which lead to the zygotic transcription of *fog*, *t48*, and other targets (Costa et al., 1994; Kölsch et al., 2007; Leptin, 1991; Leptin and Grunewald, 1990). Fog and T48 stimulate RhoA activity, which then activates ROCK and Dia, which assemble and contract the apical actin cortex (Figure 4) (Barrett et al., 1997; Dawes-Hoang et al., 2005; Homem and Peifer, 2008; Kölsch et al., 2007; Manning et al., 2013; Martin et al., 2009; Mason et al., 2013). Surface views of contracting ventral furrow cells revealed that actin and myosin form a network across the surface (Figure 3C) (Martin et al., 2009; Mason et al., 2013) with pulsatile dynamics in which the actomyosin network assembles and disassembles

in bursts (Xie and Martin, 2015) (see Appendix A for discussion of pulsatile actomyosin dynamics). This observation was surprising at the time because the prevailing model for apical constriction invoked a “purse-string” mechanism, where a circumferential belt of actomyosin constricted to cinch down the apical area. The second observation is that the myosin activating kinase, ROCK, and its activator RhoA, localize to the apical center (Mason et al., 2013), although the function of this localization was not determined (Figure 4).

The observation of an apical actomyosin network during apical constriction motivated the central question of this thesis: how is the apical actin cortex organized to produce contractile force? While the transcription factors and upstream regulators of contractility in the ventral furrow are known, the spatial organization of the apical actin cortex is not. Interestingly, *twist* and *snail* mutants neither contract normally, nor localize ROCK correctly, suggesting a functional importance for central ROCK localization in apical constriction (Mason et al., 2013; Vasquez et al., 2014). Recent work also demonstrated that apical myosin abundance and myosin motor activity both affect the speed of contraction (Vasquez et al., 2016; Xie and Martin, 2015). However, based on the fact that both the spatial organization of auxiliary proteins and also actomyosin topology determine muscle contractility, we decided to determine the spatial organization of more components of the apical actin cortex as well as the polarization of actin filaments within the apical cortex.

Questions addressed in this thesis

In an effort to understand the cellular mechanism of actomyosin contractility in apically constricting epithelial cells, I focus on two major questions. The first is to understand the composition of the apical actomyosin cortex. Outside of the core actomyosin machinery, various proteins regulate contractility and transmit forces to boundaries and neighboring cells. Chapter 2 of this thesis describes several actin cortex-related proteins and processes in apically constricting epithelial cells, where they were previously uncharacterized, and demonstrates that many proteins exhibit a specific localization pattern in the apical domain. The second major thrust of this thesis is to understand how components of the actomyosin cortex are spatially organized to contract, with a focus on the polarity of actin filaments. Are the actin filaments and myosin minifilaments spatially organized in apically constricting epithelial cells, and if so, is this organization functionally important? Chapter 3 directly addresses the question of actomyosin spatial organization in apical constriction. I identify an actomyosin topology in the contractile apex that resembles a sarcomere, in a 2-dimensional, or radial, orientation. This organization inspired our “radial sarcomere” model for epithelial cell contraction. Finally, in Chapter 4, this thesis concludes with recommendations for further lines of inquiry, and potential applications of these findings for human health.

Chapter 2: Spatial organization of new molecular components in the epithelial actin cortex

Authors: Jonathan S. Coravos[1] and Adam C. Martin[1]
Department of Biology, Massachusetts Institute of Technology, Cambridge, Massachusetts.
JC performed all experiments. JC and AM wrote the manuscript.

Abstract

Actomyosin networks, for example the actin cortex, require a collection of proteins that help generate contractile force and convert that force into cell deformation. Epithelia are one important example that uses myosin contractions of the apical actin cortex to power a cell deformation called apical constriction. Here, I use a candidate-based approach to characterize the apical actin cortex, including components of the spectrin-based membrane skeleton and actin filament end-binding proteins, as well as proteins that mediate the attachment of the cortex to the plasma membrane. Interestingly, many of these proteins exhibit a spatial localization within the apical domain, showing that the apical actin cortex is spatially organized, and suggesting localized activities for these proteins. Using RNAi knockdown, I was unable to find substantial phenotypes for any of these candidates. I propose additional experiments for determining whether these newly characterized cortical proteins and processes are functionally required for apical constriction.

Introduction

In apically constricting epithelial cells, the actin cortex forms a layer under the apical surface (Booth et al., 2014; Martin et al., 2009; Mason et al., 2013). This apical actin cortex contains myosin, which allows the actin cortex to generate contractile force. The apical actin cortex contains many additional regulatory and structural proteins. For example, mutants in proteins comprising the adherens junction, which binds the actin cortex at cell-cell contacts, lead to epithelial cell separation during apical constriction (Martin et al., 2010). Upstream activation of apical constriction occurs through RhoA (Barrett et al., 1997; Fox and Peifer, 2007; Kölsch et al., 2007; Mason et al., 2016) and its effectors ROCK (Dawes-Hoang et al., 2005; Mason et al., 2013) and the formin Dia (Homem and Peifer, 2008; Mason et al., 2013). However, we still lack a complete catalog of proteins involved in the apical actin cortex of apically constricting cells, and we do not know their organization and function in the apical domain.

A phenomenon related to the actin cortex is a process called plasma membrane blebbing. Blebbing occurs when contractions in the actin cortex lead to separation from the plasma membrane. Hydrostatic pressure from the cytoplasm causes the separated plasma membrane to inflate outward from the site of separation, after which the actin cortex reassembles underneath the inflated membrane. Myosin-dependent contractility pulls the bleb back into the plane of the cortex (Charras et al., 2008). While the biological function of blebs is not fully understood, they are useful research tools because they allow for the determination of cortical components. Using fluorescently-tagged proteins and immunostaining in blebs (Charras et al., 2006), as well as mass-

spectrometry of mechanically isolated blebs (Biro et al., 2013; Bovellan et al., 2014), the following abridged list of cortex components has been identified:

- ERM proteins, which connect the cortex and the plasma membrane
- actin crosslinkers (e.g. Fimbrin, Filamin)
- actin capping proteins (e.g. α-actinin, Tropomodulin, Adducin, Capping protein)
- actin nucleation/elongation factors (e.g. Arp2/3, Dia)
- small GTPases and their regulators (e.g. RhoA, ARHGAP1, ARHGEF7)
- actin turnover proteins (e.g. Profilin and Cofilin)

Some of these proteins have also been observed to localize to or play a role in the actin cortex of apically constricting epithelial cells, including Dia (Homem and Peifer, 2008; Mason et al., 2013), proteins that mediate actin filament disassembly and turnover (Jodoin et al., 2015), and RhoA and its regulators (Dawes-Hoang et al., 2005; Kölsch et al., 2007; Mason et al., 2013; 2016), but many others have not been investigated.

Here I add the following proteins to the list of actin cortex components in apically constricting epithelial cells: MP-RIP, β_H-Spectrin, Capping protein, Adducin, Tropomodulin, and Moesin. I found spatial patterns for these proteins in the apical cortex, with some localizing specifically to junctions, and others enriched in the medioapical region. RNAi did not substantially disrupt apical constriction for any of these proteins, but more experiments would have to be done to efficiently deplete gene activity at the embryonic stage where apical constriction occurs. In Chapter 3, I investigate the functional importance for spatial organization of apical cortex components.

Results

MP-RIP is enriched at adherens junctions

RhoA activity leads to myosin bipolar filament assembly through ROCK phosphorylation of the regulatory light chain. This assembly is counteracted by regulatory light chain dephosphorylation by myosin phosphatase, which binds myosin through the myosin binding subunit (MBS) of the phosphatase holoenzyme. In addition to assembling myosin bipolar filaments, ROCK also phosphorylates and inhibits MBS (Riento and Ridley, 2003). A paradox raised by some contractile systems is that myosin bipolar filaments can colocalize with MBS, yet remain intact (Vasquez et al., 2014).

Myosin phosphatase-Rho interacting protein (MP-RIP) is a protein that explains this paradox in some systems. MP-RIP binds the myosin binding subunit (MBS) of myosin phosphatase, the small GTPase RhoA, and localizes to myosin-based stress fibers (Surks et al., 2003). The most complete model for how MP-RIP functions is as a scaffold to mediate a switch in myosin phosphorylation in response to RhoA signaling. MP-RIP constitutively localizes myosin phosphatase to stress fibers through binding to MBS and actin filaments (Surks et al., 2005). In the absence of RhoA activity, the recruited myosin phosphatase is active and leads to myosin II regulatory light chain dephosphorylation and stress fiber disassembly. When RhoA is activated, it is recruited to MP-RIP which serves as a scaffold to bring myosin phosphatase near the RhoA-ROCK complex, which leads to myosin phosphatase inactivation and stabilized stress fibers (Riddick et al., 2008).

In the apical cortex of constricting epithelial cells, myosin phosphatase activity is essential for apical constriction (Vasquez et al., 2014), but it is unclear how myosin

phosphatase is regulated. MBS and ROCK both localize to apical myosin structures. Myosin is enriched medioapically, but is also present in fibers radiating outward to adherens junctions (Martin et al., 2010; Vasquez et al., 2014). Based on the ability of MP-RIP to regulate myosin phosphatase activity at stress fibers, I hypothesized that MP-RIP might also regulate specific actomyosin structures, such as these radiating fibers, in the apical cortex. Differences in MP-RIP localization to various structures in the apical domain might stabilize myosin in some regions while allowing turnover in others.

Figure 1

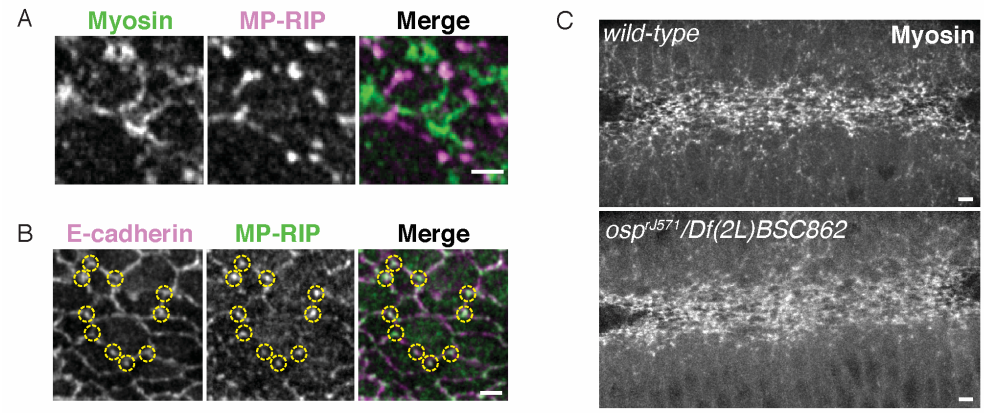

Figure 1: MP-RIP localizes the apical junctions at E-cadherin spots, but is not required for ventral furrow formation. (A) Apical maximum intensity projection (~2 µm) of myosin (SqhGFP) and MP-RIP (anti-MP-RIP) in a fixed embryo. Note the connection of myosin fibers with MP-RIP spots at the cell periphery. **(B)** Apical maximum intensity projections (~2 µm) of E-cadherin (anti-E-cadherin) and MP-RIP (anti-MP-RIP) in fixed embryo. Yellow dashed circles mark sites of MP-RIP and E-cadherin colocalization at apical spot junctions. **(C)** Embryo of maternal transheterozygotic genotype: osp^{rj571}/Df(2L)BSC862. A wild-type embryo expressing SqhGFP is included for comparison. MP-RIP is not required for normal myosin network organization or ventral furrow formation. Scale bars: 2 µm in A, B; 5 µm in C.

Using an antibody against MP-RIP, I found that MP-RIP does not colocalize closely with myosin, but localizes in discrete apical spots (Figure 1A). MP-RIP localized to E-cadherin-containing spot adherens junctions, the site of actomyosin network intercellular connections (Figure 1B). MP-RIP therefore defines a region of actin cortex proteins that localize specifically to the adherens junctions at the apical circumference.

When I tested *MP-RIP* for a loss-of function mutant phenotype, maternal transheterozygotic mutants did not exhibit a ventral furrow phenotype (Figure 1C), suggesting that MP-RIP is not required for apical constriction in the ventral furrow. One caveat is that some embryos likely carried one wild-type *MP-RIP* locus, possibly providing a zygotic rescue of the maternal mutant phenotype.

β_{heavy}-Spectrin in the apical actomyosin cortex

Spectrin-family proteins are long, flexible proteins with actin-binding, plasma-membrane binding, and regulatory domains. They line the plasma membrane and play structural and signaling roles (Liem, 2016; Machnicka et al., 2012). Flies have a single α-spectrin gene, and two isoforms of the β-spectrin gene, β-spectrin and β_H-spectrin (*karst*). In epithelia, β_H-spectrin can accumulate apically, and interact with adherens junctions or the apical determinant Crumbs (Dubreuil et al., 1998; Médina et al., 2002; Praitis et al., 2005; Thomas and Kiehart, 1994; Thomas et al., 1998). Loss-of-function *β_H-spectrin* mutants result in apical domain expansion (Lee and Thomas, 2011). Overexpression of dominant negative β_H-spectrin peptide also causes depolarization of epithelial cells and mislocalization of spectrin-associated membrane proteins, Ankyrin and Adducin (Hu et al., 1995). These results suggest that β_H-spectrin can promote spatial compartmentalization of epithelial cells membranes. *α-spectrin* also localizes to adherens junctions (Pradhan et al., 2001), and is required to maintain proper epithelial polarity (Lee et al., 1997; Ng et al., 2016). The other spectrin ortholog, α-spectrin, binds directly to the adherens junction through α-catenin and this binding stimulates spectrin skeleton assembly at the adherens junction (Pradhan et al., 2001). In addition to

homeostatic roles in epithelia, spectrins also function in epithelial morphogenesis, although their roles have only been appreciated at a gross anatomical level (Lee et al., 1993; McKeown et al., 1998; Norman and Moerman, 2002; Thomas et al., 1998; Zarnescu and Thomas, 1999).

Figure 2

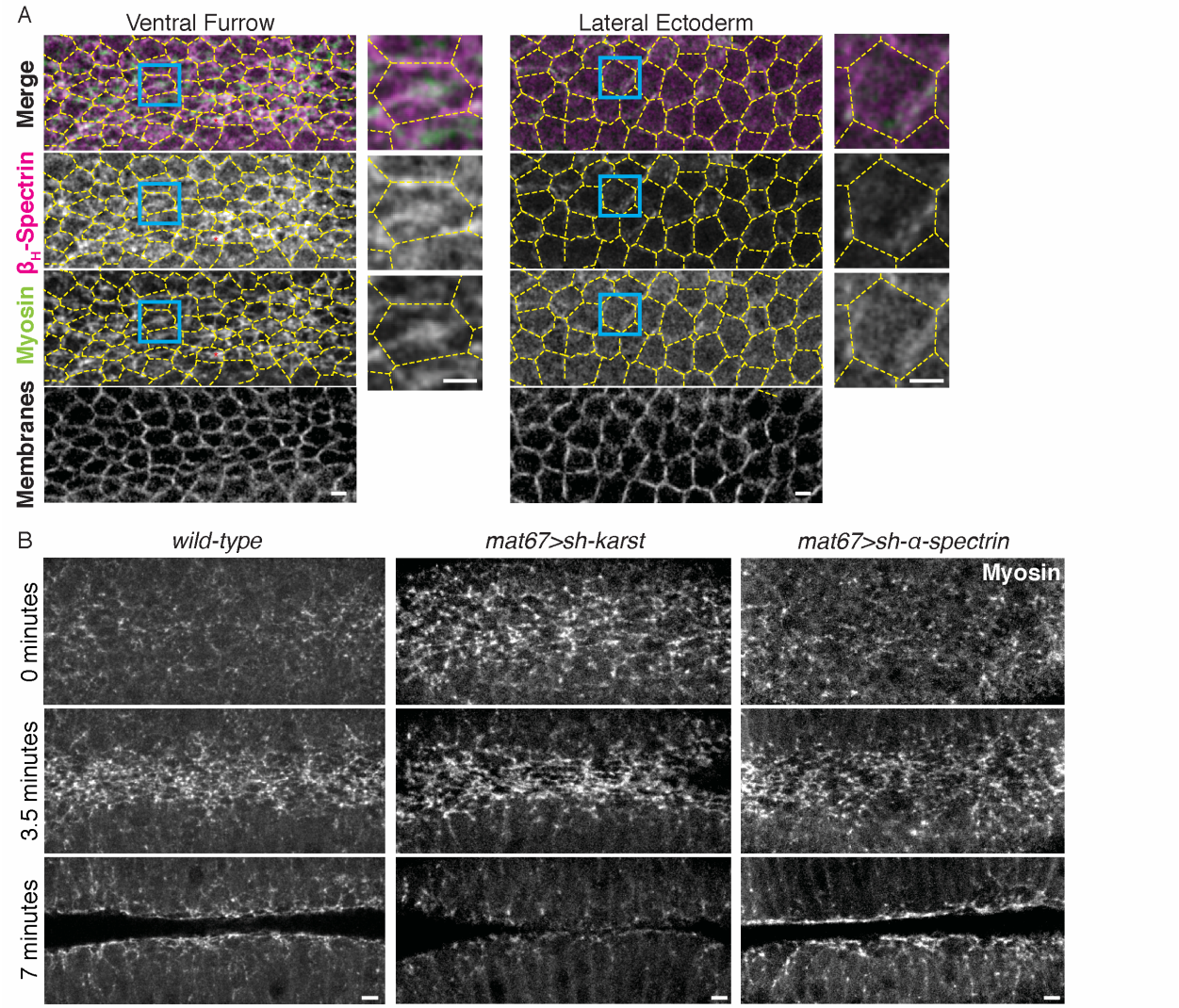

Figure 2: β_H-spectrin localizes to the apical junctions and across the apical surface, and neither β_H-spectrin nor α-spectrin has a knockdown phenotype. (A) Apical maximum intensity projection (~2 µm) of β_H-spectrin (anti-β_H-spectrin) and myosin (SqhGFP) in fixed embryos. Cell junctions are outlined in dashed yellow lines. Note the presence of β_H-spectrin across the apical surface specifically in the ventral furrow, and not in the lateral ectoderm. Cyan boxes indicate cells magnified to the right. **(B)** β_H-spectrin (karst) and α-spectrin Gal4/UAS-short hairpin knockdowns do not cause a defect in myosin network organization or ventral furrow formation. Embryos were temporally aligned by furrow closure. A wild-type embryo expressing SqhGFP is included for comparison. Scale bars: 2 µm in A, 5 µm in B.

Based on the known roles of β_H-spectrin and α-spectrin in epithelia, I hypothesized that spectrins might also display distinct localization patterns and functions in the apical actin cortex of apically constricting. First, I found that β_H-spectrin exhibits a ventral-specific localization to the apical surface, colocalizing with myosin, demonstrating that apical β_H-spectrin accumulates in the medioapical domain (central of the apical domain, see Chapter 1, Figure 2) (Figure 2A). Two possible functions of β_H-spectrin in the ventral furrow are (a) stabilization of the apical adherens junctions during the dynamic process of apical constriction, and (b) in maintaining the spatial organization of the apical cortex into medioapical and junctional domains. This second model is based on a recent finding that actin and spectrin appear in a periodic structure in axons, and are thought to organize Na^+ channels (Xu et al., 2013). Because RhoA and ROCK are present in a central spot in apical constricting cells, one possibility is that spectrin is important for maintaining this compartment (Mason et al., 2013).

To test for a β_H-spectrin function in apical constriction, I used Gal4/UAS to knockdown β_H-spectrin or *α-spectrin* (Figure 2B). In neither case did I observe a major phenotype in myosin network organization or ventral furrow formation, although it is always possible the knockdown was too weak to elicit a phenotype. Another approach would be to use the dominant negative allele *β_H33* (Lee and Thomas, 2011).

Actin filament end-binding proteins occupy distinct positions in the apical actomyosin cortex

Actin end-binding proteins regulate actin filament assembly and connect actin filaments to various binding partners. In the muscle sarcomere, for example, the barbed

end binding protein Capping protein stifles dynamics at the barbed end, and connects the actin filament barbed ends to the Z-disk through α-actinin (Papa et al., 1999). The pointed end capping protein Tropomodulin (Tmod) regulates actin filament length in the sarcomere (Mardahl-Dumesnil and Fowler, 2001). Here, I report the localization of several end-binding proteins in apically constricting cells, and find that actin end-binding proteins localize in a manner consistent with barbed ends enriched at junctions, and pointed ends enriched in the medioapical domain.

Barbed-end binding proteins: Capping protein and Adducin

Capping protein and Adducin both bind barbed ends of actin filaments, and participate in many actomyosin processes, from sarcomere contraction to cell motility (Edwards et al., 2014). Capping protein plays a complex role in actin filament dynamics, but is generally thought to bind actin filament barbed ends and limit their length (Caldwell et al., 1989). In epithelia, both Capping protein subunits localize to adherens junctions, as well as in some cases across the apical surface or cytoplasm (Schafer et al., 1992). Capping protein stabilizes E-cadherin and β-catenin at the adherens junction (Jezowska et al., 2011). *Capping protein* mutant cells can also accumulate excessive actin and be extruded (Janody and Treisman, 2006).

Adducin crosslinks spectrins and actin filaments, binding to their sides or barbed ends (Kuhlman et al., 1996; Li et al., 1998). In epithelia, Adducin localizes to and stabilizes adherens junctions (Kaiser et al., 1989; Naydenov and Ivanov, 2010), and stimulates the assembly of the spectrin skeleton (Abdi and Bennett, 2008). In flies, Adducin is encoded by *hu-li tai shao* (*hts*) (Yue and Spradling, 1992), and is required for actin ring structures that prop open cytoplasmic channels between the oocyte and

Figure 3

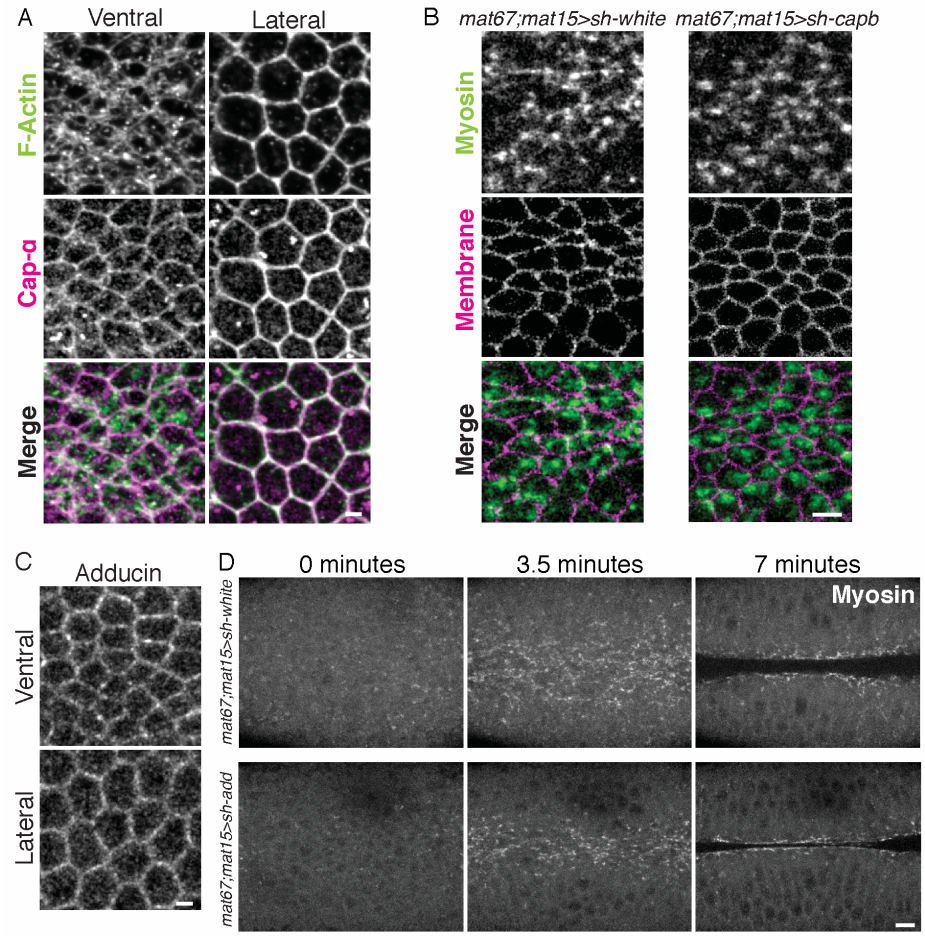

Figure 3: Capping protein and Adducin both localize to the apical periphery but not the apical center, and neither displays a knockdown phenotype. (A) Apical maximum intensity projection (~2 µm) of F-actin (phalloidin-AF568) and Capping protein α (anti-Cap-α) in ventral and lateral cells of fixed embryos. **(B)** Apical maximum intensity projection (~2 µm) in live embryos depleted of *white* or *capping protein β (cpb)* and expressing SqhGFP and Gap43-mCh. *cpb* knockdown does not cause a major defect in myosin network formation. **(C)** Apical maximum intensity projection (~2 µm) of Adducin (anti-Adducin) in ventral and lateral cells. **(D)** Apical maximum intensity projection (~2 µm) in live embryos depleted of *white* or *adducin* and expressing SqhGFP. *add* knockdown does not cause a major defect in myosin network formation or ventral furrow formation. Embryos were temporally aligned at furrow closure. Scale bars: 2 µm in A, C; 5 µm in B; 10 µm in D.

neighboring cells. *Drosophila* studies have also shown that Adducin regulates phosphorylation and basolateral recruitment of the epithelial polarity determinant Dlg (Wang et al., 2011). Together, these findings suggest that Adducin localization not only indicates the localization of actin filament barbed ends, but also regions of adherens junction stabililty and spectrin skeleton nucleation.

Here, I determined the localization of Capping protein α (*cpα* in *Drosophila*) in the apically constricting cells of the ventral furrow, and found a strong enrichment at the apical junctions (Figure 3A, and see Chapter 3, Figure 3 and Supplementary Figure 2). This implies (a) that actin filament barbed ends are enriched at the junctions, and (b) that they are capped by Capping protein. Adducin also localized at the apical junctions both in ventral and lateral cells (Figure 3C), confirming the implied distribution of barbed ends. This finding is consistent with the previous observation of Capping protein and Adducin at adherens junctions (Schafer et al., 1992) (Kaiser et al., 1989; Naydenov and Ivanov, 2010). Neither *cpa* nor *hts* knockdown, however, produced a phenotype, subject to the familiar caveat that knockdown may not have been sufficient to produce a loss-of-function phenotype (Figure 3B,D).

There are several intriguing models for how Capping protein and Adducin might operate in apical constriction. First is that Capping protein might form the basis for an α-actinin-based mechanical coupling to the adherens junction. Inhibiting Capping protein would therefore be predicted to inhibit force-propagation across the tissue, leading individual apical domains to disconnect from their neighbors, as has previously been reported for *β-catenin* mutants (Martin et al., 2010) and as has been seen with injection of the barbed-end capping drug that does not bind α-actinin, CytochalasinD (Martin et al., 2009; Mason et al., 2013). Second, Capping protein might drive the formation of branched or unbranched actin filament growth, either by capping Arp2/3-nucleated branches (Akin and Mullins, 2008), or by capturing and stabilizing formin-elongated filaments (Shekhar et al., 2015). Under this model, Capping protein should change the topology of the actin cortex, shifting it into either a more branched or unbranched state.

Different network topologies could affect the generation or propagation of force, through an effect on actin network connectivity (Backouche et al., 2006).

Pointed-end binding protein: Tropomodulin

Tropomodulin (Tmod) caps actin filament pointed ends. Tmod binding can slow or even completely stop assembly/disassembly at the already slow-growing pointed end, and has been proposed to act as a mechanism for fine-tuning actin filament length in actin networks (Fischer and Fowler, 2003). Tmod can act as a strong or "leaky" cap on actin filament pointed ends, depending on the presence of tropomyosin (Rao et al., 2014; Weber et al., 1994). In sarcomeres, these properties allow Tmod to regulate actin filament assembly and length with consequences for sarcomere length and function (Gokhin et al., 2015; Littlefield et al., 2001; Mardahl-Dumesnil and Fowler, 2001).

In epithelia, Tmod knockdown reduces basolateral membrane-associated actin filaments, shortens the epithelial height, and disrupts the spectrin-based membrane skeleton (Weber et al., 2007). Tmod also localizes to the adherens junctions and the terminal web of intestinal brush border cells, where it is required for adherens junction stability during epithelial morphogenesis, and for the proper formation of the intestinal lumen (Cox Paulson et al., 2014; Cox-Paulson et al., 2012).

Despite actin filaments being present across the entire apex, Tmod is enriched in a distinct apical domain. In contrast to barbed-end capping proteins, Tmod localizes to the middle of the apical domain, specifically in ventral furrow cells (Chapter 3: Figure 3 and Supplementary Figure 2). This localization pattern implies the presence of actin filament pointed ends in that region, and raises some possibilities for Tmod function in

the medioapical actin cortex, including regulation of actin filament length, and protection of the pointed end from depolymerization.

Membrane-cortex attachment in apically constricting cells

Membrane-cortex adhesion, defined as the strength of the mechanical connection between the plasma membrane and the actin cortex, is regulated by the Ezrin, Radixin, and Moesin (ERM) family of proteins (Neisch and Fehon, 2011). *moesin* is the only ERM gene in *Drosophila*, facilitating genetic analyses. All ERM proteins have an N-terminal FERM domain that interacts with the plasma membrane or scaffolding proteins, a C-terminal actin-binding domain, and an α-helical coiled-coil spanning the two termini. ERM proteins are activated by PIP_2-binding to the FERM domain and phosphorylation of a conserved Threonine residue (Thr559 in *Drosophila*) at the C-terminus (Fievet et al., 2004).

Moesin has been found to play a role in cortical rounding/stiffening (Kunda et al., 2008; 2012; Roubinet et al., 2011) and spindle positioning (Carreno et al., 2008; Kunda et al., 2008; Sabino et al., 2015). In *Drosophila* epithelia, Moesin also plays a role in structuring the apical domain: it is essential for the apical cytoskeletal structure of the rhabdomere (Karagiosis and Ready, 2004), follicle cells (Sherrard and Fehon, 2015), the wing imaginal disk epithelium (Neisch et al., 2013; Speck et al., 2003), and for cytoskeletal attachment to the oocyte membrane (Polesello and Payre, 2004). Motivated by this collection of examples of Moesin in individual cell morphogenesis and epithelia, I looked to see where Moesin localizes in apically constricting ventral furrow

Figure 4

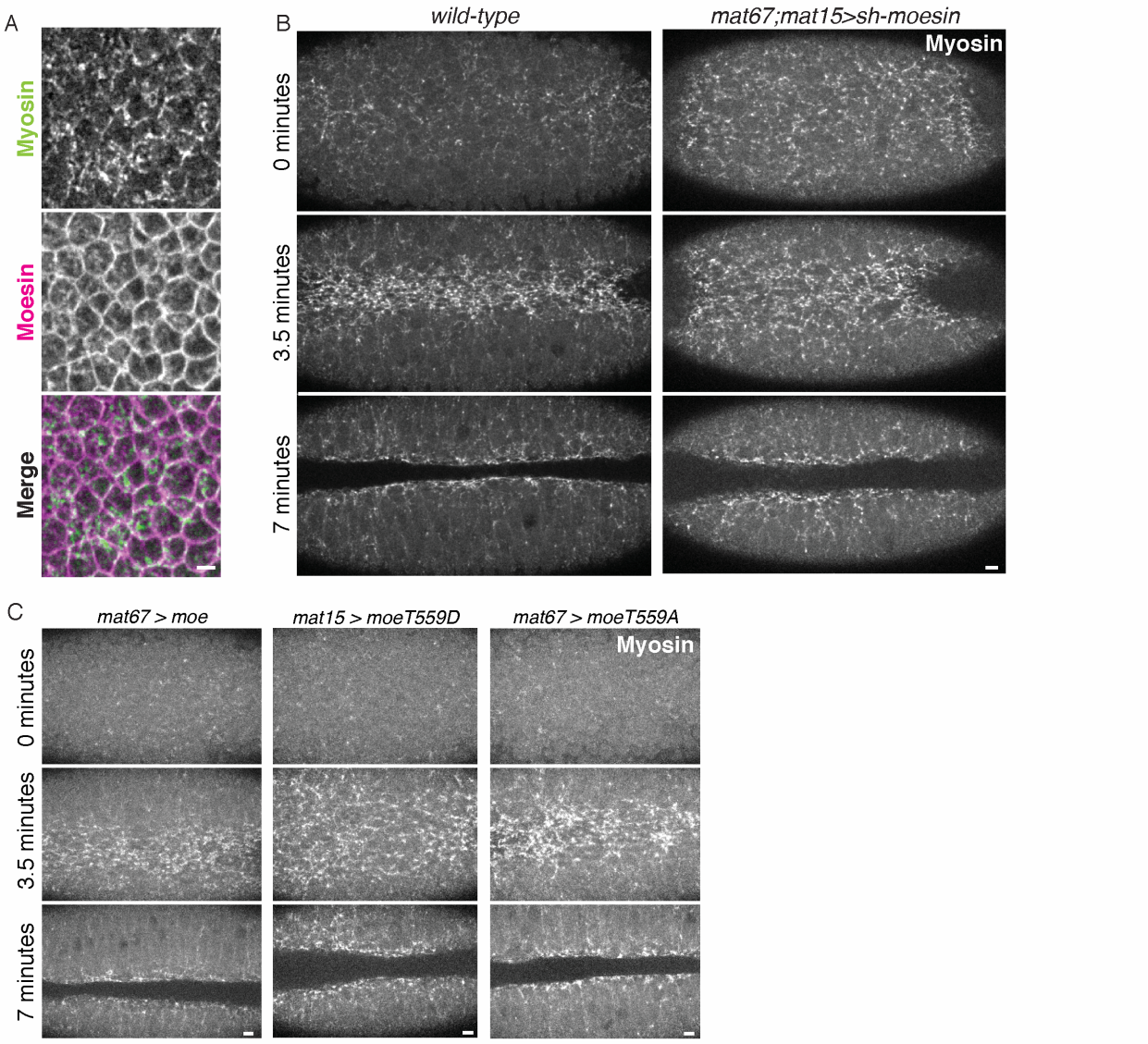

Figure 4: Moesin localizes at junctions and across the apical urface of ventral furrow cells, but does not present a knockdown phenotype. (A) Apical maximum intensity projection (~2 μm) of myosin (SqhGFP) and Moesin (anti-Moesin) in the ventral furrow. Note the Moesin localization across the apical surface. **(B)** Moesin knockdown by Gal4/UAS-short hairpin does not cause a defect in myosin organization or ventral furrow formation. A wild-type embryo expressing SqhGFP is included for comparsion. **(C)** Overexpression in a wildtype background of wild-type or phosphomutant *moesin* alleles does not cause a major defect in myosin organization or ventral furrow formation. In both B and C, embryos were temporally aligned by furrow closure. Scale bars: 2μm in A, 5 μm in B,C.

cells. Using a Moesin antibody, I determined that Moesin is localized strongly to apical junctions, and in a heterogeneous pattern across the apical surface (Figure 4A). This

localization is consistent with Moesin playing a role connecting the actin cortex to the apical plasma membrane at junctions and across the apical surface.

To test this model, I looked at myosin network organization and ventral furrow formation in embryos depleted of Moesin with a Gal4/UAS-driven short hairpin, and although there were some subtle differences between myosin networks and ventral furrow formation in the knockdown, I did not identify any reproducible or dramatic differences (Figure 4B). It is technically difficult to look at the *moesin* null mutant because it disrupts oogenesis (Polesello et al., 2002). As another method to investigate Moesin function, I used the Gal4/UAS system to overexpress two *moesin* alleles with either a glutamate or alanine substitution for the regulatory threonine (Thr559) that are designed to mimic the active or inactive states, respectively (Polesello et al., 2002). Overexpressing *moeT559D* was lethal before ventral furrow formation unless driven with the weak *mat15* Gal4 driver, in which case a ventral furrow still formed (Figure 4C). *moeT559A* could be driven with stronger Gal4 drivers without causing early lethality. Again, I observed some subtle differences between conditions, but no reproducible or dramatic differences emerged (Figure 4C).

In other systems, low membrane-cortex adhesion has been associated with blebbing (Cunningham et al., 1992; Dai and Sheetz, 1999). Interestingly, the apices of ventral cells are covered in small blebs (Sweeton et al., 1991). I therefore analyzed the spatial organization of blebs in the apical domain of apically constricting cells to determine spatial organization of membrane-cortex adhesion. Using high resolution confocal microscopy, I was able to capture precise images of blebs in the apical cortex

of apically constricting cells (Figure 5A). I confirmed that they form with the kinetics of blebs observed in cell culture, and that they form over holes in the actin cortex, initially

Figure 5

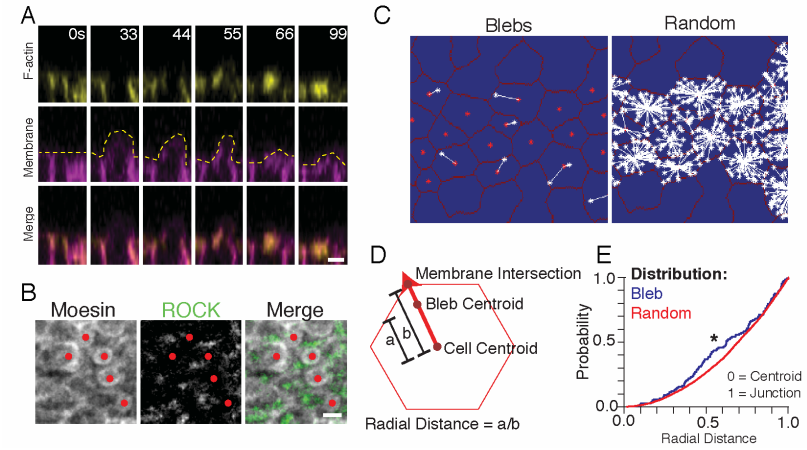

Figure 5: Ventral furrow bleb dynamics and spatial localization. (A) Cross-sectional views of a bleb in an embryo expressing Utr::Venus (F-actin) and Gap43-mCh (membrane). Yellow-dashed line marks the extent of the apical plasma membrane. Note the absence of F-actin under the newly formed bleb at 33 seconds, and the reassembly of F-actin in the bleb as it is retrated to the apical surface. **(B)** Apical projection (~2 μm) of a fixed embryo expressing Venus::ROCK^{K116A} and stained with anti-moesin to label blebs. Red dots indicate bleb location. Note the lack of overlap between ROCK fluorescence and bleb location. **(C)** Example of bleb localization and random feature localization used for calculating the radial distance metric in (D). White asterisks are feature locations (bleb or random), red asterisk is the geometric centroid, and the white line corresponds to the "a" distance in (D). Red lines are cell membrane outlines. **(D)** Schematic describing the calculation of the radial distance metric. **(E)** Cumulative probability distribution of the bleb and random feature distributions. Distributions were compared with the kolmogronov-smirnov test, asterisk indicates significance at α = 0.05. Scale bars: 2 μm in A.

lack actin filaments in the bleb, and retract as actin filaments reappear (Figure 5A, adapted from Jodoin et al., 2015). Ventral furrow blebs therefore share key properties with blebs in other systems (Charras et al., 2006; 2008). I next evaluated the spatial localization of blebs in the apical membrane, using a Moesin antibody because Moesin is one of the first known cortical proteins to appear in blebs (Charras et al., 2006). I determined that blebs occur in regions of the apical cortex lacking ROCK, suggesting a spatial distribution of blebs away from the apical center (Figure 5B). To quantitatively assess bleb localization, I recorded the radial coordinate position of blebs relative to the cell geometric centroid (Figure 5C,D). I found that, compared with randomly distributed

coordinates, blebs are enriched in the space between the geometric centroid and the cell junctions (Figure 5E). These findings demonstrate that blebs, like some apical proteins, are spatially organized, and that bleb-associated actin cortex dynamics are also spatially organized.

Discussion

The following proteins are now characterized components of the apical cortex during apical constriction in the *Drosophila* ventral furrow: MP-RIP, β_H-spectrin, Tmod, Capping protein, Adducin, β_H-spectrin, and Moesin. The major observation from this suite of experiments is that the apical actin cortex of ventral furrow cells exhibits a detailed spatial organization of these components. β_H-spectrin localizes across the apical surface, Moesin localizes to junctions and the medioapical zone, Adducin and Capping protein localize to junctions, and Tmod localizes to the medioapical zone. MP-RIP localizes to apical adherens junctions that colocalize with myosin. Blebs are enriched in the space between the geometric centroid and the junctions (Figure 6). This spatial organization is striking, but its function is unclear. Chapter 3 investigates this question in depth. Following are some speculations for how the spatial organization of this collection of cortical components might play a role in apical constriction and ventral furrow formation.

β_H-spectrin and Adducin both act in the spectrin-based membrane skeleton, and their presence in the apical cortex raises an interesting possibility for a role for spectrin in apical constriction. Two major possibilities exist for spectrin function. First, spectrin could regulate the spatial organization of the cortex. The apical cortex displays a spatial organization of components, with ROCK localized to the center of the apical domain (Mason et al., 2013). With their ability to simultaneously bind actin filaments, the plasma membrane, and various adaptor proteins, spectrins have the potential to regulate this spatial organization, as they do in axons (Xu et al., 2013). The second interesting possibility for spectrin is that, as in erythrocytes, spectrin could provide mechanical

Figure 6

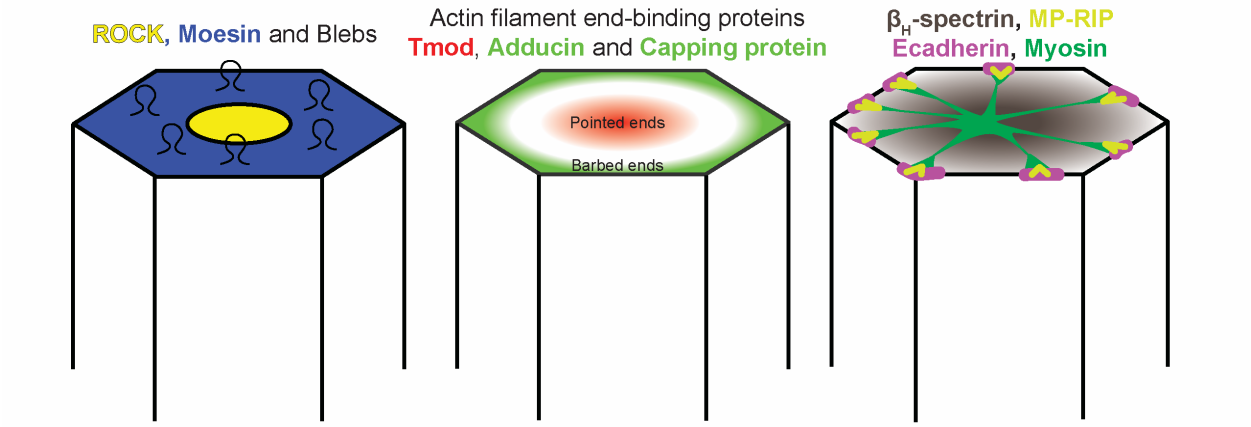

Figure 6. Schematics displaying the spatial localization of actin cortex-related associated proteins. Moesin localizes across the apical surface, ROCK localizes the the medioapical center, and blebs are enriched between the medioapical center and the junctions. Tmod is enriched medioapically, and Adducin and Capping protein are enriched junctionally, indicating the presence of pointed ends and barbed ends in their respective zones. β_H-spectrin localizes across the apical surface. MP-RIP colocalizes with E-cadherin and myosin in spots at the apical junctions. Not drawn to scale.

structure to cells that are deforming. It is possible that in the absence of the spectrin-based membrane skeleton, the apical membrane would lose integrity and bleb away from a contracting actin cortex, or that neighboring cells would tear apart from each other as the apical cortices of neighboring cells ruptured. This model requires sufficient knockdown of β_H-spectrin, or, alternatively, one could disrupt β_H-spectrin binding to the membrane by overexpressing the competing peptide β_H33 (Lee and Thomas, 2011). I recommend performing these experiments in embryos expressing fluorescent myosin (Sqh::GFP) and a membrane marker (Gap43::mCherry), to investigate the effects of spectrin disruption on the stability of the intercellular myosin network, or on the apical morphology or decrease in area of ventral epithelial cells.

I also found that actin filament end-binding proteins exhibit localization patterns in the apical domain, with barbed end binding proteins Adducin and Capping protein α enriched at the junctions, and the pointed end-binding protein Tmod enriched in the

medioapical zone. This observation has interesting implications for the organization of the actin cortex (see Chapter 3 for more discussion), but also for localized function of end-binding proteins in apical constriction. For example, Capping protein is known to anchor sarcomere actin filaments to the Z-disk through α-actinin (Papa et al., 1999), and α-actinin is also present at some adherens junctions (Tang and Brieher, 2012). Capping protein might therefore regulate actin filament hand-off to α-actinin at adherens junctions in the ventral furrow. I propose looking for α-actinin localization at adherens junctions and evaluating the α-actinin knockdown phenotype, paying special attention to possible effects at the adherens junction. In both of these experiments, I recommend using the live *ubi>EcadGFP* fly line, which has bright apical E-cadherin labeling and should reveal colocalization with α-actinin antibody staining, or adherens junction perturbations caused by α-actinin knockdown.

Tmod might play a role in regulating actin filament length in the apical cortex, as it does in sarcomeres (Gokhin et al., 2015). Because the connectivity of actin networks influences the distance over which forces are transmitted in the cortex (Backouche et al., 2006), filament length could have an effect on mechanical force propagation in the apical cortex. I propose testing this possibility by looking in *tmod* knockdowns for a defect in the persistence of myosin fluorescence during dynamic contractions, which is a proxy for force-generation (Xie and Martin, 2015). In the event of a phenotype, it would then be interesting to image the apical actin cortex with a super resolution approach to elucidate structural differences in the wild-type and *tmod*-depleted actin cortex.

Understanding any machine requires having a full parts list, and there are several clear next steps for filling out this list for the contracting apical domain of epithelial cells. In this discussion, I have already advocated searching for α-actinin in the apical cortex. I also recommend investigating the role of tropomyosin, which is required for tight Tmod pointed end capping. Candidate-based searches, however, will only go so far, and the complete parts list should be generated with an unbiased method. For this, I suggest immunological purification of the apical cortex, followed by mass spectrometry. There are several proteins one could use for "bait" in this approach. Because Moesin is one of the first proteins to appear in the assembling cortex (Charras et al., 2006), using the Moesin-actin binding domain is one approach, especially since it is a GFP-tagged probe (GFP::MoeABD) long in use in the field. To find ventral furrow-specific cortical components, two populations of GFP::MoeABD embryos should be collected, wild-type and ventralized, in which most cells acquire ventral furrow fates. Analyzing the GFP-pulldown pellet from these two samples would potentially collect a broad range of cortex-associated proteins. Proteins enriched in ventralized embryos would constitute a putative parts list of cortex-associated proteins with specialized functions in apical constriction. Another possibility for actin cortex component analysis is to adapt the bleb isolation protocol used in HeLa cells (Biro et al., 2013) to S2R+ *Drosophila* cells. Using blebs isolated from contracting S2R+ cells (Rogers et al., 2004) and using unstimulated S2R+ cells for comparison, one could generate a parts list of contraction-associated cortical components for validation by RNAi screening *in vivo*.

Experimental Procedures

Antibodies Used

Antibody	Use	Concentration	Source
R β_H-Spectrin	FA	1:10000	Graham Thomas, Penn State University, University Park, PA
R MP-RIP	FA	1:500	Sigma
R Moesin	FA	1:5000	Sebastien Carreno, University of Montreal, Canada
M anti-adducin	FA	1:500	DSHB
R anti-Capα	FA	1:200	Janody Lab, Instituto Gulbenkain de Ciencia, Oeiras, Portugal
Rt anti-E-cadherin	FA	1:50	DSHB

R = rabbit, M = mouse, Rt = Rat
FA = paraformaldehyde fixation
DSHB = Developmental Studies Hybridoma Bank, University of Iowa

Fly Stocks

Genotype	Source
OregonR	1
y,v;P{TRiP.HMS00882}attP2 **(alias: sh-karst)**	1
y,w;P{TRiP.GL01173}attP2 **(alias: sh-αSpec)**	1
y,v;P{TRiP.HMS00886}attP2 **(alias: sh-moesin)**	1
y,v;P{TRiP.HMS00017}attP2 **(alias: *sh-white*)**	1
y,v;P{TRiP.HMS02349}attP2 **(alias: sh-capb)**	1
y,v;P{TRiP.HMS01736}attP40 **(alias: sh-adducin)**	1
P{UASp-DmoeTA}	2
P{UASp-DmoeTD}	2
P{UASp-DmoeWT}	2
y w sqh^{AX3};P{w$^+$ sqh-Sqh::GFP}42 **(alias: SqhGFP**)	3
P{sqh-gap43::mCherry}attp2/Tm3 **(alias: Gap43-mCh)**	4
P{mat-Tub-Gal4}67 **(alias: mat67)**	5
P{mat-Tub-Gal4}15 **(alias: mat15)**	5
mat67, SqhGFP; mat15, Gap43-mCh	4
SqhGFP; mat15	4
mat67, SqhGFP	4
mat67,SqhGFP; mat15, Gap43-mCh	4
P{PZ}osp^{rj571}/CyO	1
Df(2L)BSC862/CyO	1
P{PZ}osp^{rj571};P{w+ sqh-SqhGFP}	1
P{UASp-Venus::rock^{K116A} }attP40	6
P{sqh-Utr::Venus}/Tm3	7

Sources

1. Bloomington Drosophila Stock Center, Indiana University
2. Gift from Francois Payre
3. Gift from A. Royou
4. This study
5. Gift from D. St. Johnston
6. Gift from J. Zallen
7. Gift from A. Sokac

Fly Genetics

All flies analyzed were generated using the stocks listed in the above table. All fixed image visualizations of myosin (Figure 1A, Figure 2A, Figure 4A) were performed in *sqh^{AX3};P{w^{+} sqh-Sqh::GFP}42*. To analyze knockdown phenotypes (Figure 2B; 3B,D; and 4B), females carrying the UAS-driven short hairpin (e.g. *sh-moesin*) were crossed to males carrying either or both maternal Gal4 drivers, *mat67* and *mat15* with *SqhGFP* or *Gap43-mCh* to visualize myosin and membranes, respectively. Female F1 offspring from this cross (e.g. *mat67,SqhGFP/+; mat15/sh-moesin*) were mated to OregonR males, and embryos from these crosses were analyzed for a phenotype. Moesin phosphoallele phenotypes (Figure 4C) were also analyzed in embryos of mothers with the following genotype, where XX is WT or TA: mat67, SqhGFP/UASMoeXX or SqhGFP/UASMoeTD; mat15/+. In Figure 6E, embryos are of maternal genotype *mat67/UAS-moeWT::GFP* or *mat67/UAS-moeTA::GFP*. To analyze the *osp* (*MP-RIP*) mutant phenotype (Figure 3C), flies of the following genotypes were crossed: *osp^{rj571}/CyO; P{SqhGFP}* and *Df(2L)BSC862/CyO*. *osp^{rj571}/ Df(2L)BSC862; SqhGFP/+* females were collected, crossed to Oregon R, and their embryos were analyzed for mutant phenotypes. Bleb dynamics (Figure 5A) were examined in embryos laid by *Gap43-mCherry/sqh-Utr::Venus* females crossed to OregonR males. ROCK was

visualized (Figure 5B) in embryos laid by *P{UAS-Venus::rock^{k116A}}attP40/+;mat15/+* females crossed to Oregon R males.

Bleb analysis

Bleb positions were manually annotated (Figure 5) by identifying protruding membranes that appeared above cells. A bleb-centroid distance metric was calculated by generating a ray from the geometric centroid through the bleb position, forming a third point at the intersection of the ray and the edge of the cell. The bleb-centroid distance metric is the ratio of the bleb-centroid distance to the membrane-centroid distance, where a value of 1 is a position on the cell edge and a value of 0 is a position on the cell centroid. To evaluate the spatial distribution of the bleb-centroid distance metric, I generated a random set of points and calculated their distances from corresponding cell centroids. Because these distributions were not normal, I compared them using a two-sample Kolmogorov-Smirnov test with an alpha of 0.05.

Imaging and image processing

See Chapter 3, Experimental Procedures

Chapter 3: Apical sarcomere-like actomyosin contracts nonmuscle *Drosophila* epithelial cells

Reprinted with permission from Elsevier:
Jonathan S. Coravos, Adam C. Martin. 2016. Apical sarcomere-like actomyosin contracts nonmuscle *Drosophila* epithelial cells. *Dev. Cell*. Volume 39 , Issue 3 , 346 – 358
JC and AM designed and performed experiments, analyzed data, and wrote the manuscript.

Abstract

Actomyosin networks generate contractile force that changes cell and tissue shape. In muscle cells, actin filaments and myosin II appear in a polarized structure called a sarcomere, where myosin II is localized in the center. Nonmuscle cortical actomyosin networks are thought to contract when nonmuscle myosin II (myosin) is activated throughout a mixed-polarity actin network. Here, we identified a mutant version of the myosin-activating kinase, ROCK, that localizes diffusely, rather than centrally, in epithelial cell apices. Surprisingly, this mutant inhibits constriction, suggesting that centrally localized apical ROCK/myosin activity promotes contraction. We determined actin cytoskeletal polarity by developing a barbed end incorporation assay for *Drosophila* embryos, which revealed barbed end enrichment at junctions. Our results demonstrate that epithelial cells contract with a spatially organized apical actomyosin cortex, involving a polarized actin cytoskeleton and centrally positioned myosin, with cell-scale order that resembles a muscle sarcomere.

Introduction

Cell and tissue shape changes emerge from forces generated by myosin II and actin filaments. At the molecular scale, myosin II forms bipolar filaments with motor domains at both ends of a rod, which bind and move towards actin filament barbed ends (Sellers, 1991) (Fig. 1A). In muscle sarcomeres, this molecular apparatus is arranged and repeated at a larger scale, with actin filament barbed ends anchored at the sarcomere edges, and pointed ends oriented inward. Bipolar myosin II filaments overlap with actin filament pointed ends and, when the muscle is stimulated, pull in the actin filament arrays, shortening the sarcomere and contracting the muscle (Huxley and Hanson, 1954).

In cortical nonmuscle contexts, like individual cells (Charras et al., 2006; Flanagan et al., 2001), cell-cell epithelial interfaces (Simoes et al., 2014; Simões et al., 2010), and the apical surface of epithelial cells (Barrett et al., 1997; Clay and Halloran, 2013; Dawes-Hoang et al., 2005; Lee and Harland, 2007; Wójciak-Stothard et al., 2001), the contractile molecular actomyosin apparatus is still responsible for force generation, but actin filament networks are not thought to exhibit well-defined polarity. In these contexts, mixed-polarity actin networks are thought to contract from activation of nonmuscle myosin II (myosin) throughout the network (Fig. 1A). This myosin activation often occurs downstream of RhoA (Ridley and Hall, 1992) and its effector, the myosin-activating kinase, Rho associated coiled-coil kinase (ROCK, *rock*) (Amano et al., 1996; Mizuno et al., 1999; Winter et al., 2001). Interestingly, actin networks reconstituted *in vitro* also begin with a mixed-polarity actin network, but contract into actomyosin asters after global activation of myosin in the network (Backouche et al., 2006; Köster et al.,

2016; Murrell and Gardel, 2012; Stachowiak et al., 2012). Based on these cases and other work, it has been proposed that nonmuscle cortical actin networks generate and orient forces through intrinsic properties of a uniformly activated actomyosin network (Murrell et al., 2015; Vignaud et al., 2012), emerging possibly from the asymmetry in actin filament response to tension and compression (Stachowiak et al., 2012) or from actomyosin advection that carries upstream regulators of contractility (Munjal et al., 2015). In epithelia undergoing morphogenesis, the polarity of actin filament networks has not been determined, limiting our understanding of the mechanism of epithelial contractility (Mason et al., 2013; Munjal et al., 2015; Röper, 2012).

We investigated the importance of cell-scale actomyosin polarity in the columnar epithelial cells of the *Drosophila* ventral furrow. Apical constriction in these cells promotes invagination of the prospective mesoderm, and leads to the formation of the ventral furrow (Martin et al., 2009; Polyakov et al., 2014; Rauzi et al., 2015). We have previously shown that ROCK is enriched in the center of the apical domain (medioapical), displaying a type of cell polarity we termed radial cell polarity, in which proteins are polarized along the radial axis from the centroid to cell edge (Mason et al., 2013; Vasquez et al., 2014). Mutation or depletion of the ventral furrow transcription factor Twist disrupts medioapical ROCK polarization and disrupts apical constriction (Mason et al., 2013; Xie and Martin, 2015). As a transcription factor, Twist is several steps removed from the mechanism of actomyosin contractility and could have pleiotropic effects. Demonstrating the importance of ROCK localization in apical constriction therefore requires a direct perturbation of ROCK localization.

We identified a ROCK mutant that fails to polarize within the medioapical domain and demonstrated that medioapically polarized ROCK and myosin activity are required for apical constriction and tissue folding. We also determined that the apical actin network exhibits a cell-scale actin filament polarity, with pointed ends in the center of the apex and barbed ends around the apical periphery, suggesting that apical myosin binds and pulls inward on actin filament networks with barbed ends oriented towards the cell junctions. Finally, we show that the actin cytoskeleton is required to polarize ROCK within the apical domain, consistent with the idea that actomyosin feedback reinforces contractility (Munjal et al., 2015; Priya et al., 2015).

Results

Apically diffuse ROCK is insufficient for epithelial folding

To determine the function of medioapical ROCK polarization, we screened a collection of Venus-tagged and UAS-driven ROCK truncation mutants (*rock*^{wt} = *UASp>Venus::rock*$^{1\text{-}1391}$, see Supplementary Experimental Procedures, Fly Stocks) (Simoes et al., 2014) for alleles that failed to localize in a radially polarized focus in the apical domain of ventral furrow cells. Our screen revealed that any construct including the coiled-coil domain was capable of exhibiting a medioapical polarization (Fig. 1B, columns 1-3 and 5). In contrast, deleting a portion of the coiled coil domain resulted in a mutant (ROCK$^{\Delta 547\text{-}923}$) that localized across the apex (Fig. 1B, column 6). ROCK$^{\Delta 547\text{-}923}$ retains the N-terminal kinase domain and a C-terminal RhoA-binding domain, but removes a portion of the Shroom-binding domain, which interacts with the actin-ROCK scaffold protein, Shroom (Hildebrand and Soriano, 1999; Mohan et al., 2012; Nishimura and Takeichi, 2008). However, we confirmed previous work showing that *shroom* knock-down does not disrupt ventral furrow formation or ROCK localization (Fig. S1A,B) (Simoes et al., 2014). This is consistent with the fact that ROCK$^{\Delta 835\text{-}937}$, which lacks only the Shroom-binding domain, exhibits normal ROCK localization (Fig. 1B, column 5).

We next determined whether the apically enriched but diffuse ROCK$^{\Delta 547\text{-}923}$ disrupted myosin localization. We expressed Venus-tagged *rock*^{wt} and *rock*$^{\Delta 547\text{-}923}$ in the *rock*^{2} null mutant background, with *rock*$^{\Delta 547\text{-}923}$ being expressed at a level close to that of wild-type GFP-tagged *rock* expressed with its endogenous promoter (Fig. S1C). The localization of both proteins in the *rock* null background recapitulated the localization of the overexpressed proteins in our screen, including ventral-specific apical localization,

Figure 1

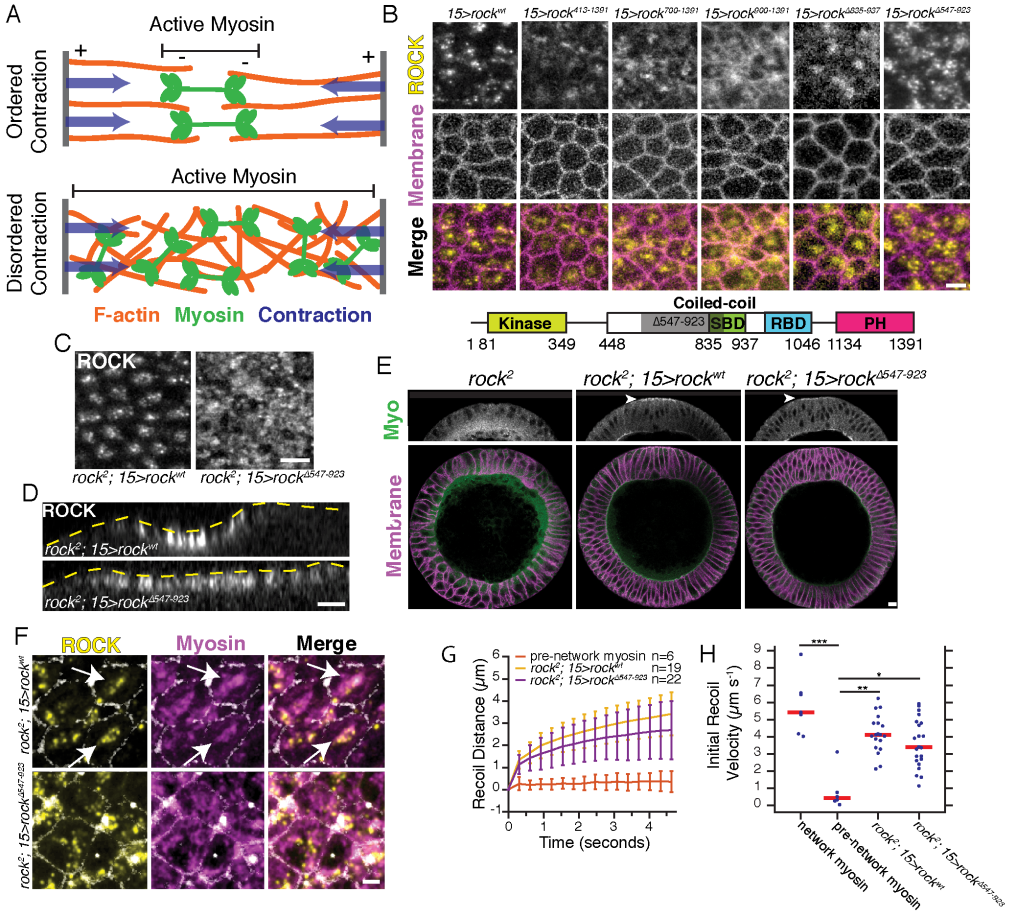

Figure 1. Diffuse apical ROCK is insufficient for tissue folding. (**A**) Models for actomyosin contraction. (**B**) Apical surfaces of ventral furrow cells in embryos expressing the indicated Venus-tagged *rock* transgenes in the presence of endogenous wild-type ROCK. SBD = Shroom-binding domain, RBD = RhoA binding domain, PH = pleckstrin homology. Shaded region indicates deleted region in ROCK$^{\Delta 547\text{-}923}$. (**C**) Apical surfaces of ventral furrow cells with ROCK^{wt} or ROCK$^{\Delta 547\text{-}923}$ expressed in *rock*^{2} null mutant background. (**D**) Cross-section views of the ventral side of embryos. Yellow dashed lined represents the embryo surface. Embryos were aligned in time by the onset of ROCK accumulation. The ventral domain appears smaller in *rock*^{wt} because cells have contracted their apical area. (**E**) Cross-sections of fixed embryos stained for myosin heavy chain (Myo) and Neurotactin (Membrane). Genotypes are the *rock*^{2} null mutant or the *rock*^{2} mutant expressing either *rock*^{wt} or *rock*$^{\Delta 547\text{-}923}$. Arrowheads indicate apical myosin specific for ventral domain. (**F**) Apical surface views of *rock*^{wt} or *rock*$^{\Delta 547\text{-}923}$ expressed in *rock*^{2} null background and immunostaining of myosin heavy chain. Arrows show polarized myosin. (**G**) Recoil distance of fluorescent ROCK signal away from laser cut in ventral furrow epithelium after laser ablation at t = 0. In the pre-network myosin condition, the ablation was performed in wild-type embryos expressing RLC::GFP, which was used instead of ROCK fluorescence to track recoil distance. n is cuts per condition, and bars represent ± 1 s.d. (**H**) Initial recoil velocity following (~ 300 ms) laser ablation in RLC::GFP embryos prior to (pre-network myosin) or after (network myosin) the establishment of the supracellular myosin network. Initial recoil velocity was also measured in *rock*^{2} germline clones expressing either *rock*^{wt} or *rock*$^{\Delta 547\text{-}923}$. From left to right, n = 7, 6, 19, 22 cuts. Red bars represent median. Comparisons were performed with the Kruskal-Wallis test. Images B-D were separately contrast adjusted to illustrate intracellular distribution of ROCK. Scale bars = 5 μm (B,C,E,F), 10 μm (D). See also Figure S1.

and the more dispersed apical localization of ROCK$^{\Delta 547\text{-}923}$ (Fig. 1C,D). In contrast to the *rock*^{2} mutant, which lacks apical myosin in the ventral furrow (Dawes-Hoang et al., 2005), both *rock*^{wt} and *rock*$^{\Delta 547\text{-}923}$ result in apical myosin, suggesting that the *in vivo* ROCK kinase activity of *rock*$^{\Delta 547\text{-}923}$ is normal (Fig. 1E). Moreover, the reduction in basal myosin in ventral cells occurred normally in both *rock*^{wt} and *rock*$^{\Delta 547\text{-}923}$ mutants, demonstrating that the *rock*$^{\Delta 547\text{-}923}$ mutant does not lead to inappropriate regulation of basal myosin (Fig. 1E). In surface views of ventral cells, myosin localization mirrored that of ROCK, such that in *rock*$^{\Delta 547\text{-}923}$, myosin localized across the apical surface instead of concentrating into a medioapically-centered network (Fig. 1F). Thus, the *rock*$^{\Delta 547\text{-}923}$ mutant appears to retain *in vivo* myosin-activating activity, but ROCK and myosin exhibit a more uniform distribution across the apical cortex. Consistent with this interpretation, a recent study showed that the *in vitro* kinase activity of a *rock* mutant similar to *rock*$^{\Delta 547\text{-}923}$ was identical to that of wild-type ROCK (Truebestein et al., 2015).

Despite exhibiting apical ROCK and myosin localization, the *rock*$^{\Delta 547\text{-}923}$ mutant failed to rescue ventral furrow formation in *rock*^{2} germline clones (Fig. 1D, Movie S1). The *rock*$^{\Delta 547\text{-}923}$ mutant did cause an initial flattening of the ventral domain, but failed to make a furrow. To determine whether the rock$^{\Delta 547\text{-}923}$ mutant promoted tissue-level tension, we performed laser cutting experiments in the ventral tissue of *rock*^{2} mutants expressing *rock*^{wt} or *rock*$^{\Delta 547\text{-}923}$. To determine recoil velocities, we tracked the displacement of fluorescent ROCK away from the laser cut. We found that both conditions resulted in similar initial recoil velocities, suggesting that both alleles generated epithelial tension (Fig. 1G,H; S1D,E). In wild-type embryos expressing fluorescently-tagged myosin, we measured recoil velocities before and after the

accumulation of a myosin network, and we found that *rock*^{wt} and *rock*$^{\Delta 547\text{-}923}$ generate more tension than the ventral epithelium prior to apical contractility onset, and slightly less than the wild-type myosin network condition (Fig. 1G,H). The ability of *rock*$^{\Delta 547\text{-}923}$ to rescue tension argues that the *in vivo* kinase activity of ROCK$^{\Delta 547\text{-}923}$ is not affected and that its furrow phenotype resulted from another property of the mutant protein. One possibility is that ROCK needs to be medioapically localized to efficiently contract cells

Diffuse apical ROCK kinase activity dominantly inhibits apical constriction

To further investigate the importance of proper ROCK localization, we expressed *rock*$^{\Delta 547\text{-}923}$ in the presence of endogenous *rock* (Fig. S1F). We found that expressing *rock*$^{\Delta 547\text{-}923}$, but not *rock*^{wt}, blocked apical constriction and tissue folding even in the presence of endogenous wild-type ROCK (Fig. 2A-C; Movie S2). If reduced kinase activity or lower expression of ROCK$^{\Delta 547\text{-}923}$ and thus, loss-of-function, were the reason for the failure of *rock*$^{\Delta 547\text{-}923}$ to promote tissue folding, expressing *rock*$^{\Delta 547\text{-}923}$ in the presence of endogenous *rock* would not be expected to cause a folding defect. Because ectopic *rock*^{wt} was expressed more strongly than *rock*$^{\Delta 547\text{-}923}$ and did not perturb apical constriction and folding, increased ROCK protein amount was not the reason for the *rock*$^{\Delta 547\text{-}923}$ tissue folding phenotype (Fig. S1F). The differences in expression levels indicate that ROCK$^{\Delta 547\text{-}923}$ is probably less stable than ROCK^{wt}.

To determine if the dominant negative effect of *rock*$^{\Delta 547\text{-}923}$ expression was the result of mislocalized kinase activity, we examined whether a kinase-dead mutation K(116)A suppressed the *rock*$^{\Delta 547\text{-}923}$ phenotype (Fig. 2A-C, Movie S2).

Figure 2

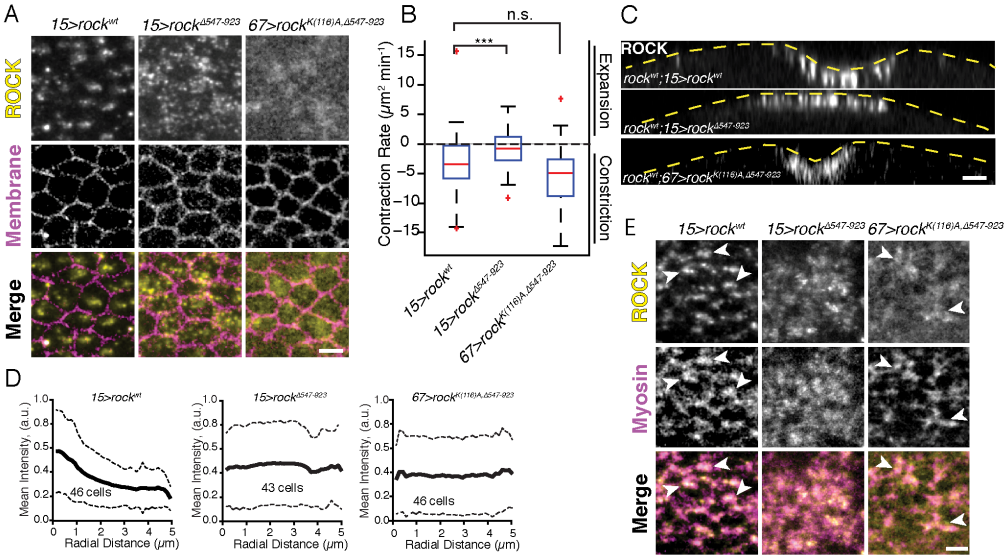

Figure 2. Diffuse ROCK dominantly inhibits apical constriction and tissue folding. (**A**) Apical surfaces of embryos expressing Venus::ROCK^{wt}, Venus::ROCK$^{\Delta 547\text{-}923}$, or Venus::ROCK$^{K(116)A,\ \Delta 547\text{-}923}$ transgenes in wild-type *rock* background. (**B**) Quantification of apical area contraction rate in embryos expressing *rock* variants from (A) with the maternal Gal4 drivers, *mat15* or *mat67*. For each condition, from left to right n = 90, 104, 122 cells and 2 embryos. Red line is median, box represents 25th-75th percentile, and whiskers represent ± 2.7 s.d.. Statistical comparisons were made with the Kruskal-Wallis test. (**C**) Cross-sections of live embryos with the same genotypes as (A). Dashed yellow line indicates the apical surface of the embryo. Embryos were aligned in time by onset of ROCK accumulation. (**D**) Quantification of normalized intensity distribution of Venus::ROCK^{wt}, Venus::ROCK$^{\Delta 547\text{-}923}$, and Venus::ROCK$^{K(116)A,\ \Delta 547\text{-}923}$ from cell centroid to the cell junction (radial distance). Solid lines represent mean, and dashed lines represent ± 1 s.d.. Each plot represents cells quantified from one representative embryo. (**E**) Apical myosin localization (RLC::mCherry) in *rock* mutants expressed in a wild-type background. ROCK and myosin colocalize in foci for *rock*^{wt} and *rock*$^{K(116)A,\ \Delta 547\text{-}923}$ (arrowheads). In A,C,E, images were separately contrast adjusted to illustrate intracellular distribution of ROCK, but not myosin. Scale bars = 5μm (A,C,E). See also Figure S1.

ROCK$^{K(116)A,\Delta 547\text{-}923}$ was expressed at a greater level than ROCK$^{\Delta 547\text{-}923}$ (Fig. S1F), and the K(116)A substitution suppressed the dominant negative ROCK$^{\Delta 547\text{-}923}$ phenotype, suggesting that *rock*$^{\Delta 547\text{-}923}$ inhibited contraction through incorrect kinase localization. By expressing the various *rock* alleles with labeled membranes, we were also able to quantify the radial distribution of ROCK fluorescence in each case, and found that whereas ROCK expressed via an endogenous promoter (Fig. S1G) and ectopic ROCK^{wt} are radially polarized around the cell geometric centroid, both ROCK$^{\Delta 547\text{-}923}$ and ROCK$^{K(116)A,\Delta 547\text{-}923}$ exhibited a flat distribution on the radial axis (Fig. 2D). Thus, the dominant effect of *rock*$^{\Delta 547\text{-}923}$ requires kinase activity and is associated with a flat

distribution of ROCK localization across the apical surface. We propose that inhibition of apical constriction and tissue folding upon ectopic *rock*$^{\Delta 547\text{-}923}$ expression is a result of ROCK kinase activity localized across the apical domain. Expressed in the wild-type *rock* background, *rock*$^{\Delta 547\text{-}923}$ also caused myosin to localize more diffusely across the apex, rather than in a polarized manner, as was observed with *rock*^{wt} overexpression (Fig. 2E). We found similar localization patterns for ROCK^{wt} and ROCK$^{\Delta 547\text{-}923}$ in the squamous epithelium of the amnioserosa (Fig. S1H), suggesting that medioapical ROCK activity and localization could play a role in concentrating myosin in the apical domain of other nonmuscle epithelial cells.

The apical actin cortex is polarized with junctional barbed ends and medial pointed ends

We next wanted to determine why a polarized distribution of ROCK and myosin was important for apical constriction. Because actin filament orientation influences contraction (Murrell et al., 2015; Reymann et al., 2012), we determined whether actin networks are also polarized in the apical cortex. Labeling actin networks with a protein that binds the sides of actin filaments does not detect polarity because the apical actin cortex forms a dense actin network. We therefore analyzed the localization of proteins that bind either the pointed or barbed ends of actin filaments. Surprisingly, we found that different end-binding proteins exhibited distinct localization patterns. Barbed end-binding proteins, such as adducin (Kuhlman et al., 1996; Xu et al., 2013) and capping protein α (Cap-α) (Amândio et al., 2014; Isenberg et al., 1980; Wear et al., 2003), were

Figure 3

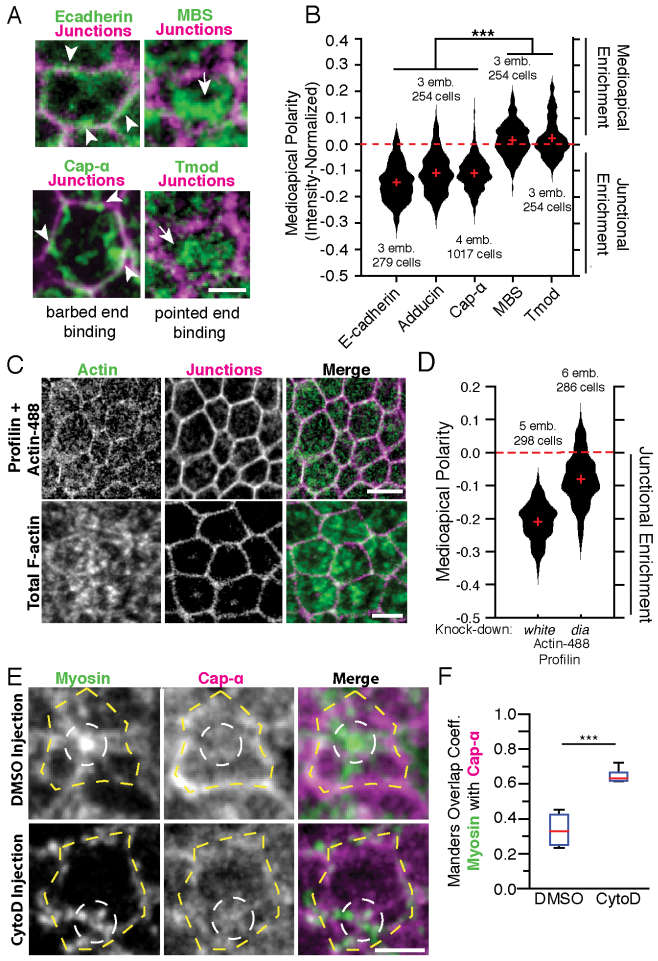

Figure 3. The apical actin cortex in ventral furrow cells is polarized with pointed ends enriched medioapically and barbed ends enriched at junctions. (A) Apical surfaces of fixed embryos stained with antibodies against indicated proteins or a Tmod::GFP transgenic line. Arrowheads indicate junctional staining of E-cadherin and Cap-α structures. Arrows indicate medioapical MBS and tmod. MBS and tmod staining were performed in the same embryos to determine relative localization. Junctions were identified using subapical E-cadherin or F-actin. (B) Medioapical polarity or mean medioapical intensity minus mean junctional intensity (positive value means medioapical enrichment). Red crosses represent medians, and the dotted red line indicates no enrichment in either the medioapical or junctional domains. Statistical comparisons were made with Kruskal-Wallis. emb. = number of embryos analyzed, and cell = total number of cells analyzed. (C) Apical surface of embryos that were fixed minutes after injection with mixture of actin-488 and profilin. Bottom images show total F-actin (Utr::GFP) for comparison. (D) Medioapical polarity in *white-RNAi* (control) and *dia-RNAi* knock-down embryos injected with actin-488 fluorescence. Red crosses indicate median, and emb. = number of embryos analyzed, and cell = total number of cells analyzed. Statistical comparison with Wilcoxon Rank Sum, distributions differ significantly, α = 0.01. (E) RLC::GFP embryos fixed and stained for Cap-α that were injected with DMSO or CytoD (250 µg/mL in DMSO). White dashed circles highlight myosin and yellow dashed lines highlight junctions. (F) Manders overlap coefficient for myosin colocalization with Cap-α after Costes thresholding. Each data point corresponds to the ventral domain of 1 embryo. n = 6 embryos for each condition. Red line is median, box represents 25th-75th percentile, and whiskers represent ± 2.7 s.d.. Statistical comparison with Wilcoxon Rank Sum. Scale bars = 2 µm (A,E), 5 µm (C). See also Figure S2.

enriched at the junctional domain (Fig. 3A). We quantified this enrichment by determining the difference in fluorescence intensity between medioapical and junctional domains and normalizing this value to total fluorescence intensity. Using this metric, junctional proteins, such as E-cadherin, exhibit a negative value. The intensity distribution of adducin and Cap-α also exhibited strong negative values, demonstrating junctional enrichment (Fig. 3B, S2A). In contrast, we found that the pointed end capping protein, tropomodulin (tmod), was localized in the center of the apical domain (Fowler et al., 1993; Weber et al., 1994), and MBS, a myosin binding protein that localizes to the center of the apical domain (Vasquez et al., 2014), colocalized with tmod (Fig. 3A). We quantified colocalization between tmod and MBS with the Manders Overlap Coefficient, which measures the amount of overlap between two signals in thresholded images, which were generated using the Costes method for rigorous and reproducible thresholding (Costes et al., 2004; Manders et al., 1993). We calculated a Manders Overlap Coefficient of 0.61 indicating that 61% of MBS signal colocalizes with tmod signal, and suggesting that pointed ends are enriched in the zone containing myosin at the apical center. The apical enrichment of tmod is specific to the ventral furrow, and adducin and Cap-α localize to junctions in cells adjacent to the ventral furrow region (Fig. S2B,C). Thus, specifically in contractile ventral furrow cells, barbed and pointed end-binding proteins exhibit distinct distributions, suggesting that actin networks have barbed ends enriched at apical junctions and pointed ends enriched in the apical center with myosin.

To independently determine the position of actin filament barbed ends we injected fluorescently-labeled actin monomers into embryos and fixed the embryos to

identify the position of actin incorporation (Symons and Mitchison, 1991; Tang and Brieher, 2012). To ensure actin incorporated only at barbed ends, we injected an equimolar mixture of actin-488 and purified recombinant *Drosophila* profilin (*chickadee*) (Fig. S2D,E). Proflin-actin heterodimers can only bind to actin filament barbed ends because profilin inhibits spontaneous nucleation and pointed end assembly (Pollard and Cooper, 1984; Schutt et al., 1993), and because profilin-actin is recruited to growing barbed-ends by the formin, Dia (Goode and Eck, 2007). We fixed embryos within minutes of injection, and measured the intensity distribution of actin fluorescence incorporation in the apical cortex of ventral furrow cells. Compared to the distribution of total F-actin, labeled barbed ends were enriched at junctions (Fig. 3C,D, S2F), with some observed cases of medioapical incorporation, which could be the result of *de novo* assembly by medioapical Dia (Mason et al., 2013). Actin incorporation at junctions was reduced by *dia* RNAi, suggesting that junctional actin assembly was partially dependent on Dia (Fig. 3D, S2G). This result was consistent with previous reports of actin assembly at epithelial cell junctions (Kobielak et al., 2003; Kovacs et al., 2002; Leerberg et al., 2014; Verma et al., 2012), and confirmed that the apical cortex of ventral furrow cells has a biased polarity with actin filament barbed ends enriched at junctions.

We next examined what happens to apical cortex organization upon treatment with Cytochalasin D (CytoD), which disrupts apical constriction and the attachment of the actin network to the junctions (Mason et al., 2013). Normally, myosin is enriched in the apical center with Cap-α enriched at the junctions. Injecting embryos with CytoD, but not DMSO, caused Cap-α to abnormally colocalize with myosin structures (Fig. 3E,F,

S2H). Quantifying colocalization with the Manders Overlap Coefficient, we found that there is low colocalization between myosin and Cap-α in DMSO control injections, indicating Cap-α and myosin localize to distinct structures. In contrast, after CytoD injection, the overlap coefficient was high, indicating that myosin and Cap-α colocalize strongly (Fig. 3F). The change in myosin/Cap-α colocalization indicated that CytoD inverts the cellular actin organization, which is also associated with a lack of force on cell junctions and a failure to apically constrict (Martin et al., 2010; Mason et al., 2013).

ROCK activity continuously sustains apical myosin and constricted cell shape

Given the central position of myosin and the cell-scale polarity of the apical actin cortex, we hypothesized that medioapical ROCK stabilizes myosin in the medioapical domain. In this position, myosin could sustain tension on polarized actin networks emanating from opposite sides of the cell and thus, stabilize cell shape. The requirement of ROCK to sustain a contraction is difficult to test, because *rock* mutants fail to initiate constriction (Dawes-Hoang et al., 2005). We therefore needed a method to precisely and temporally control ROCK activity, allowing us to inhibit ROCK after the onset of myosin contraction. We accomplished this by developing a technique to image an embryo under confocal microscopy while simultaneously injecting it with a drug or vehicle (Fig. S3A). We first determined that embryos can tolerate being pierced by a needle. Despite leaking some yolk around the embedded needle, embryos proceeded through early gastrulation (Movie S3). When we injected drugs during imaging, we inserted the needle immediately before injection, limiting the damage to the embryo.

Myosin accumulation and apical area reduction proceeded normally in pierced, uninjected embryos (Fig. S3B,C)

Figure 4

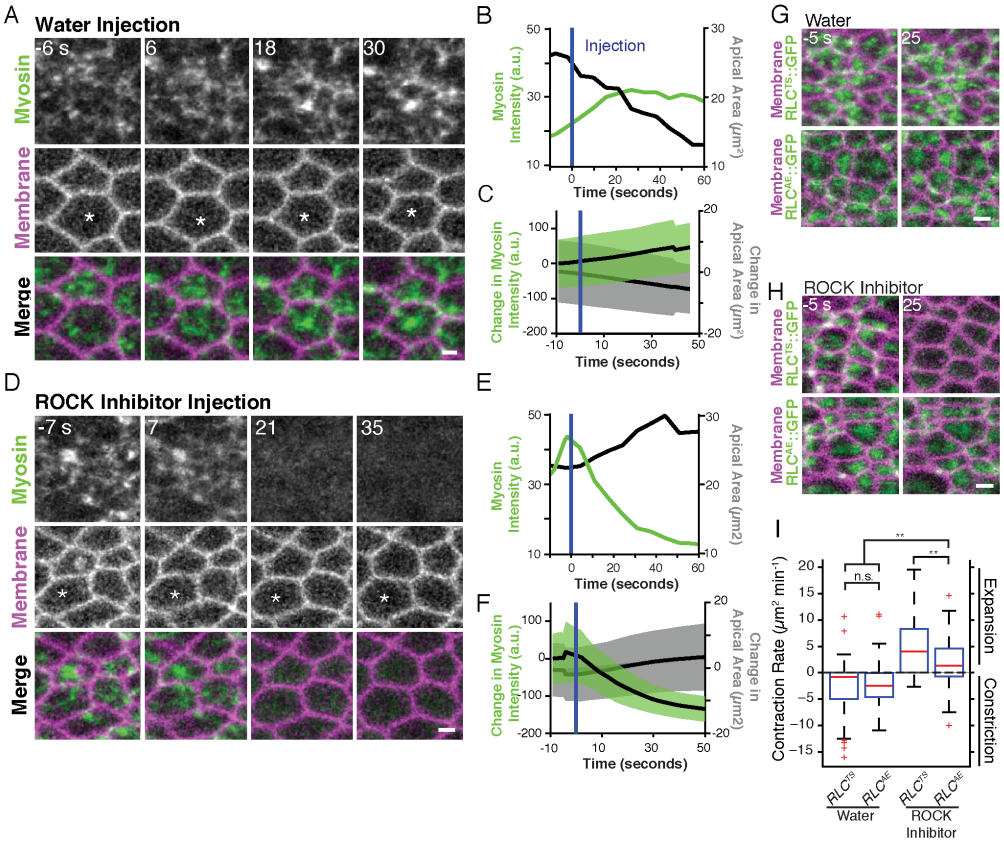

Figure 4. ROCK activity continuously stabilizes apical myosin and sustains apical constriction. (**A-C**) Apical surfaces of cells in a live embryo expressing RLC::GFP (myosin regulatory light chain) and Gap43::mCherry (membranes). Water injection occurs at t = 0. (**B**) Myosin fluorescence intensity and apical area for the cell marked in (asterisk, A). Blue vertical line indicates the injection time. (**C**) Mean myosin intensity and apical area (n=164 cells, 3 embryos). Dark lines are means, and shaded areas are ± 1 s.d. (**D-F**) Same as (A-C) but with ROCK inhibitor (Y-27632, 50 mM). In (F), mean myosin intensity and apical area (n = 259 cells, 3 embryos). (**G**) Water injection and (**H**) ROCK inhibitor injection into embryos expressing myosin RLC phosphomutants. RLC^{TS}::GFP and RLC^{AE}::GFP were expressed in a RLC hypomorphic mutant background (*sqh*^{1} germline clones). RLC^{TS} is the wild-type protein, and RLC^{AE} is a possible phosphomimetic mutant. (**I**) Quantification of contraction rate in embryos from the indicated conditions. Red line is median, box represents 25th-75th percentile, and whiskers represent ± 2.7 s.d.. From left to right n = 2 embryos and 188 cells, 3 embryos and 217 cells, 3 embryos and 208 cells, 3 embryos and 195 cells. Statistical comparison calculated with Kruskal-Wallis. Scale bars = 2 μm (A,D,G,H). See also Figure S3.

We used this technique to determine how apical myosin levels and apical area respond to acute inhibition of ROCK with the ROCK inhibitor Y-27632. Injecting embryos with water during ventral furrow formation did not impede either myosin

accumulation or apical constriction (Fig. 4A-C). In contrast, within 15 seconds of Y-27632 injection, apical myosin fluorescence faded dramatically, and the apical area relaxed (Fig. 4D-F; Movie S4). The rapid decrease in myosin intensity probably reflects the activity of myosin phosphatase, which opposes the myosin regulatory light chain phosphorylating activity of ROCK (Ito et al., 2004; Piekny and Mains, 2002; Totsukawa et al., 2004; Vasquez et al., 2014). ROCK phosphorylates many substrates, so to determine whether the ROCK inhibitor effect occurred through ROCK phosphorylation of myosin, we asked whether a mutant myosin regulatory light chain (RLC^{AE}) designed to mimic constitutive phosphorylation by ROCK would suppress the ROCK inhibitor effects (Vasquez et al., 2014; Winter et al., 2001). RLC^{AE} partially suppressed both the loss of myosin fluorescence and apical relaxation (Fig. 4G-I), showing that at least part of the ROCK inhibitor effect operates through myosin regulatory light chain phosphorylation. The incomplete suppression might result from improper myosin localization in this mutant (Vasquez et al., 2014), the mutant lacking normal motor activity (Kamisoyama et al., 1994), or a complementary role for ROCK phosphorylation of other substrates. These data show that in ventral furrow cells, ROCK activity is continuously required to maintain apical myosin during apical constriction and that cell shape change (i.e. apical constriction) is reversible by acute ROCK inhibition even after the initial actomyosin network contraction. This result is consistent with the model that polarized ROCK sustains tension across the apical surface by contributing to myosin localization in the center of the apex where it can bind and pull on polarized actin networks emanating from opposite sides of the cell.

Figure 5

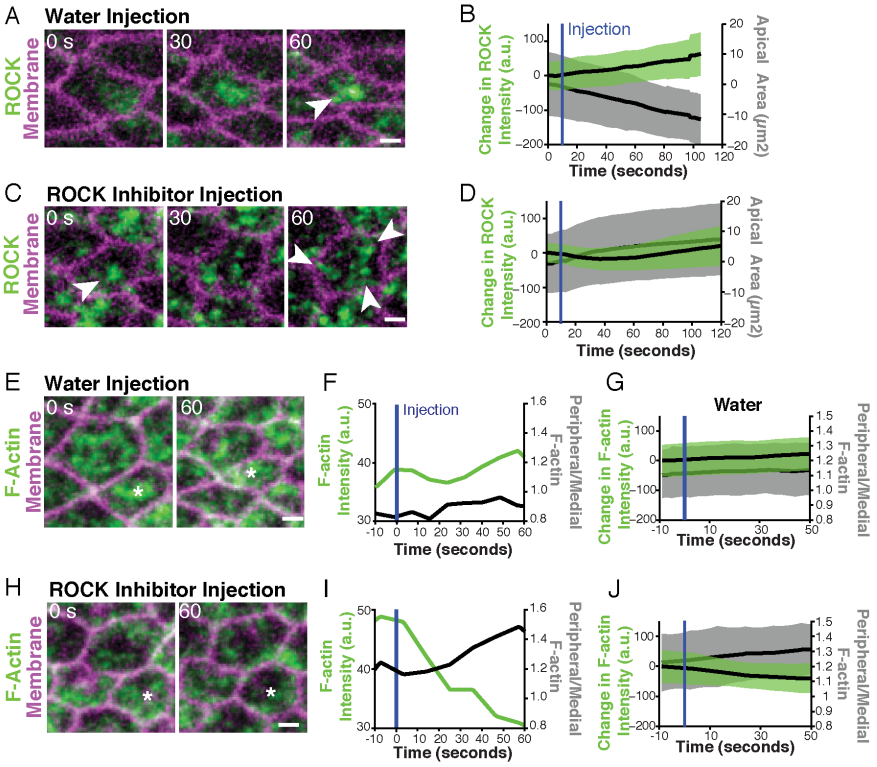

Figure 5. ROCK continuously maintains ROCK medioapical polarity and medioapical F-actin. (**A**) Surface views of ventral cells in embryo expressing GFP::ROCK and Gap43::mCherry injected with water after t = 0. (**B**) Dark lines represent means, and shaded areas indicate ± 1 s.d. (n = 90 cells, 2 embryos).. (**C,D**) Same as (A,B) but with ROCK inhibitor (Y-27632, 50 mM solution) injection (n = 177 cells, 3 embryos).) (**E**) Surface views of ventral furrow cells expressing Utr::GFP (F-actin), and Gap43::mCherry (membranes) injected with water after the t = 0 second frame. (**F**) Total F-actin intensity and ratio of mean peripheral (1 μm-thick outer shell) to mean medioapical F-actin in asterisk-marked cell from (E). Blue vertical line indicates the time of injection. (**G**) Mean F-actin intensity and the ratio of peripheral F-actin intensity to medioapical intensity before and after injection (n = 240 cells, 3 embryos). Dark lines represent means, and shaded areas indicate ± 1 s.d. (**H-J**) Same as (E-G) but with ROCK inhibitor injection. ROCK inhibitor acutely disrupts medioapical F-actin (asterisk, H). In (J), n = 150 cells, 2 embryos. Scale bars = 2 μm (A,C,E,H). See also Figures S3 and S4.

ROCK localization requires continuous ROCK activity and Dia

Because ROCK polarity is a central feature of establishing this efficient contractile organization, we next investigated what is responsible for positioning ROCK in the center of the apical cortex. While we speculate that RhoA is important for this process, it is not clear how active RhoA would localize to the middle of the cell apex. Importantly, we found that within a minute of ROCK inhibition, the radial organization of ROCK was disrupted; rather than being polarized, ROCK became distributed into many

Figure 6

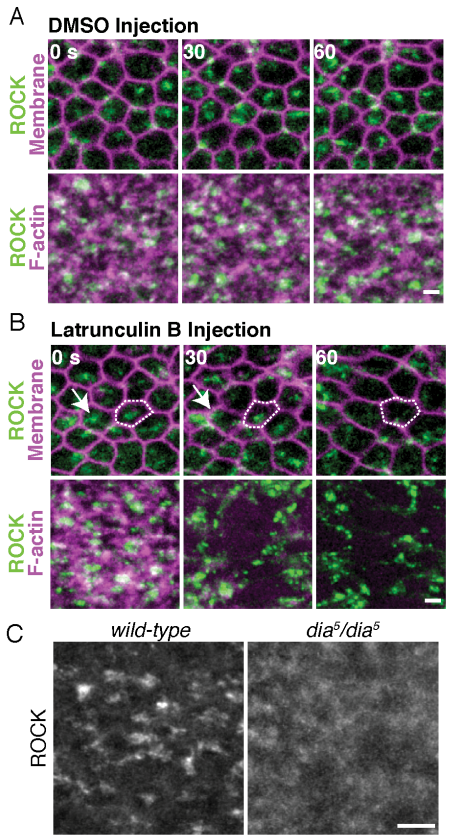

Figure 6. ROCK localization to medioapical foci requires the actin cytoskeleton and Dia. (**A**) Apical views of ventral furrow cells in embryos expressing ubi-GFP::ROCK, Gap43::mCherry (Membrane) or GFP::ROCK, Utr::mCherry (F-actin) and injected with DMSO after 0 sec time point. (**B**) Same as (A) but with Latrunculin B injection. Disrupted ROCK polarity (white outline and arrow). (**C**) Apical ROCK in wild-type and maternal *dia*^{5} mutant ventral cells. Scale bars = 2 μm (A,B), 5 μm (C). See also Figure S5

small puncta spread across the entire apical surface, of which some emerged from the original cluster, and others appeared after inhibition (Fig. 5A-D; Movie S5). On the same time scale, ROCK inhibition caused F-actin networks to redistribute to the apical periphery, and decrease in intensity (Fig. 5E-J). ROCK inhibition also affected E-cadherin localization, causing it to spread across the apical surface but remain apical (Fig. S4A-F). ROCK inhibition did not affect the apical-basal localization of Par3, showing that ROCK regulates the apical cortex, but probably not through Par3 or apical-basal polarity (Fig. S4G). ROCK activity therefore continuously stabilizes the

medioapical ROCK polarity, the medioapical F-actin cytoskeleton, and junctional E-cadherin.

Because ROCK affects the actin cytoskeleton (Fig. 5H) and because the apical actin cortex exhibits a polarity, we tested whether actin was important for ROCK localization. Depolymerizing F-actin with injected Latrunculin B, a G-actin sequestering toxin, caused ROCK foci to disintegrate or migrate to cell junctions (Fig. 6A,B). This effect was associated with the loss of the F-actin cytoskeleton, suggesting that ROCK might be physically linked to F-actin (Fig. 6A,B; lower panels). In addition, *dia*, which is required for actin cortex polarity (Fig. 3D) and ventral furrow formation (Homem and Peifer, 2008), was also required for ROCK medioapical focus formation. Hypomorphic dia^{5} mutants failed to polarize ROCK in the apical domain (Fig. 6C), despite ROCK being expressed at a similar level as in wild-type controls (Fig. S5A). These experiments show that ROCK localization depends on its own activity and the actin cytoskeleton, especially *dia*, and most probably RhoA as well.

Discussion

Here, we demonstrated that the apical actomyosin cortex of constricting ventral furrow cells is polarized, with barbed ends enriched at the periphery and pointed ends enriched in the apical center. We demonstrated this actin polarity in two independent ways: (1) Two barbed end binding proteins are enriched at the junctions, whereas the pointed end binding protein tropomodulin is enriched in the apical center; (2) Incorporation of actin onto actin filament barbed ends is biased to junctions. Interestingly, we also found that a ROCK mutant that localizes apically but is dispersed diffusely across the apex does not effectively constrict cells. This suggests that

enrichment of myosin near the center of the apical domain is important for constriction. Finally, the maintenance of apical myosin and cell shape depends on the continuous activity of ROCK, suggesting a model in which myosin in the center of the cell apex bridges antiparallel actin networks emanating from opposite sides of the cell to sustain and transmit force across the cell apex (Fig. 7A).

Figure 7

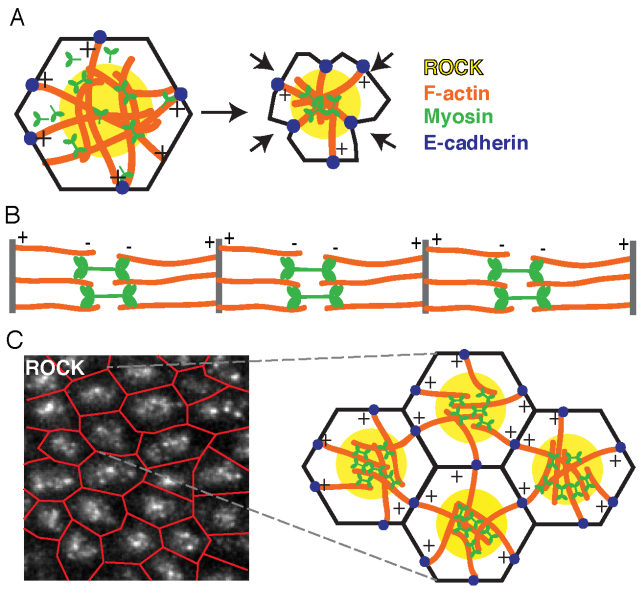

Figure 7. Model of apical constriction mechanism in ventral furrow cells. (**A**) Illustration of actin filament polarity and ROCK myosin localization during apical constriction. We term this organization a "radial sarcomere". (**B**) Illustration of muscle fiber (or myofibril). (**C**) Illustration of ventral furrow tissue, where contractile units/cells are linked at the junctions (red lines, ROCK image) and operate together to contract and deform the epithelium.

Similarities and Differences with Muscle Sarcomeres

The cortex of ventral furrow cells resembles a sarcomere in two ways: (1) actin filaments are arranged with barbed ends at the edge of the contractile unit and pointed ends in the center, and (2) myosin is localized to the center of the contractile unit where it can bridge and contract actin filaments (Fig. 7A). These results were surprising given the prevailing view that some nonmuscle cells contract through global activation of myosin across a mixed-polarity actin cytoskeleton (Murrell et al., 2015). On the

spectrum of actin network order ranging from isotropic/mixed-polarity to muscle sarcomere order, the contractile actomyosin structure in ventral furrow cells is more like a muscle sarcomere than previously appreciated. One reason apically constricting epithelial cells might use sarcomere-like actomyosin to contract is that the contractile network must attach to and sustain tension on intercellular junctions to prevent relaxation of cell shape changes, just as muscle myosin pulls on actin filaments attached to sarcomere boundaries to contract the sarcomere. As in a muscle sarcomere, centrally activated myosin in epithelial cells is positioned, with its barbed end-directed motor activity, to pull on both sides of the cell, and to bridge contractile forces across the apical domain; indeed, when mechanical coupling to one side fails, the central myosin travels away from the center, which suggests that myosin indeed bridges actin networks from opposite sides of a cell (Jodoin et al., 2015). *In vitro* models of actomyosin contractility lack the boundary condition of a sarcomere Z-band or epithelial cell junction, limiting comparisons of *in vitro* and *in vivo* network organization. However, *in vitro* actomyosin networks contract in a manner that leads to barbed end accumulation at the center of contracted actomyosin foci (Köster et al., 2016). We were able to obtain this inverted, barbed ends-in, orientation of *in vitro* actomyosin gels by slowing actin polymerization and decoupling the actomyosin network from the junctions with cytochalasin D. In this case the actomyosin network contracts, but without pulling on the cell junctions, and apical constriction does not happen (Mason et al., 2013). This suggests that the proper orientation of actin filaments is necessary for the transmission of force from the contracting network to the peripheral junctions, and that without this coupling and proper actin filament orientation, contraction of the network proceeds like

an *in vitro* actomyosin network, and without pulling on the apical junctions to contract the apical area.

In addition to differences in the degree of actin filament order, we note several contrasts between muscle sarcomeres and the organization of the apical actin cortex of ventral furrow cells. First, muscle sarcomeres are thought to be stable structures, although there is some evidence that thin filament turnover affects sarcomere length (Bai et al., 2007; Littlefield et al., 2001). In contrast, the actomyosin structure in ventral furrow epithelial cells is highly dynamic, appearing and disappearing over the course of minutes, with myosin, ROCK, and actin pulsing (Martin et al., 2009; Mason et al., 2013; Vasquez et al., 2014) and remodeling (Jodoin et al., 2015). Perhaps related to this dynamic behavior, actin cytoskeletal polarity and medioapical myosin localization are less pronounced in the apical cortex of ventral furrow cells, with cytoskeletal polarity markers showing an enrichment, rather than total exclusion from complementary domains, and with myosin structures sometimes projecting to the cell periphery. We speculate that the requirement for medioapical ROCK may reflect a need for rapid assembly of a contractile structure, and to maintain contractile forces during a transient and dynamic contractile process. It may also reflect the ability of ventral furrow epithelial cells to contract ~90% of their apical area (Martin et al., 2009), compared to sarcomeres which contract only ~30% of their length (Huxley and Niedergerke, 1954). In slower nonmuscle contractile processes, order may be capable of emerging spontaneously through self-organization. We note, however, that ROCK localization has not been determined in smooth muscle where ROCK is known to play a role in calcium

sensitization and force maintenance (Lan et al., 2015; Uehata et al., 1997). Our data suggests that ROCK localization could support its function in other contexts.

A second distinction between ventral furrow cells and muscle cells is that muscle myofibrils are comprised of one-dimensional arrays of sarcomere contractile units (Fig. 7B), whereas actomyosin in the ventral furrow is organized in a two-dimensional array. One could therefore think of the ventral furrow as a collection of "radial sarcomeres" linked together in a 2-dimensional grid to contract the epithelial sheet (Fig.7C). We speculate that the sarcomere-like organization in a two-dimensional contractile tissue is required to allow tension to reduce the apical area of cells and fold the sheet, possibly by reducing compressional and bending stiffness of the apical domain. Interestingly, $ROCK^{wt}$ and $ROCK^{\Delta 547\text{-}923}$ produce comparable levels of epithelial tension as inferred by tissue recoil following laser cutting, but $ROCK^{\Delta 547\text{-}923}$ does not invaginate, which could reflect increased stiffness in the epithelium. In addition, the $ROCK^{\Delta 547\text{-}923}$ mutant flattens the tissue, suggesting that diffuse apical myosin is able to generate tension that flattens the tissue, but is unable to efficiently contract and fold the tissue. This interpretation agrees with models of ventral furrow formation in which contraction of the apical area propagates changes to the rest of the cell, leading to the acquisition of a wedge-shaped cells and tissue folding (He et al., 2014; Polyakov et al., 2014).

ROCK pattern formation

An important outstanding question is how ROCK becomes polarized in the middle of the apical surface, which is a basis for the formation of this polygonal grid of contractile units. Here, we provide evidence that the coiled-coil domain of ROCK, ROCK

kinase activity, the actin cytoskeleton, and Dia are all required for ROCK focus formation. Because Dia is required for robust apical actin network polarity, it is possible that the polarity of the actin network is important to localize ROCK to the apical center. ROCK could be important to localize itself through myosin-induced flows, as suggested in earlier work (Munjal et al., 2015). Future work is needed to establish the link between actin and ROCK polarization and the importance of the coiled-coil domain. Interestingly, ROCK has been shown to interact with stress fibers in other systems (Chen et al., 2002; Katoh et al., 2001; Newell-Litwa et al., 2015), which resemble the fibrous actomyosin cytoskeleton in ventral furrow cells and may represent a conserved role for ROCK localization to polarized actin structures.

Experimental Procedures

Image Processing and Quantitative Analyses

All images were processed using Fiji (http://fiji.sc/wiki/index.php/Fiji) and MATLAB (The MathWorks). Displayed images were processed with a Gaussian filter (σ = 0.7). All still and movie frames are Z-projections through 2–5 μm of apical depth. For myosin, projections are maximum intensity, and for all other fluorescent proteins, projections are summed intensity. To display differences in ROCK distribution, image display parameters were sometimes (Fig. 1B,C,D; 2A,C,E; Movies S1, S2, S5) optimized for each image to effectively display the distribution of ROCK fluorescence intensity across the apical area. Membrane images are single sections at the bottom of the apical projection. For analyzing myosin intensity, images were background subtracted by determining the mean pixel intensity in a region >5 μm below the apical surface, and subtracting that value from all pixels in the maximum intensity projection. In Figures, asterisks indicate significance threshold α, i.e. * = significant at α = 0.01, ** = significant at α = 0.001, etc.

Expressions for junctional and medioapical intensity were also used for quantifying medioapical polarity, ρ, of actin polarity markers and fluorescent actin incorporation (Fig. 3B,D; S2C). In this case, the peripheral domain was defined as the 0.4 μm outermost shell of the cell apex to reflect junctional rather than peripheral localization. We calculated ρ as the difference between mean medioapical intensity and mean junctional intensity, normalized by the mean total intensity (Vasquez et al., 2014):

$$\rho = \frac{\overline{I}_m - \overline{I_p}}{\overline{I}_t}$$

In Fig. 3B and Fig. 3D, the medioapical polarity was calculated as above with normalization by mean pixel intensity in the cell in order to ignore differences in the measurement due to overall intensity of the probe. This was important because fluorescence from different reagents and different embryos was being compared, and different reagents and embryos had different mean fluorescent intensity profiles. Radial intensity profiles (Fig. 2D; S1G; S2F) were calculated by representing a cell apical area in polar coordinates, where the origin of the coordinate plot is the cell geometric centroid, and each pixel occupies a coordinate position defined by its radial distance from the origin, r, and its angular position, *Θ.* We generated the radial intensity profile by determining the mean pixel intensity as a function *r,* where Θ_r is the number of pixels at radius r:

$$\langle I(r) \rangle = \frac{\sum_{k=0}^{\theta_r} I_k(r)}{\theta_r}$$

To analyze embryos injected with fluorescently labeled actin (Fig. 3D), we generated an image mask to select the surface of the embryo for further analysis. In x-z cross-sections of the image volume, we applied a Sobel edge detection algorithm to the summed signal of all fluorescent channels to find the surface of the embryo. We dilated this edge ~2 μm into the surface of the tissue. Next, viewing the masked pixels in the x-y plane, we closed the image to eliminate holes in the mask. We projected the brightest 2 pixels in each z dimension from the mask for each channel of the underlying image, and projected the sum of these pixels onto an x-y plane. This approach allowed us to identify the apical 2 μm of tissue across the imaged embryo, regardless of position in z. Code for surface masking is available here:

https://github.com/jcoravos/surface_embryo. For additional information on quantitative image analayses, see Supplemental Experimental Procedures.

Imaging

All imaging was performed with a Zeiss LSM 710 confocal microscope. A 40x/1.2 Apochromat water objective was used for live imaging, and a 63x/1.4 Apochromat was used for fixed imaging (Carl Zeiss). An argon ion, 561nm diode, 594nm HeNe, and 633nm HeNe lasers were used for fluorophore excitation. Pinhole settings ranged from 1-2 airy units. We used the following approximate band pass filters, adjusting to minimize channel bleed through: For Venus: 519-578 nm, for GFP and AF-488: 488-558 nm, for Cherry and AF-568: 580-696 nm, and for AF-647 675-700 nm.

Embryo Injection

Embryos were injected with dsRNA in water, or profilin:actin-488 (10 μM each) in G-Buffer (2mM Tris pH 8, 0.2 mM ATP, 0.5 mM DTT, 0.1 mM $CaCl_2$, 1 mM $NaN_{3)}$, or Y-27632 (50 mM) in water, Latrunculin B (5 mg/mL) in DMSO, or Cytochalasin D (0.25 mg/mL) in DMSO (Enzo Life Sciences, Farmingdale, NY). For all injections, embryos were first dechorionated in 50% bleach and washed with water, and mounted with embryo glue, and desiccated for 5 minutes with Drierite (Drierite Company). Before injection, halocarbon 700 and 27 oil (3:1 ratio) was layered over embryos.

To inject profilin:actin and label actin filament barbed ends (Fig. 3C,D; S2D-G), we purified *Drosophila* profilin (*chickadee*) (see Supplemental Experimental Procedures), and verified its activity by determining its effect on actin filament assembly

in a pyrene-actin assembly assay. We centrifuged fluorophore-labeled actin to pellet and discard actin filaments, and mixed active profilin with fluorophore-labeled actin monomers to a final concentration of 10 µM each in G buffer (5 mM Tris-HCl pH8, 0.2 mM ATP, 0.5 mM DTT, 0.2 mM $CaCl_2$, and 1 mM NaN_3). We let the mixture stand for 10 minutes at 4°C, and proceeded to inject profilin actin as described below. Embryos injected with profilin:actin-488 were incubated for <1 minute to allow incorporation, but to prevent saturation of the apical actin meshwork with fluorescent actin, and then removed from the embryo glue in a petri dish with heptane and fixed in PFA.

For simultaneous imaging and injection of Y-27632 or Latrunculin B, embryos were mounted on a No. 1 coverslip ventral side down over a window scraped in the embryo glue with a razor blade. The window in the embryo glue allows the embryo to be image with an inverted objective, while still holding the embryo in place as it is pierced with the needle and injected during imaging.

Laser Cutting and Recoil Analysis

Laser ablations (Fig. 1G,H; S1D,E) were performed using a 2-photon Mai-Tai laser set to 800 nm on a LSM710 confocal microscope (Zeiss) through a 40x/1.2 objective. Laser power set between 25% to produce sufficient power to ablate, rather than bleach, the tissue, but not so much as to boil the embryo. Ablations were performed in a 1-pixel wide and 50-pixel long line (0.08nm x 4µm) parallel to the dorso-ventral axis of the embryo. Recoil distance was measured in FIJI by manually measuring the distance across the opening in the frame before ablation and every time point after ablation (time resolution was 320 ms per frame). In *rock* mutant embryos,

fluorescence from Venus::ROCK was used to determine the opening in the tissue. "Pre-network myosin" and "network myosin" ablations were performed in *y w sqh^{AX3};P{w^{+} sqh::GFP}42* embryos, using fluorescence from Sqh::GFP to track recoil distance. Pre-network myosin ablations were performed at the onset of myosin accumulation, but before the appearance of an intercellular connected myosin network. Ablations performed after this network appeared were classified as network myosin ablations.

We determined initial recoil velocity by calculating the displacement of the tissue over the first 320ms time step and dividing by the elapsed time. Recoil distance was plotted by smoothing displacement curves from individual recoil experiments with a kernel of 3 time steps and a loess filter. Recoil distance fitting was performed with a non-linear regression fit to a Kelvin-Voigt model:

$$\epsilon(t) = \frac{\sigma_0}{E}(1 - exp^{(-t\frac{E}{\eta})})$$

where ε is strain, σ_0 is initial stress, E is the elastic modulus, and η is the viscous drag coefficient. We report the fitted value of σ_0/E for each curve in Supplemental Fig. 1E. Fitting parameters are reported in Fig. S1.

Antibodies

Antibody	Use	Concentration	Source
R anti-Zipper	MH & FA	1:500	Wieschaus Lab, Princeton University, Princeton, NJ
M anti-Neurotactin	MH	1:100	DSHB, contributed by C. Goodman
R anti-Dia	WB	1:5000	Steve Wasserman, UCSD, San Diego, CA
M anti-GFP	WB	1:1000	Roche
M anti-tubulin	WB	1:5000	Sigma
M anti-Rho1 (conc.)	FA	1:500	DSHB
R anti-MBS	FA	1:500	Tan Laboratory, University of Missouri, Columbia, MO
M anti-adducin	FA	1:500	DSHB
R anti-Capα	FA	1:200	Janody Lab, Instituto Gulbenkain de Ciencia, Oeiras, Portugal

R = rabbit, M = mouse
MH = methanol/heat-fixation, FA = paraformaldehyde fixation, WB = western blot
DSHB = Developmental Studies Hybridoma Bank, University of Iowa

Fly Stocks

Genotype	Source
OreR	2
y,w,rock^{2} FRT^{19A}/FM7	2
P{UASp-Venus::rock$^{1-1391}$}attp40 (alias: *rock^{wt}*)	3
P{UASp-Venus::rock$^{413-1391}$}attp40	3
P{UASp-Venus::rock$^{700-1391}$}attp40	3
P{UASp-Venus::rock$^{900-1391}$}attp40	3
P{UASp-Venus::rock$^{\Delta 835-937}$}attp40	3
P{UASp-Venus::rock$^{\Delta 547-923}$}attp40	3
P{UASp-Venus::rock$^{K\ (116)A,\ \Delta 547-923}$}attp40	3
y,w,rock^{2} FRT^{19A}/FM7; P{UASp-Venus::rock$^{1-1391}$}attp40	1
y,w,rock^{2} FRT^{19A}/FM7; P{UASp-Venus::rock$^{\Delta 547-923}$}attp40	1
y w rock^{2} FRT^{19A}/FM7; P{UASp-Venus::rock$^{K\ (116)A,\ \Delta 547-923}$}attp40	1
ovo^{D},hsFLP,FRT^{101}/C (1)Dx/FM7	3
ovo^{D},hsFLP,FRT^{101}/ C (1)Dx/FM7; P{mat-Tub-Gal4}15	1
y,w ; ; P{mat-Tub-Gal4}15 (alias: *mat15*)	4
w ; P{mat-Tub-Gal4}67 (alias: *mat67*)	4
sqh-sqh::mCherry^{M9}, P{mat-Tub-Gal4}15/TM3	1
P{sqh-gap43::mCherry-7}, P{mat-Tub-Gal4}15/TM3	1
sqh-sqh::mCherry^{B1}, P{mat-Tub-Gal4}67/CyO	1
P{mat-Tub-Gal4}67;P{sqh-gap43::mCherry}attp2/Tm3	1
y w sqh^{AX3};P{w^{+} sqh::GFP}42	5
w; Sp/Cyo; P{sqh-gap43::mCherry} (attP2), P{w+ sqh-sqh::GFP}/TM3	1
ovo^{D1} FRT^{101}/Y; hsFLP-38/hsFLP-38	2
sqh^{1} FRT^{101}/FM7; P{w^{+} sqh-sqh^{TS}::GFP}attP1 P{w^{+} sqh-gap43::mCherry}attP40/CyO	6
sqh^{1} FRT^{101}/FM7; P{w^{+} sqh-sqh^{AE}::GFP}attP1 P{w^{+} sqh-gap43::mCherry}attP40/CyO	6
w;; sqh-utr::GFP/TM3	7
P{ubi-GFP::rock}/TM3	8
P{sqh-gap43::mCherry-7}/Tm3	1
sqh-utr::mCherry/ (CyO)	7
hsFLP;Sco/CyO	2
ovo^{D},FRT^{40A}/CyO	2
dia^{5},FRT^{40A}/Cyo;P{ubi-GFP::rock}/Tm3	1,2
sqh-sqh::mCherry^{a11}/CyO	1
w; P{mat-Tub-Gal4}67, UAS-bazGFP^{r1}/CyO	9
P{GawB}c381	2
yw;Mi{PT-GFSTF.0}tmod[MI07502-GFSTF.0]TM6C,Sb,Tb	2
w; P{ubi-p63E-shg.GFP}	10
y,sc,v; P{TRiP.HMS00308}attP2 (alias*: sh-dia*)	2
y,v;P{TRiP.HMS00017}attP2 (alias: *sh-white*)	2
rock^{2};P{rock-GFP::ROCK} (BAC)	11

Sources

1. This study
2. Bloomington Drosophila Stock Center, Indiana University
3. Gifts from J. Zallen and S. Simões
4. Gifts from D. St. Johnston
5. Gift from A. Royou
6. Vasquez et al., 2014
7. Gift from T. Lecuit
8 Gift from Y. Bellaïche
9. Gifts from Y. Wang and E. Wieschaus
10. Kyoto Drosophila Genomics and Genetic Resources
11. Gift from V. Hatini, prior to publication

Fly Genetics

To analyze *rock*^{wt} or *rock*$^{\Delta 547\text{-}923}$ expression in maternal *rock*^{2} null-mutant background (Fig. 1C-H; S1C-E; Movie S1), we imaged the embryos laid by germline-null mothers (Chou et al., 1993) generated by heat-shocking larvae (2 hours at 37°C, 3 days) with the following genotypes: *y,w,rock*^{2} *FRT*^{19A}*/ovo*^{D}*, hsFLP,FRT*^{19A}*; P{UASp-Venus:: rock*^{xx}*}attp40/ P{mat-Tub-Gal4}15* (where xx is wild-type or Δ547-923). RLC phosphomimetic alleles (Fig. 4G-I) were also examined in *sqh*^{1} germline clones of heat-shocked larvae with the following genotypes *sqh*^{1} *FRT*^{101}*/ ovo*^{D}*,hsFLP,FRT*^{101}*; P{w*$^{+}$ *sqh-sqh*^{xx}*::GFP}attP1 P{w*$^{+}$ *sqh-gap43::mCherry}attP40/+*. *rock* expression and localization in *dia*^{5} germline clones (Fig. 6C; S5A) was obtained by heat-shocking larvae with the genotype: *hsFLP*/+; *dia*^{5}*,FRT*^{40A}*/ovo*^{D}*,FRT*^{40A}*;P{ubi-GFP::rock}*/+, determining ROCK expression level with western, and localization with confocal imaging. We also visualized ectopic *rock* transgene expression in wild-type *rock* background (Fig. 1B; 2A-E; S1A,B,F, Movie S2) by imaging the embryos laid by mothers of the following genotypes: *P{UASp-Venus:: rock*^{xx}*}attp40/+; P{sqh-gap43::mCherry-7}, P{mat-Tub-Gal4}15/+ P{UASp-Venus:: rock*^{xx}*}attp40/+; sqh-sqh::mCherry*^{M9}*, P{mat-Tub-Gal4}15/+ P{UASp-Venus:: rock*^{xx}*}attp40/sqh-sqh::mCherry*^{B1}*,P{mat-Tub-Gal4}67 P{UASp-Venus::*

rock^{xx}}attp40/P{mat-Tub-Gal4}67;P{sqh-gap43::mCherry}attp2 (where xx is 1-1391, Δ547-923, or K (116)A,Δ547-923). We drove ectopic expression of ROCK mutants in the amnioserosa (Fig. S1H) with the following zygotic genotypes: *P{UASp-Venus:: rock^{xx}}attp40/ P{ubi-p63E-shg.GFP};; P{GawB}c381/*+ (where xx is 1-1391 or Δ547-923).

To visualize the effects of ROCK inhibitor (Fig. 4,5;S4; Movies S4 and S5), Latrunculin B (Fig. 6A,B), or Cytochalasin D (Fig. 3E;S2H) on myosin, ROCK, actin, Par3, and E-cadherin localization, we injected inhibitors into the following genotypes: *sqh^{AX3};P{w^{+} sqh::GFP}42/+; P{sqh-gap43::mCherry} (attP2), P{w+ sqh-sqh::GFP}/*+. *sqh-utr::GFP/P{sqh-gap43::mCherry-7}. P{ubi-GFP::rock}/P{sqh-gap43::mCherry-7}. P{mat-Tub-Gal4}67, UAS-bazGFP^{r1}/sqh-sqh::mCherry^{a11}* (Fig. S4C). *sqh-sqh::mCherry^{a11}/ P{ubi-p63E-shg.GFP}*.

To deplete *white* or *dia* (Fig. 3D;S2G), we drove expression of a short-hairpin against *dia* or *white* in the following genotypes *P{mat-Tub-Gal4}67/P{TRiP.HMS00308}attP2; P{mat-Tub-Gal4}15/*+ or *P{mat-Tub-Gal4}67/P{TRiP.HMS00017}attP2; P{mat-Tub-Gal4}15/*+. Tropomodulin was visualized (Fig. 3A,B;S2A-C) by formaldehyde fixing the fluorescent protein trap line *yw;Mi{PT-GFSTF.0}tmod[MI07502-GFSTF.0]/TM6C,Sb,Tb* and visualizing endogenous GFP fluorescence.

Immunostaining and Western Blotting

Antibodies and corresponding concentrations used in this paper are listed in Supplementary Experimental Procedures (Antibodies). For fixed imaging, all embryos

were first dechorionated in 50% bleach and then either methanol/heat fixed or, to preserve actin cytoskeletal structure, formaldehyde (FA) fixed. Methanol/heat fixed embryos appear in Fig. 1E, and FA-fixed embryos appear in Fig. 1F; 3A,C,E; S2A,B,G,H). For methanol/heat fixations, embryos were placed in boiling Triton salt solution (0.03% Triton X-100 and 0.4% NaCl in water), cooled on ice, and then devitellinized by vortexing in a 1:1 heptane/methanol solution. FA-fixed embryos were fixed in a 1:1 solution of 8% FA in 0.1 M phosphate buffer, pH 7.4, and heptane for 25 min, transferred to a Petri dish, and manually devitellinized using a syringe needle. Both FA and methanol/heat-fixed embryos were blocked overnight in 10% BSA in PBS-Tw (PBS with 0.1% Tween), and then immunostained with primary antibodies, suspended in 5% BSA in PBS-Tw (PBS with 0.1% Tween) for 2 hours at room temperature. This was followed by 3 10 minute washes in PBS-Tw, and then by incubation with secondary Alexa-fluor conjugated antibodies reactive to the appropriate species. After a final 3 10 minute washes in PBS-Tw, both FA and methanol/heat-fixed embryos were mounted in AquaPolymount (Polysciences, Inc. Warrington, PA). For cross-sections (Fig. 1D), Methanol/heat-fixed and stained embryos were post-fixed in 4% FA in PBS-Tw for 30 minutes, washed three times in PBS-Tw, and equilibrated in 50% glycerol in PBS. Embryos were sectioned with an X-acto blade in 50% glycerol in PBS, and transferred to AquaPolymount for mounting.

Western blotting (Fig. S1C,F;S5A) was performed by picking 2- to 3-hour old embryos and grinding in sample buffer (1 embryo/2µL 1X sample buffer). Sample were then boiled for 5 minutes, centrifuged at 15000xg for 10 minutes, and stored at -20°C. Samples were run on 8-10% SDS-PAGE gels. Protein was transferred to 0.45-µm

nitrocellulose membrane (Bio-Rad Laboratories) and detected using indicated primary antibodies and horseradish peroxidase–labeled secondary antibodies (Jackson ImmunoResearch Laboratories, Inc.).

RNAi

dsRNA was synthesized as previously described (Simoes et al., 2014). Templates to produce dsRNA against both *Shrm isoforms, ShrmA*, *ShrmB*, and a non-expressed gene (*FLP*, used as control) were made by PCR of genomic DNA preps from flies carrying *hsFLP*. The following primers, including 5' T7 promoter sequences for dsRNA synthesis by T7 RNA polymerase, were used to generate the PCR templates: for *Shrm isoforms A and B,*
TAATACGACTCACTATAGGGAGACCACGCCTCATACTTGCCGCGTCAGAG,
TAATACGACTCACTATAGGGAGACCACCTCTGGCTGCTTGTCGTGCACATC,
TAATACGACTCACTATAGGGAGACCACGAGGAACTGCAGCTGATGCAGCGC,
TAATACGACTCACTATAGGGAGACCACCGCATCGCTGAGGGAGCTAAGCTG, and for *FLP*, TAATACGACTCACTATAGGGAGACCACCAGCAATCAAGAGAGCCACATTC, and TAATACGACTCACTATAGGGAGACCACTCCCACAACATTAGTCAACTCCG. dsRNA was synthesized from PCR amplified templates using MEGAscript T7 (Ambion). To visualize the effect of Shroom knock-down on ROCK focus formation (Fig. S1A,B), dsRNA was injected (~ 0.05nL of 1mg/mL dsRNA) into embryos expressing *ubi>GFP::ROCK* and *gap43::mCherry* at age 0-30 minutes. Embryos were incubated for ~3 hours at room temperature until the onset of ventral furrow formation and imaged

using confocal microscopy. Efficacy of dsRNA was determined by recapitulating the loss of ROCK planar polarity in lateral cells, as reported in Simoes et al., 2014.

Profilin and actin purification

Recombinant profilin expressed from the pMW172-chickadee plasmid (a gift from D. Kovar, U. Chicago) was purified from *Escherichia coil* strain BL21 cells using poly-L-proline Sepharose. Overnight bacterial culture was induced at OD_{600} = 0.6-0.8 with 0.5 mM IPTG for 5 hours at 37°C. Cells were pelleted at 4700 rpm for 10 min at 4ºC and stored at -80°C. Pellets were resuspended to 50 mL in profilin buffer with PMSF and protease-inhibitors (20 mM Tris-HCl pH 7.5, 150 mM KCl, 0.2mM DTT, 500 µM PMSF, 1x Leupeptin/Pepstatin A) and sonicated until no longer viscous. Sonicate was centrifuged at 9,500 rpm at 4°C for 25 min, and the supernatant was added to PLP-column (pre-equilibrated with profilin buffer) and allowed to flow through by gravity. The column was washed with 30 mL of profilin buffer, then 30 mL 2 M urea in profilin buffer. Profilin was eluted in 50 mL 7 M urea in profilin buffer, and protein-containing fractions were pooled. Profilin was then concentrated in 5-7kD MW cut-off dialysis tubing overnight, and concentrated again in 3kD MW cut-off centrifuge tube at 3,000 rpm. Precipitated protein was pelleted, and supernatant was aliquoted, flash frozen, and stored at -80°C.

The poly-L-proline (PLP) column was prepared by coupling PLP (Sigma P3886) to CnBr-Sepharose (Sigma C9210-15G). In clean PYREX, CnBr-Sepharose (15 g) was soaked in 1.0 mM HCl for 15 minutes. Swollen beads were rinsed and resuspended to 50 mL in coupling buffer (0.1 M $NaHCO_3$, 0.5 M NaCl, pH 8.3). 500 mg PLP was

dissolved in 10 mL coupling buffer. CnBr-Sepharose suspension was split into four 25 mL volumes, to which 2.5 mL PLP was added and rocked overnight at 4°C. Coupled beads were collected in a tabletop centrifuge, washed in coupling buffer, collected, washed in 100 mM Tris/HCl, pH 8.0, and resuspended in 100 mM Tris/HCl, pH 8.0, and incubated for 2 hours rocking at 4°C. Beads were washed 3 times in profilin buffer, and stored in profilin buffer with 0.04% NaN_3 at 4°C.

Profilin activity was measured using a pyrene actin assembly assay. Actin used in pyrene assembly and for injections into embryos was purified as previously described using rabbit muscle acetone powder (Pel-Freez, Rogers AZ) and a cycle of polymerization, depolymerization, and gel filtration (Spudich and Watt, 1971). Purified actin was stored in G Buffer. Purified Ca-ATP-actin was converted to Mg-ATP-actin by 5 minutes incubation in Mg-exchange buffer (final conc. 50 µM $MgCl_2$, 200 µM EGTA), and was then added to individual wells of a 96-well plate with polymerization buffer (final conc. 2.5 µM actin (10% pyrene-labelled), 50 mM KCl, 1 mM $MgCl_2$, 1 mM EGTA, 10 mM Imidazole HCl, pH. 7.0) and Antifoam (final conc. 0.5 ppm Sigma Antifoam 204 A6426). Flourescence data from 150 µL reactions were read using a Spectramax Microplate Reader (Molecular Devices, Sunnyvale, CA). To determine profilin activity, reactions supplemented with profilin (2.5 µM) were compared to unsupplemented reactions, keeping buffer concentrations equivalent.

Purified rabbit skeletal muscle actin was labeled by thawing 500 µL of 50 µM actin and dialyzing overnight against 5 mM Tris-HCl pH 8.0, 0.2 mM $CaCl_2$ to remove DTT. Alexa-fluor-488-maleimide (final conc. 200 µM, Sigma-Aldrich) was added and incubated 5 hours at 4°C with rotation. DTT (2µM final conc.) was added to stop the

labeling reaction, and reaction solution was centrifuged at 90k rpm for 15 minutes to remove precipitate. Labeled actin was then loaded onto a Superose 6 column (GE Healthcare Lifesciences) to separate actin from free label. Actin-containing fractions were collected, pooled, and stored at -80°C.

Image Processing and Quantitative Analysis

We used custom MATLAB software, Embryo Development Geometry Explorer (Gelbart et al., 2012), to segment membrane images for quantification of apical area and change in fluorescence intensity or distribution. For non-continuous representations of apical area (e.g. Fig. 2B,4I) apical area change was calculated as change in apical area (μm^2) over 30 seconds, measured after the establishment of a stable myosin network. Comparisons of apical area change were made using the Kruskal-Wallis test because data were not always normally distributed.

Myosin, ROCK, and F-actin intensities were calculated as total intensity I_t, where p_t is the total number of pixels in a cell, and I_k is the pixel intensity:

$$I_t = \sum_{k=1}^{p_t} I_k$$

For comparisons of many cells across several embryos, total intensity over time for each cell was normalized such that at t_0, $I_t = 0$. This allowed us to compare changes in fluorescent intensity across many cells and embryos with different mean fluorescent intensities, and thereby determine the response of fluorescent intensity to ROCK inhibitor or water injection.

Peripheral:medioapical ratio (Fig. 5F,I) was determined by dividing the mean peripheral

intensity (I_j) by the mean medioapical intensity (I_m):

$$\overline{I}_p = \frac{\sum_{k=1}^{p_p} I_k}{p_p}$$

$$\overline{I}_m = \frac{\sum_{k=1}^{p_t} I_k - \sum_{k=1}^{p_p} I_k}{p_t - p_p}$$

$$Peripheral : Medioapical = \frac{\overline{I}_p}{\overline{I}_m}$$

where p_t is the total number of pixels in the apex, p_p is the total number of pixels in 1 µm shell at the cell periphery, and I_k is the pixel intensity.

Embryo preparation for live imaging

For live imaging, embryos were dechorionated with 50% bleach then washed with water and mounted, ventral side up, onto a slide coated with embryo glue (double-sided tape soaked in heptane). Spacer coverslips (No. 1.5) were attached to glue and a coverslip (No. 1) was attached to create a chamber. Halocarbon 27 oil (Sigma-Aldrich, St. Louis MO) was added to the chamber. Embryos were not compressed. All imaging occurred at room temperature (~23°C).

Supplementary Information

Supplementary Figures

Figure S1, related to Figure 1 and Figure 2

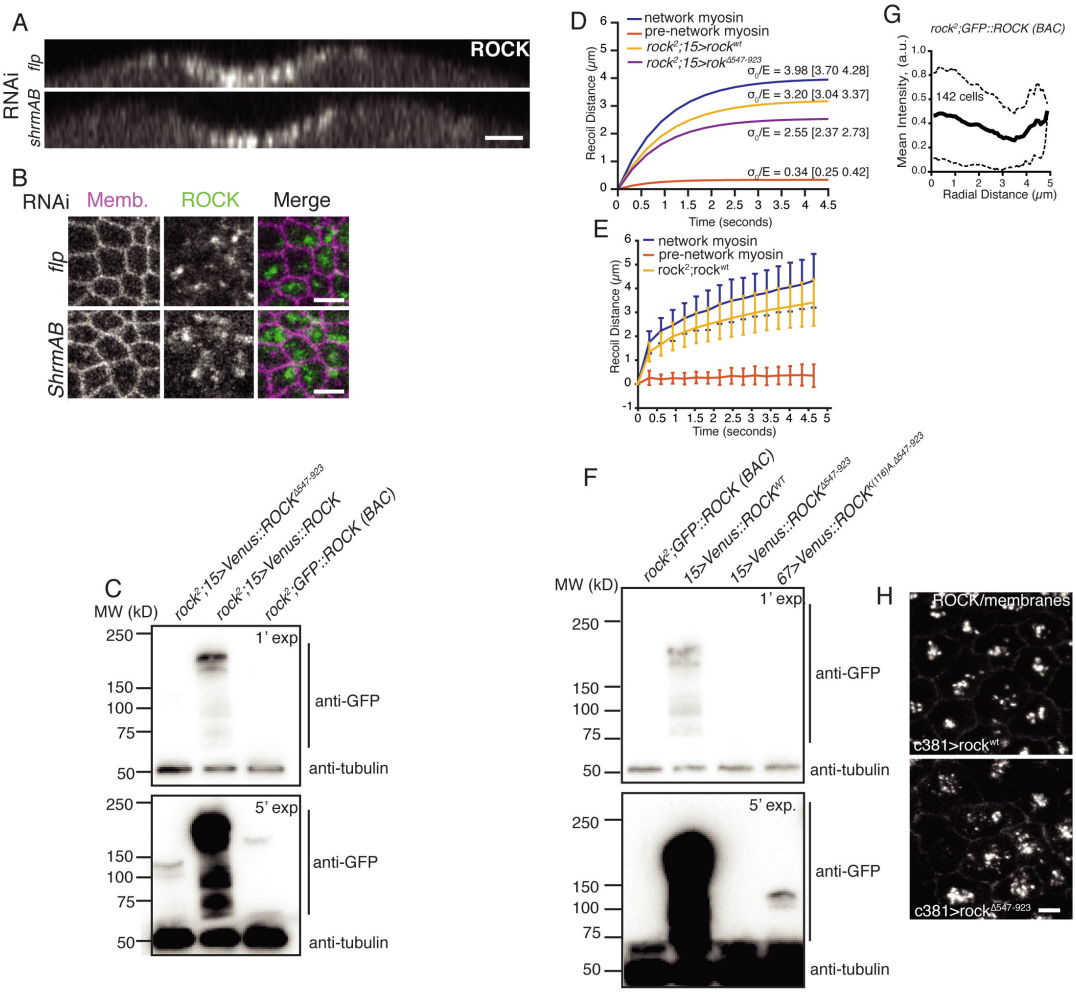

Figure S1. Shroom is not required for ventral furrow formation, expression levels of ROCK transgenes, and additional quantification of epithelial tension. (**A**) Cross-section views of ventral furrows in embryos expressing *ubi>GFP::ROCK.* Embryos were injected and incubated for 3 hours with dsRNA against either *flp* (non-expressed gene used as control) or *shrm* isoforms *shrmA* and *shrmB.* (**B**) Surface views of embryos expressing *ubi>GFP::ROCK* and Gap43::mCherry after incubation with injected dsRNA against either *flp* or both *Shroom.* (**C**) Corresponds to Fig. 1C,D. Expression levels of *UAS-Venus::rock*^{wt} (187kD) and *UAS-Venus::rock*$^{\Delta 547\text{-}923}$ (142 kD) expressed under the control of *mat15* in a *rock*^{2} null background, and of a GFP-tagged version of ROCK expressed with its endogenous promoter in a *rock*^{2} null background (GFP::ROCK (BAC), 187kD). (**D**) Corresponds to Fig. 1F,G. Kelvin-Voigt model fit with non-linear regression to tissue recoil. The initial stress (σ_0) over the elastic modulus (E) predicted by the fit are listed for each fitted equation. In the order of the graph legend, R^2 and root mean square error are (0.595,0.865); (0.0545, 0.330); (0.556, 0.758); and (0.323,0.971). The low R^2 for the pre-network myosin was expected because the tissue did not recoil as would be expected in a Kelvin-Voigt material. (**E**) Corresponds to Fig. 1F,G. Comparison of tissue recoil distance after laser ablation at t = 0 for *rock*^{wt} expressed in *rock*^{2} null background, or for pre-network and network myosin. From top to bottom order of the legend, n = 7, 6, and 19 cuts. Bars indicate ± 1 s.d. (**F**) Corresponds to Fig. 2. Expression levels of Venus-tagged ROCK transgenes expressed under the control of *mat15* or the stronger Gal4 driver, *mat67*, in a wild-type *rock* background. A GFP-tagged version of the endogenous locus in a *rock*^{2} null background is included for comparison, but was not detectable at the longer exposure time. (**G**) Corresponds to Fig. 2D. Radial intensity profile of ROCK fluorescence in fixed embyros expressing *rock-GFP::ROCK* in the *rock*^{2} null background. Note the increased intensity at the radial center, like *rock*^{wt} in Fig. 2D. The bump at the edge represents junctional fluorescence, which is only captured in fixed embryos, but not in live embryos represented in Fig. 2D. Dotted lines represent ± 1 s.d.. All cells were analyzed from one representative embryo. (**H**) Expression of *rock*^{wt} and *rock*$^{\Delta 547\text{-}923}$ in amnioserosa cells with the *c381* Gal4 driver. Membranes are labeled with E-cadherin::GFP. Scale bars = 5 μm (A,C).

Figure S2, related to Figure 3

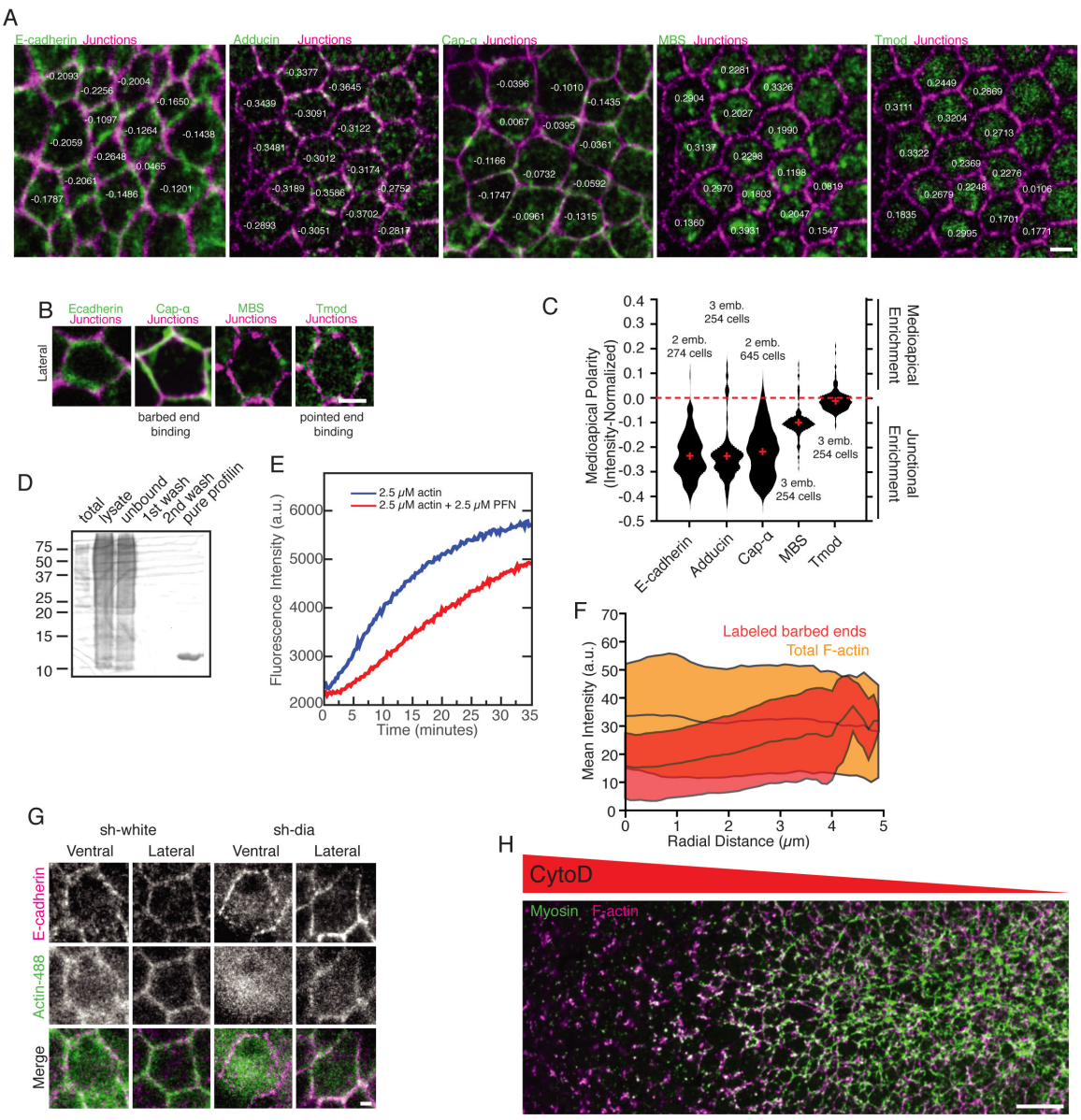

Figure S2. Actin filament polarity, profilin purification, and *in vitro* activity. (**A**) Corresponds to Fig. 3A,B. Medioapical polarity metric for individual ventral cells. Junctions are subapical adducin or F-actin, overlayed with apical adducin, mbs, Cap ✔, tmod, or E-cadherin. (**B,C**) Corresponds to Fig. 3A,B, and shows the apical organization of cytoskeletal polarity in non-contracting lateral epithelial cells. emb. and cell indicate the number of embryos and cells analyzed per condition, respectively. Red crosses indicate median. (**D**) Coomassie stained gel showing the purification of *Drosophila* profilin (*chickadee*). The pure profilin fraction was used for experiments in Fig. 3C,D. (**E**) Demonstration of profilin activity in a pyrene-actin assembly assay. The reduced actin polymerization rate demonstrates that profilin binds actin monomers and inhibits spontaneous actin filament nucleation. (**F**) Corresponds with Fig. 3C. Radial intensity distribution of total F-actin (35 cells) or actin-488 (71 cells) after actin-profilin injection. Plot represents mean intensity along radial axis among cells in single representative embryos. Shaded area represents ± 1 s.d. (**G**) Corresponds with Fig. 3D. Examples of ventral and lateral cells after injection of actin-profilin. Comparison of control knockdown (*white*) and *dia* knockdown. Note the reduction in ventral cells of junctional incorporation (column 3, row 2). (**H**) Whole ventral furrow depiction of injected embryo used in Fig. 3H. Cytochalasin D (250 µg/mL) was injected in one end of an embryo expressing RLC::GFP, the embryo was quickly fixed, and stained for F-actin (phalloidin) and Cap ✔ (shown in Fig. 3H). Note the gradient in drug effect from left to right, panels in 3H were taken from a region in the middle. Scale bar = 2 µm (A,B), 1 µm (G), 10 µm (H).

Figure S3, related to Figure 4 and Figure 5

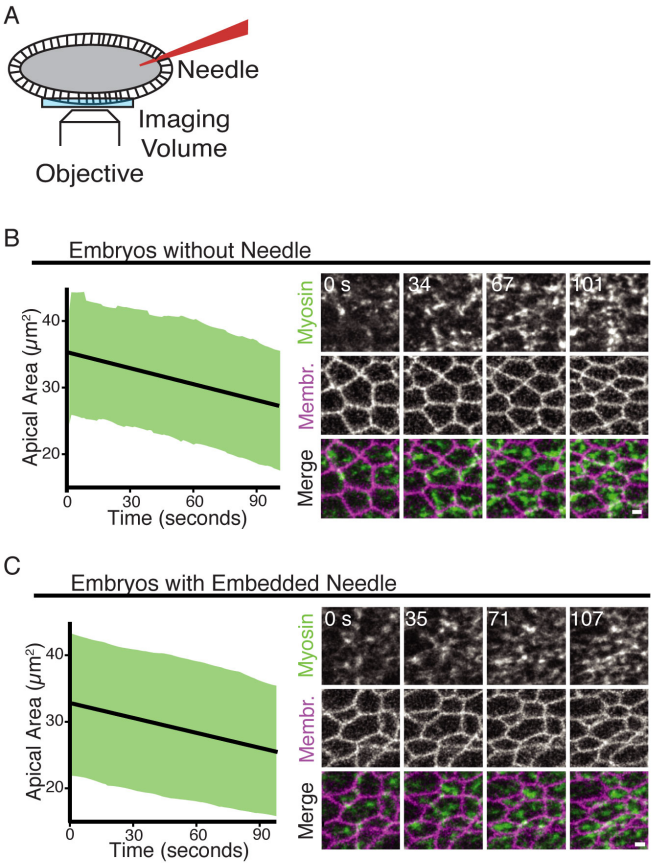

Figure S3. Live embryo injection controls. (**A**) Schematic illustrating simultaneous imaging and injection apparatus. Embryo on coverslip over objective was pierced with a needle and injected during image acquisition. Not drawn to scale. (**B**) Unpierced embryos expressing RLC::GFP (myosin) and Gap43::mCherry (membranes) undergo apical constriction (-4.85 μm^2/min, 95% CI [-4.70 -5.01], linear regression fit to the mean, R^2 = 0.975) and assemble a myosin network (183 cells, 2 embryos). (**C**) Embryos with an embedded needle similarly undergo apical constriction (-4.48 μm^2/min, 95% CI [-4.45 -4.51], linear regression fit to the mean, R^2 =0.998) and assemble a myosin network (224 cells, 2 embryos). Green shading is ± 1 s.d. around the mean, not the linear model. Scale bars = 2 μm (B,C).

Figure S4, related to Figure 5

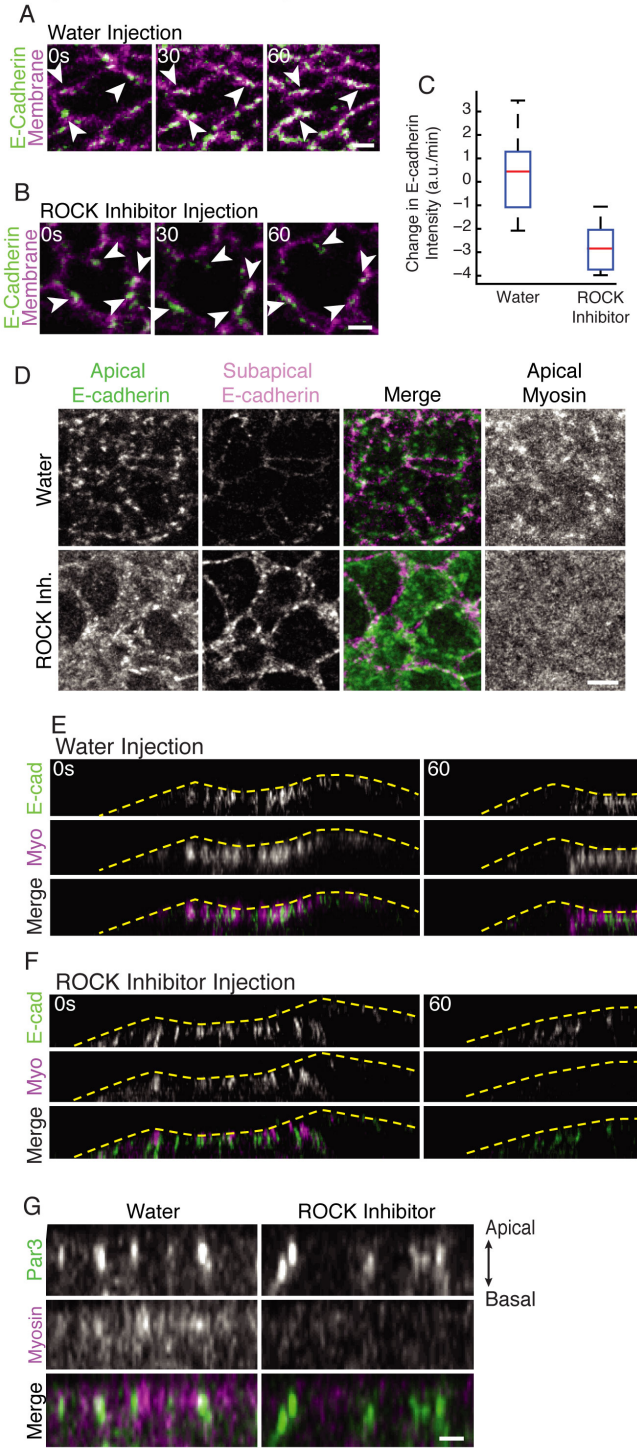

Figure S4. ROCK inhibition disrupts apical E-cadherin organization. (**A**) Water injection does not perturb E-cadherin localization. Images are ventral surface views of embryos expressing E-cadherin::GFP, and Gap43::mCherry (membranes) injected with water after acquiring t = 0 second frame. Arrowheads highlight persistent spot adherens junctions. (**B**) Same as (A) but with ROCK inhibitor injection. ROCK inhibition decreases intensity of peripheral E-cadherin (arrowheads show examples of spot junctions). (**C**) Quantification of apical E-cadherin puncta like those annotated in (A, B). Mean fluorescence intensity in puncta was tracked over 1 minute after water or ROCK inhibitor injection. 20 spot junctions from 2 embryos quantified for each condition. Red line is median, box represents 25^{th}-75^{th} percentile, and whiskers represent ± 2.7 s.d.. Comparison is significantly different (Wilcoxon Rank Sum, α = 0.001)**.** (**D**) ROCK inhibition disrupts E-cadherin's restriction to intercellular contacts. Images are apical surface of ventral furrow cells showing E-cadherin in embryos injected with water or ROCK inhibitor, fixed, and manually devitellinized to view protein localization in the apical domain. Subapical E-cadherin signal is shown to delimit cells, and myosin signal (RLC::mCherry is shown to report successful ROCK inhibition. (**E**) E-cadherin signal remains apical after ROCK inhibition, despite fading intensity. Cross sections of ventral furrow in an embryos expressing E-cadherin::GFP and RLC::mCherry (myosin). In (A) embryo injected with water at t = 0, and in (**F**) embryo injected with ROCK inhibitor at t = 0. In (B) (**G**) ROCK inhibition does not affect Par3 or apical-basal polarity. Cross sections of embryos expressing Par3::GFP and RLC::mCherry (myosin). Par3 remains apical after ROCK inhibitor injection, despite loss of myosin. Scale bars = 2μm (A,B,G), 5 μm (D,E,F).

Figure S5, related to Figure 6

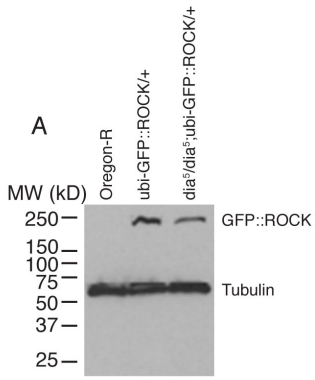

Figure S5. Expression of *ubi-GFP::ROCK* in wild-type and *dia*^{5} maternal/zygotic mutants. (**A**) Expression levels of *ubi-GFP::ROCK* expressing embryos or *dia* germline clone mutants expressing *ubi-GFP::ROCK*. Corresponds to Figure 6C.

Supplementary Movies

Accessible at http://dx.doi.org/10.1016/j.devcel.2016.09.023

Movie S1. Venus::ROCK^{wt} and Venus::ROCK$^{\Delta 547\text{-}923}$ in a *rock*^{2} null mutant. Apical maximum intensity projection of Venus::ROCK^{wt} (top) and Venus::ROCK$^{\Delta 547\text{-}923}$ (bottom) expressed in *rock*^{2} null mutant background and with the *mat15* Gal4 driver. Note that Venus::ROCK^{wt} (top) rescues *rock*^{2} and forms a furrow, whereas Venus::ROCK$^{\Delta 547\text{-}923}$ fails to form a furrow, even after 10 minutes. Movies were separately contrast adjusted to illustrate fluorescence distribution.

Movie S2. Wild-type and mutant ROCK expressed in wild-type background. Venus::ROCK^{wt} (top), Venus::ROCK$^{\Delta 547\text{-}923}$ (middle), and Venus::ROCK$^{K(116)A,\Delta 547\text{-}923}$ (bottom) expressed in under the control of *mat15*, *mat15* and *mat67*, respectively. Apical maximum intensity projection of ROCK (yellow) ectopically expressed in combination with Gap43::mCherry labeling membranes (magenta). In Venus::ROCK^{wt}, ROCK spots present before apical constriction are not apical, and may be aggregates resulting from the high expression levels of Venus::ROCK^{wt} relative to other ROCK transgenes. Note in Venus::ROCK$^{\Delta 547\text{-}923}$ (middle) that ventral cells do not efficiently constrict and ventral tissue fail to invaginate. Venus::ROCK$^{K(116)A,\Delta 547\text{-}923}$ (bottom) invaginates normally. Movies were separately contrast adjusted to illustrate fluorescence distribution.

Movie S3. Embryos begin gastrulation despite an embedded needle. Brightfield lateral view of an embryo developing with an embedded drug (phalloidin)-loaded needle. The local defects near the needle do not seem to globally perturb tissue movements.

Movie S4. Apical myosin fades within 20 seconds of ROCK inhibitor injection. Apical maximum intensity projection of an embryos expressing fluorescently-labeled myosin RLC Sqh::GFP (green) and labeled membranes Gap43::mCherry (magenta). The time of water injection (top) and ROCK inhibitor injection (bottom) is indicated by frame label.

Movie S5. Medioapical ROCK polarization is lost within a minute of ROCK inhibitor injection. Apical maximum intensity projection of an embryo expressing fluorescently-labeled ROCK (*ubi-GFP::ROCK*) (green) and membrane-labeling Gap43::mCherry (magenta). The time of water injection (top) and ROCK inhibitor injection (bottom) is indicated by frame label. Time of injection indicated by frame label. Movies were separately contrast adjusted because ROCK fluorescence intensity increases dramatically after ROCK inhibition.

Chapter 4: Discussion

Major Conclusions

One of many functions of the actomyosin force-generating machine is to power cell shape changes in epithelia, which in turn build the structures of the growing embryo. Here, I add to our knowledge of contractile actomyosin in epithelia in two ways. First, I add several proteins to the parts list of the constricting apical cortex, and demonstrate that they exhibit spatial organization. Second, I show that epithelial cells can apically constrict using a spatially organized actomyosin structure we term the radial sarcomere.

The new components of the constricting apical actomyosin cortex identified here are β_H-spectrin, Moesin, Tmod, Adducin, Capping protein, and MP-RIP. All are spatially distributed, some with patterns specific to the apically constricting ventral cells. These findings show that the spectrin-based membrane skeleton and actin end-binding proteins are spatially organized in the apical domain, and may play functional roles in apical constriction and epithelial morphogenesis.

For β_H-spectrin, Adducin, Moesin, and Capping protein, RNAi knockdown did not reveal a striking defect in ventral furrow formation or myosin network organization. This negative result indicates either that the knockdown target does not play a functional role in apical constriction, or that the knockdown was not sufficient to reveal a function. RNAi does not produce null phenotypes, and unfortunately, analyzing a true null mutant for these proteins is difficult because all are essential during oogenesis. Moreover, strong RNAi knockdown can cause defects before ventral furrow formation, killing the embryo or perturbing the tissue in such a way as to complicate analysis during ventral furrow formation. For this reason, I could not rule out a role for these proteins in ventral furrow formation, and I proposed several alternative perturbations, for example,

overexpressing dominant negative constructs to inhibit the function of the wild-type protein.

In the absence of an identified function for many of these proteins, their localization patterns still suggest an organization in the apical cortex of an apically constricting epithelial cell. Actin end-binding proteins localized in a way that suggests actin filaments are organized with barbed ends at junctions and pointed ends in the medioapical area. This enrichment was confirmed by an *in vivo* barbed end labeling assay. Bleb and Moesin localization also suggest a spatial pattern to the actin cortex, perhaps indicating a spatial organization to membrane-cortex adhesion, or a spatial organization to actin cortex turnover. These newly characterized proteins add to the previously reported apical localization of actomyosin regulatory proteins, RhoA, ROCK, RhoGEF2, and Dia (Mason et al., 2013; Mason et al., 2016).

The “radial sarcomere” model addresses a second major question: is the spatial organization of the apical actin cortex functionally important? Two major features emerged from investigating this question. First, the actin cytoskeleton in apically constricting cells has a sarcomere-like polarity, with actin filament barbed ends arrayed at junctions, and pointed ends arrayed in the apical center. Second, myosin, and its activating kinase ROCK, are localized in the region of pointed end enrichment. Using a ROCK mutant that localizes across the apical surface, we demonstrated that medioapical ROCK localization is essential for apical constriction and epithelial folding. Future experiments will be needed to determine the functional importance of other spatially organized actin cortex components, like actin end-binding proteins and β_H-spectrin.

Establishing the spatial organization of the apical actin cortex

This thesis leaves unanswered several important questions, which I recommend as topics for further inquiry. First, what determines the spatial organization of the apical actomyosin cortex? Previous studies have made it clear that the transcription factors that define the ventral furrow, Twist and Snail, are also required for the medioapical localization of ROCK (Leptin, 1991; Mason et al., 2013). Chapter 3 demonstrates that the medioapical localization of ROCK in the apex is essential for constriction, but the mechanism by which ROCK becomes localized is unclear. I also have not clearly defined how any of the other spatially localized proteins and blebs achieve the localization patterns they exhibit in Chapter 2. Considering that these proteins are all associated with the apical membrane or the apical actin cortex, I suspect that the same mechanism will ultimately regulate the spatial organization of the entire apical cortex.

We have some information to shape further efforts to solve this question. First, ROCK localization requires its own activity, and second, ROCK localization requires Dia and an intact actin cytoskeleton. These findings suggest a feedback loop in which ROCK activity operates through the actin cytoskeleton to concentrate itself in a spot at the medioapical center. This could occur through actomyosin contractility, which is capable of generating some degree of cortical organization (Köster et al., 2016; Munjal et al., 2015), or through ROCK phosphorylation of other substrates. Alternatively, an upstream signal could direct ROCK to the medioapical region. Somewhere between the transcription factor Twist and ROCK, a protein in the signaling cascade could localize to the medioapical domain and from there control the spatial organization of cortex.

Another possibility is that microtubules could spatially regulate the apical cortex, perhaps inhibiting RhoA activity at junctions and/or promoting its localization in the center. Precedent for this model comes from studies showing that microtubule plus ends can either deposit or absorb RhoGEF2 from the plasma membrane (Bulgakova et al., 2013; Ratheesh et al., 2012; Rogers et al., 2004). In fact, preliminary evidence demonstrates a defect in apical constriction with microtubule depolymerization by colchicine, in which myosin and ROCK slowly condense in the medioapical region. Ventral cells then lose most intercellular connections, and fail to invaginate (data not shown). This colchicine effect somewhat resembles junctional mutant phenotypes (Martin et al., 2010) or injections of a low concentration of actin barbed end capping drug, Cytochalasin D, that disconnects the actin cytoskeleton from adherens junctions (Mason et al., 2013). An issue in this model is how microtubules can discriminate between the junctional and medioapical actin cortex. Microtubules are anchored at the microtubule organizing center, which in epithelia is apical to the nucleus. In apically constricting cells, the junctions will therefore be farther away from the nucleus than the medioapical domain. Differences in microtubule length could perhaps be a mechanism to distinguish between the medioapical and junctional domains.

Attachment of the actin cortex to adherens junctions

A second pressing question is how actin filament barbed ends that are growing near junctions can be transferred and stably attached to the adherens junctions. Here, I identified a sarcomere-like organization to actin and myosin. The connection to the adherens junction clearly depends on β-catenin and α-catenin, which directly binds actin

filaments (Buckley et al., 2014; Desai et al., 2013; Martin et al., 2010), but it remains unclear how dynamic actin filaments initially establish a connection to the adherens junctions at the edge of the structure. Proteins analyzed in Chapter 2 raise two possibilities for how adherens junctions could capture actin filaments growing and moving in the apical domain. First, α-actinin at adherens junctions (Tang and Brieher, 2012) could bind Capping protein-capped barbed ends, as is observed at the Z-disk in muscle sarcomeres (Papa et al., 1999). This α-actinin/Capping protein/barbed end complex might then present the actin filament to the adherens junction and allow α-catenin to directly bind the actin filament. Alternatively, adherens junction-associated Adducin (Naydenov and Ivanov, 2010) is known to stimulate spectrin skeleton assembly at the membrane (Abdi and Bennett, 2008), and also to recruit spectrin to the actin filament barbed ends (Li et al., 1998). Spectrin skeletons could grow out from adherens junctions and create a net to capture free actin filament barbed ends, which would then be transferred to α-catenin at the adherens junction itself. Either of these mechanisms could allow adherens junctions to capture free actin filament barbed ends in the radial sarcomere, allowing force transmission from the contractile apparatus to the cell-cell junctions and across the tissue.

Related to the question of how adherens junctions attach to actin filaments is how this connection can be maintained in a dynamic state. Recent observations identified transient separations in the actin cortex between the central zone of myosin activation and the junctions, and these separations are repaired in an actin turnover-dependent manner (Figure 1, originally published in Coravos et al., 2016) (Jodoin et al., 2015). If either of the above scaffolding mechanisms are involved in maintaining cortex-

adherens junction attachment, they will also likely need to be constantly replenished as the attachment cycles through breaks and repairs. This cycling raises the question of what regulates the appropriate level of attachment at the adherens junction.

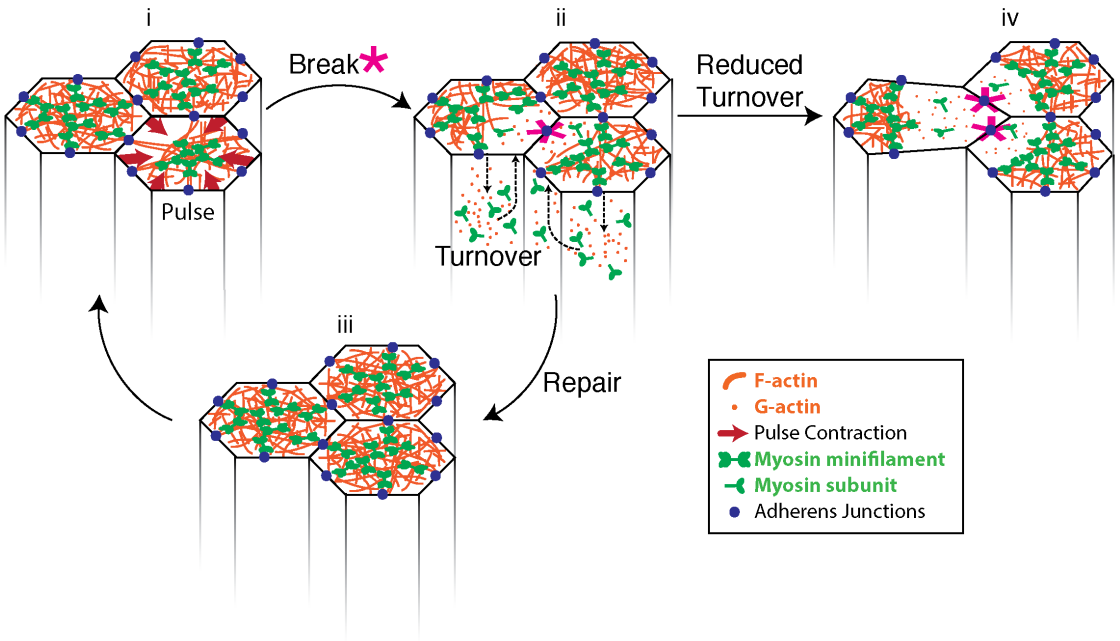

Figure 1. Actomyosin turnover sustains intercellular actomyosin connectivity. **(i)** During epithelial morphogenesis, actomyosin pulses (dark red arrows) lead to contractions, **(ii)** contractility can disrupt intercellular actomyosin connections to adherens junctions (magenta asterisk). **(iii)** actomyosin turnover repairs these connections in wild-type cells, **(iv)** but with reduced turnover, tears appear in the epithelium between cells, interfering with morphogenesis.

Radial sarcomeres in other epithelia and smooth muscle

Finally, is the radial sarcomere a conserved mechanism for cells to generate contractile force? ROCK localization and actin filament polarity should be determined in some of the cases where actin and myosin networks correlate with cellular contractility, for example in the neural tube (Christodoulou and Skourides, 2015), the gastrulating *C. elegans* embryo (Roh-Johnson et al., 2012), and the *Drosophila* salivary gland (Booth et al., 2014). Another important context of contractile force is in the specialized epithelia of the vascular endothelium, which assembles cell-spanning actin networks in response to

histamines, thrombin, and other ligands. In endothelia, these ligands stimulate $G\alpha_{12/13}$, RhoA, and ROCK, and lead to the assembly of actin networks, which pull on adherens junctions and cause vascular permeability (Spindler et al., 2010; van Nieuw Amerongen et al., 1998; Amerongen et a., 2000; Wójciak-Stothard et al., 2001). It would be interesting to obtain high-resolution localization data of endogenous ROCK and to determine actin filament polarity in this system.

If the radial sarcomere is a common mechanism for epithelial contractility, it may also operate in smooth muscle. Because smooth muscles are not thought to transmit forces at cell-cell adherens junctions, but rather through structures called dense bodies in the smooth muscle syncytium, the radial sarcomere would appear differently. ROCK would localize at areas of actin filament pointed end overlap between dense bodies, and force would be transmitted to dense bodies, which are known sites of barbed end accumulation (Bond and Somlyo, 1982). ROCK localization should therefore be evaluated in smooth muscle. An interesting additional question in smooth muscle is whether Ca^{2+} sensitization, which is known to be mediated by ROCK (Somlyo and Somlyo, 2003; Uehata et al., 1997), might depend on translocation of ROCK to specific locations, for example in between dense bodies. If the radial sarcomere, and more generally, ROCK localization, is a common mechanism for contractile force generation in smooth muscle and nonmuscle, it may be a productive framework for developing new therapeutics for actomyosin contractility-related pathologies.

Implications for cardiovascular disease and pulmonary fibrosis

The general rationale connecting ROCK and actomyosin contractility to disease is that changes in ROCK expression or enzymatic activity, either through functional single nucleotide polymorphisms or copy number variation, leads to disease (Knipe et al., 2015; Morgan-Fisher et al., 2013; Schofield and Bernard, 2013; Shimokawa et al., 2016). This thinking has led to models for ROCK in fibrotic and cardiovascular disease, and cancer, in which changes in activity level causes disease. However, work in this thesis shows that ROCK localization can be essential for its function. Moreover, ROCK has been found to localize to specific subcellular structures in other cellular contexts (Katoh et al., 2001; Muliyil and Narasimha, 2014; Simões et al., 2010; Bardet et al., 2013). The two human ROCK orthologs, ROCK1 and ROCK2, also localize to distinct subcellular domains in Chinese Hamster Ovary cells (Newell-Litwa et al., 2015). ROCK-related diseases are therefore likely to arise not only from changes in activity, but also from changes in localization.

Current approaches to treat ROCK-associated diseases use one of several small molecule ATP-competitors with ROCK specificity. The first compound (Y-27632) is unsuitable for humans due to toxicity, but another compound (fasudil) has been approved in Japan since 1992 for cerebral vasospasm (Shibuya et al., 1992; Suzuki et al., 2007). Still, fasudil is a relatively weak inhibitor, and is approved for a narrow range of conditions.

Based on this thesis, a new possibility for modulating ROCK function would be to interfere with ROCK localization. This could be accomplished by finding a therapeutic strategy to mimic the mutant phenotype of $ROCK^{\Delta 547\text{-}923}$. Though I have not

demonstrated why this mutant fails to localize properly, it seems likely that it is either through the inability of ROCK$^{\Delta 547\text{-}923}$ to bind a partner that normally binds in the deleted region, or because ROCK$^{\Delta 547\text{-}923}$ is unable to dimerize and generate dimeric binding interfaces. In either case, an intracellular coiled-coil peptide would likely impede ROCK localization. Precedent for such compounds exists (Fosgerau and Hoffmann, 2015). Such a compound could recapitulate the experimental therapeutic benefits seen with ROCK inhibition, for example regression of pulmonary fibrosis (Zhou et al., 2013), or amelioration of cardiovascular symptoms (Shimokawa et al., 2016), but with lower risk of off-target effects, and possibly with greater potency.

Appendix: Actomyosin pulsing in tissue integrity maintenance during morphogenesis

Jonathan S. Coravos, Frank M. Mason Adam C. Martin. Available online 2016.
http://dx.doi.org/10.1016/j.tcb.2016.11.008

Summary

The actomyosin cytoskeleton is responsible for many changes in cell and tissue shape. For a long time, the actomyosin cytoskeleton has been known to exhibit dynamic contractile behavior. Recently, discrete actomyosin assembly/disassembly cycles have also been observed in cells. These so-called actomyosin pulses have been observed in a variety of contexts, including cell polarization and division, and in epithelia, where they occur during tissue contraction, folding, and extension. In epithelia, evidence suggests that actomyosin pulsing, and more generally, actomyosin turnover, is required to maintain tissue integrity during contractile processes. This review explores possible functions for pulsing in the many instances during which pulsing has been observed, and also highlights proposed molecular mechanisms that drive pulsing.

The pulsatile behavior of nonmuslce myosin 2 and filamentous actin

Nonmuscle myosin 2 (Myo2) and filamentous actin (F-actin) comprise a molecular machine capable of generating contractile force and changing cell shape (Kasza and Zallen, 2011; Lecuit et al., 2011; Vicente-Manzanares et al., 2009). Localization of F-actin and Myo2 (actomyosin) to specific subcellular structures, like the lamella, stress fibers, apical networks or adherens junctions, is critical to cellular actomyosin function (Murrell et al., 2015). Dynamics in both the spatial and temporal regulation of actomyosin have been observed in a growing number of biological contexts, especially in developmental systems, raising the question of how spatiotemporal actomyosin dynamics affect actomyosin function. One class of temporal actomyosin dynamics is a process broadly described as actomyosin pulsing, in which F-actin and Myo2 first assemble in a subcellular structure and then disassemble, on the time scale of minutes or less (Figure 1). Neither the mechanism nor the function of actomyosin pulsing is fully understood. In this review, we discuss observations of actomyosin pulsing in cellular and developmental contexts, we explore possible biological functions for pulsing, and we evaluate proposed molecular mechanisms for actomyosin pulsing.

Pulsed actomyosin accumulation is thought to generate contractile stress on the actomyosin cytoskeleton, which transmits force to cellular neighbors or substrates when attached to a cell's adhesion receptors (Gardel et al., 2008; Roh-Johnson et al., 2012; Thievessen et al., 2013). Actomyosin pulses also often correspond with an accumulation and dissipation of F-actin (Blanchard et al., 2010; He et al., 2010; Mason et al., 2013; Rauzi et al., 2010; Valencia-Expósito et al., 2016). In some biological

Figure 1

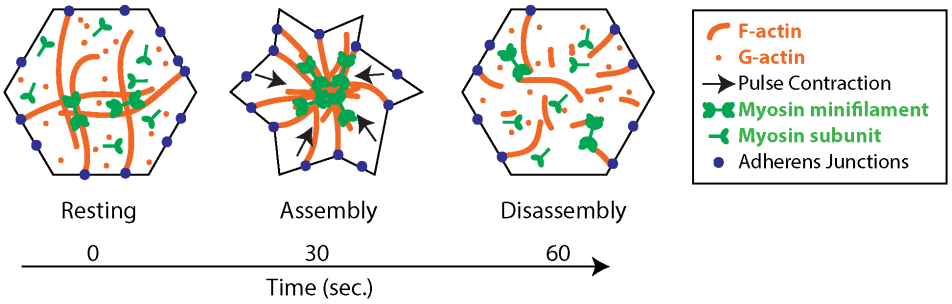

Figure 1. A generalized schematic of actomyosin pulsing. Over the course of approximately one minute, Myo2 minifilaments assemble and contract a filamentous actin cytoskeletal network. This contraction can pull on cell adhesion receptors like adherens junctions or focal adhesions. Pulsed contraction is often followed by relaxation involving disassembly of Myo2 and the F-actin cytoskeleton.

contexts, repetitive actomyosin pulses exhibit *bona fide* oscillatory behavior that can be identified as a dominant frequency using Fourier analysis (Gorfinkiel, 2016; Koride et al., 2014; Sokolow et al., 2012; Solon et al., 2009). In other contexts, however, actomyosin pulses may not occur at a well-defined frequency and are possibly stochastic (Xie and Martin, 2015). Another important distinction in discussing actomyosin spatiotemporal dynamics is that between pulses and traveling waves, recently reviewed by (Allard and Mogilner, 2013). These two phenomena are probably related, and sometimes occur together (Munro et al., 2004; Rauzi et al., 2010; Saravanan et al., 2013). We limit this review to a discussion of pulsing.

Actomyosin pulsing has been observed in cultured cells, and in developmental contexts like single-celled embryos or epithelia undergoing morphogenesis. Work in cultured cells has demonstrated that cortical actomyosin pulses can emerge after microtubule depolymerization (Bornens et al., 1989; Paluch et al., 2005; Pletjushkina et al., 2001). Cortical pulses have also been observed during mitosis, where they maintain volume symmetry across the cleavage furrow during cytokinesis (Sedzinski et al., 2011). In endothelial cells, retraction cycles were shown to be triggered by bursts of

Ca^{2+} that activate myosin (Tsai and Meyer, 2012). In developmental contexts, actomyosin pulsing was first reported in the *C. elegans* zygote where pulsing is involved in establishing anterior-posterior polarity preceding the first cell division (Munro et al., 2004). Pulsing was later observed in the *Drosophila* embryo in several contexts: in apical constriction of epithelial cells of the ventral furrow (Martin et al., 2009), salivary gland (Booth et al., 2014), and renal tubules (Saxena et al., 2014); in constrictions of the amnioserosa cells during dorsal closure (Blanchard et al., 2010; David et al., 2010; Solon et al., 2009); during extension of the germband (Fernandez-Gonzalez and Zallen, 2011; Rauzi et al., 2010; Sawyer et al., 2011); and in the follicular epithelium surrounding and shaping the developing oocyte (He et al., 2010; Valencia-Expósito et al., 2016). Actomyosin pulses have also been observed during convergence and extension in the *Drosophila* germband. They appear to shrink pre-existing cell contacts (Rauzi et al., 2010), and drive elongation of junctions, leading to tissue extension (Collinet et al., 2015; Yu and Fernandez-Gonzalez, 2016).

With improvements in live microscopy and the adaptation of F-actin and Myo2 fluorescent probes for more animal models, pulsing has also been observed in vertebrates. In the 8-cell mammalian blastocyst, actomyosin pulsing corresponds to an increase in cortical tension leading to embryo compaction (Maître et al., 2015). During *Xenopus* neural tube formation, Ca^{2+} bursts trigger accumulation of F-actin across the apical surface of neuroepithelial cells, driving apical constriction (Christodoulou and Skourides, 2015). In addition, actomyosin pulsing occurs during *Xenopus* gastrulation and mesoderm convergent extension (Kim and Davidson, 2011; Skoglund et al., 2008), and corresponds to dynamics in cell-cell adhesive adherens junction complexes and F-

actin (Pfister et al., 2016). Thus, actomyosin pulsing is a widely conserved mechanism for generating contractile force both in individual cells and tissues.

Biological functions of actomyosin pulsing

It is clear that pulsing can be correlated with cell shape change, suggesting that increased actomyosin concentration in contracting domains promotes temporary increases in mechanical force. However, pulsing may do more than change cell shape. As mentioned above, in individual cells, actomyosin pulsing may maintain cell volume symmetry across the cleavage furrow during cytokinesis (Sedzinski et al., 2011). In tissues, it is tempting to speculate that pulsing coordinates tissue-wide cell shape changes and tissue deformation. While there have been some observations of spatial patterns in pulsing behavior (Saravanan et al., 2013; Solon et al., 2009; Xie and Martin, 2015), it has been difficult to determine the importance of these patterns because perturbations of pulsing behavior intrinsically affect Myo2 motor activity. Nevertheless, several intriguing models have emerged.

In epithelia, there is substantial evidence suggesting that pulsing and actomyosin turnover are critical for tissue mechanical integrity during morphogenesis. A challenge in addressing the function of pulsing is to find perturbations that disrupt pulsing without obliterating the actomyosin machine. In a system involving a folding epithelium, the *Drosophila* ventral furrow, numerous perturbations have been found that abrogate actomyosin pulsing, while leaving the actomyosin machinery more-or-less intact (Jodoin et al., 2015; Vasquez et al., 2014). These perturbations include disrupting either Myo2 or F-actin turnover directly, or disrupting this dynamic turnover by interfering with

upstream RhoA signaling dynamics. Interestingly, both types of perturbation lead to a phenotype where actin cortexes of neighboring cells separate from each other, at least in part through the actomyosin network separating from intercellular junctions. This has led to a model for actomyosin pulsing in maintaining tissue integrity during intercellular actomyosin contractility (Figure 2). In the *Drosophila* ventral furrow cells, the connection between the actomyosin network and the adherens junction is dynamic in the unperturbed, and contracting, epithelia (Figure 2i); this connection is sometimes lost (Figure 2ii), and subsequently repaired through turnover of actin and Myo2 (Figure 2iii) (Jodoin et al., 2015). In the absence of turnover, intercellular connections cannot be repaired, leading to the formation of additional breaks and tearing the epithelium (Figure 2iv).

The importance of turnover during contraction reveals a paradox regarding contractility in a tissue. Cortical Myo2 and F-actin can generate a strong force, yet contraction also clusters Myo2 and F-actin, leading to disconnection of the intercellular actomyosin networks. To continuously transmit force to the cell junctions and to neighboring cells, the actomyosin network in the middle of a cell or apical domain has to maintain connections to distal adhesive structures at the cell periphery (Jodoin et al., 2015; Martin et al., 2010; Roh-Johnson et al., 2012). Modeling studies have demonstrated that actin filament turnover is an effective mechanism for dispersing contracted networks and sustaining force generation across a surface (Mak et al., 2016). Clustering can lead to the loss of global connectivity of the cytoskeletal network (Figure 2ii). Actin turnover allows actomyosin clusters to dissipate, redistributing the

network to enable further large contractions (Figure 2iii) (Mak et al., 2016). Therefore, pulsing may allow

Figure 2

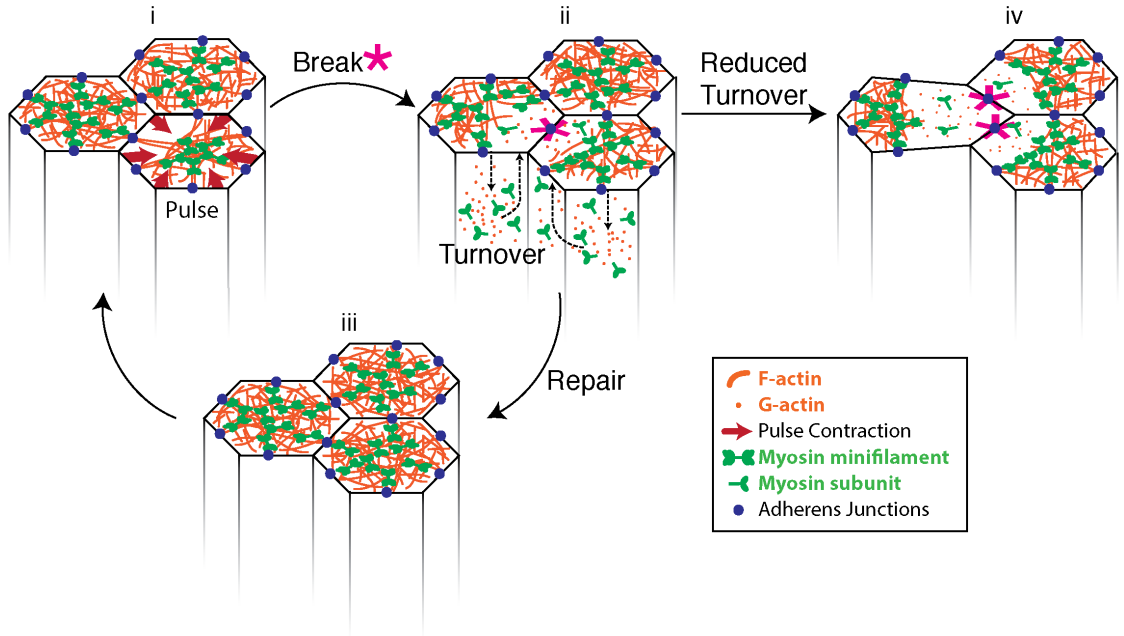

Figure 2. Actomyosin turnover sustains intercellular actomyosin connectivity. **(i)** During epithelial morphogenesis, actomyosin pulses (dark red arrows) lead to contractions, **(ii)** contractility can disrupt intercellular actomyosin connections to adherens junctions (magenta asterisk). **(iii)** actomyosin turnover repairs these connections in wild-type cells, **(iv)** but with reduced turnover, tears appear in the epithelium between cells, interfering with morphogenesis.

an intercellular actomyosin network to sustain contractility by counter-acting the clustering tendency of contracting actomyosin networks.

Pulsing may also (or alternatively) represent a transition state in actomyosin contractility. In several systems that exhibit pulsing, actomyosin pulses precede a more sustained contraction. For example, during *Drosophila* ventral furrow formation, early actomyosin pulses initially produce reversible, or “unratcheted”, contractions, where cell area expands after the pulse induces contraction. Relaxation was recently found to depend on the presence of a negative regulator of RhoA activity (see below), suggesting that pulse relaxation, or the unratcheted state, represents transient RhoA inactivation (Mason et al., 2016). This state then evolves to one in which more persistent actomyosin correlates with sustained, or “ratcheted”, cell constriction (Xie and

Martin, 2015). A similar pattern appears in *Drosophila* dorsal closure, where early actomyosin pulses correspond with constricting and relaxing cell area, followed by sustained contraction and persistent Myo2 (Blanchard et al., 2010; Sokolow et al., 2012; Solon et al., 2009). Actomyosin pulsing might therefore reflect an intermediate state in the activation of Myo2 contractility where there is limited cell shape change. One can think of the "unratcheted" pulses as an idling state of the actomyosin motor, which actomyosin passes through before achieving a state that allows sustained contraction (Teo and Yap, 2016).

Figure 3

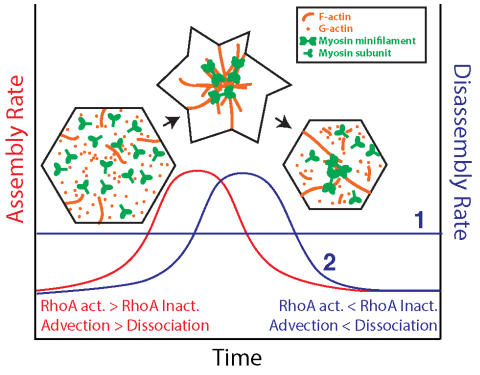

Figure 3. Model for Myo2 and actin turnover in actomyosin pulses. Actomyosin pulse assembly occurs through a combination of RhoA activation via a RhoGEF, and actomyosin advection. Disassembly occurs through a combination of RhoA inactivation through a RhoGAP, and through dissociation of actomyosin from the apical actin cortex. The balance between assembly and disassembly is determined by the relative amount of RhoA activation/deactivation, or advection/dissociation. It is unclear whether disassembly is occurring at a constant rate (blue curve 1) or spikes after pulse assembly (blue curve 2).

Mechanisms for actomyosin pulsing

Actomyosin contractility is regulated by the small GTPase RhoA. RhoA in turn is regulated by GTPase-activating proteins (GAPs) and guanine nucleotide exchange factors (GEFs), which respectively promote the inactive GDP-bound or active GTP-

bound states of RhoA (Ridley, 2015). Two RhoA effectors that are particularly important for contraction are the formin Diaphanous (Dia), which nucleates/elongates unbranched F-actin, and Rho-Kinase (ROCK), which activates Myo2 through direct phosphorylation of the myosin regulatory light chain (Amano et al., 1996), and indirectly through inhibition of myosin phosphatase (Kimura et al., 1996). Importantly, actomyosin contractility and pulsing has only been observed with Myo2, and not other non-contractile myosins. Phosphorylation of the regulatory light chain assembles myosin into bipolar filaments, which are capable of binding and contracting F-actin (Sellers, 1991). Starting with this well-established parts list, the past five years have seen a growing effort to determine a molecular mechanism for actomyosin pulsing.

ROCK, “active” RhoA, and even a RhoGEF (*Drosophila* RhoGEF2) have all been observed to pulse in *Drosophila* epithelia (Munjal et al., 2015; Vasquez et al., 2014). This suggested the possibility that there is dynamic regulation of the RhoA GTPase. Such dynamics would require a negative regulator of RhoA. In the *Drosophila* ventral furrow, negative regulation was recently found to be mediated by a RhoGAP, C-GAP (Mason et al., 2016). In this system, the peak in RhoGEF2 signal precedes the peak Myo2 signal by about 10 seconds. C-GAP depletion prevents the Myo2 disappearance after increases in Myo2. C-GAP overexpression causes myosin to disappear completely after a Myo2 pulse. Thus, in the ventral furrow, RhoGEF2 appears to initiate pulses, presumably by increasing the actomyosin assembly rate, and C-GAP terminates the pulse, either through constant disassembly (Figure 3, curve 1) or by increasing the disassembly rate after assembly (Figure 3, curve 2). Interestingly, removal of C-GAP from the ventral furrow disrupts not only pulsing, but also the spatial organization of

RhoA pathway components (Mason et al., 2016). Future insight into the timing of C-GAP and its mechanism of recruitment will be important for elucidating the mechanism of pulsing. Additionally, it will be important to determine whether negative regulation of RhoA is a conserved mechanism to regulate pulsing dynamics in other cellular and developmental contexts.

A non-mutually exclusive hypothesis, is that actomyosin pulsing is a self-organized processes (Munjal et al., 2015). Pulses could be initiated through a low level of actomyosin activity resulting in “advection” or flow of F-actin, myosin, and membrane associated proteins, such as ROCK, into a cluster (Munjal et al., 2015). Flow of proteins that regulate actomyosin contractility, such as ROCK, would result in a more sustained contraction. Disassembly of the pulse would occur through delayed negative feedback, possibly through the recruitment of myosin phosphatase to advection-assembled actomyosin structures (Munjal et al., 2015; Vasquez et al., 2014). In this model, pulsing results from the balance between a protein’s advective flow into the protein cluster and the dissociation of that protein from the membrane. A pulse cycle would represent the net flow of a protein into a cluster, slowing of this flow, and then dissociation outcompeting flow, which would represent pulse disassembly (Figure 3). Although such a mechanism can explain pulsing without the need for active regulation by RhoA, it is possible that advection could also mediate the behavior of proteins that regulate RhoA (i.e. GEFs and GAPs).

Evidence from other systems suggests that RhoA activity is dynamic and that RhoA dynamics mediates actomyosin dynamics. In mitosis, RhoA flux through the GTP hydrolysis cycle regulates the formation of the actomyosin cytokinetic furrow (Miller and

Bement, 2009; Zanin et al., 2013). In addition, bursts or “flares” of Rho-GTP correlate with bursts of F-actin accumulation at apical adherens junctions in interphase cells depleted of the RhoA-binding protein anillin (Reyes et al., 2014), and cortical waves of RhoA activity have been observed after anaphase of frog or echinoderm embryonic cells (Bement et al., 2015). The protrusion-retraction cycle at the leading edge of migrating fibroblasts requires negative regulation of RhoA through Protein Kinase A (PKA) induced recruitment of Rho GDP-dissociation inhibitor (RhoGDI) (Tkachenko et al., 2011). Overall, these studies suggest that actomyosin contractile systems with behaviors such as pulsing, cycling, or waves are associated with dynamic regulation of RhoA, which could serve as a “pacemaker”. Processes such as advection could serve as a source of delayed negative feedback to regulate RhoA, for instance by recruiting an inhibitor of RhoA. Identifying further regulators of RhoA activity and how they are recruited is thus likely to be important for understanding what regulates the timing of different pulsing behaviors.

Concluding remarks

Pulsing has been observed and characterized in a growing number of biological contexts. We suspect that actomyosin pulsing will be observed in even more cases as fluorescent actin and Myo2 probes are visualized in more tissues. Though the mechanism of pulsing is not fully understood, actomyosin pulses have already been implicated in cell shape change by correlating the appearance of pulses with cell shape change. Current challenges are to determine the biological functions and the molecular mechanism(s) governing this widespread phenomenon.

In addition to exploring the models we review here, we see several opportunities for productive inquiry. First, it will be important to determine the function of actomyosin pulsing in additional systems. This requires careful analysis of mutants in genes that promote actomyosin assembly and disassembly, which could include: 1) actin regulators, 2) myosin phosphatase or genes that regulate Myo2 filament assembly, such as Protein Kinase C and Casein Kinase II, which phosphorylate the Myo2 heavy chain (Murakami et al., 1998), and 3) RhoA inhibitors, such as GAPs, RhoGDI, ubiquitin ligases, and kinases (Ridley, 2001). Second, we propose adding additional complexity to reconstituted actomyosin assemblies to determine the molecular mechanism by which dynamic cellular actomyosin networks generate and sustain force. Specifically, it is important to determine how actin filament turnover, myosin minifilament turnover, and adherens-junction-like boundaries affect the assembly and force-generating capacity of *in vitro* networks assembled with purified components. Third, because actomyosin dynamics have been correlated in several contexts with cell shape change, we look forward to experimental approaches that build functional evidence for this connection. For these experiments, we advocate the use of point-mutants with precise effects on biochemical activities, rather than global inhibition of myosin or actin with drugs, null mutants, or knockdown experiments. Fourth, we still do not understand what directs the location of an actomyosin pulse. Fifth, we advocate searches for proteins outside of the core actomyosin machinery, for example aPKC (David et al., 2013) and Crumbs (Flores-Benitez et al., 2015), that impinge on actomyosin dynamics. Finally, we are excited about using the newest generation of *in vivo* biomechanical sensors, like lipid droplets embedded in epithelia (Campàs et al., 2014) or single-walled carbon

nanotubules (Tan et al., 2016) that can provide direct measurements of the material properties of cells and tissues experiencing dynamic actomyosin contractility. These tools will allow researchers to determine the relationship between actomyosin dynamics and cell and tissue forces and determine how tissue form emerges from dynamic and heterogeneous cell behaviors.

Finally, one of the areas for which actomyosin pulsing presents an exciting explanatory potential is in regard to neural tube defects, which represent a relatively common human birth defect (Wallingford et al., 2013). Pulsatile actin dynamics were recently observed in *Xenopus* neural tube closure (Christodoulou and Skourides, 2015), and disrupting pulses by elevating cytosolic Ca^{2+} levels promoted neural tube defects. It was separately observed that the actin severing protein, cofilin, is important for neural tube closure (Escuin et al., 2015; Gurniak et al., 2005; Mahaffey et al., 2013). This suggests that actin turnover, and possibly actomyosin pulsing, is critical for neural tube morphogenesis. Because of the evidence from *Drosophila* tissue folding, it would be productive to investigate epithelial integrity during folding of the neural tube in these cases where actomyosin turnover is defective.

Acknowledgments

We thank Soline Chanet, Claudia G. Vasquez, Shicong Xie, and Michael Mak for helpful discussions and comments.

References

Abdi, K.M., and Bennett, V. (2008). Adducin promotes micrometer-scale organization of beta2-spectrin in lateral membranes of bronchial epithelial cells. Mol. Biol. Cell *19*, 536–545.

Akin, O., and Mullins, R.D. (2008). Capping Protein Increases the Rate of Actin-Based Motility by Promoting Filament Nucleation by the Arp2/3 Complex. Cell *133*, 841–851.

Ali, F., Paré, P.D., and Seow, C.Y. (2011). Models of contractile units and their assembly in smooth muscle. Canadian Journal of Physiology and Pharmacology *83*, 825–831.

Allard, J., and Mogilner, A. (2013). Traveling waves in actin dynamics and cell motility. Curr. Opin. Cell Biol. *25*, 107–115.

Amano, M., Ito, M., Kimura, K., Fukata, Y., Chihara, K., Nakano, T., Matsuura, Y., and Kaibuchi, K. (1996). Phosphorylation and Activation of Myosin by Rho-associated Kinase (Rho-kinase). Journal of Biological Chemistry *271*, 20246–20249.

Amândio, A.R., Gaspar, P., Whited, J.L., and Janody, F. (2014). Subunits of the Drosophila Actin-Capping Protein Heterodimer Regulate Each Other at Multiple Levels. PLoS ONE *9*, e96326.

Backouche, F., Haviv, L., Groswasser, D., and Bernheim-Groswasser, A. (2006). Active gels: dynamics of patterning and self-organization. Phys Biol *3*, 264–273.

Bai, J., Hartwig, J.H., and Perrimon, N. (2007). SALS, a WH2-domain-containing protein, promotes sarcomeric actin filament elongation from pointed ends during Drosophila muscle growth. Developmental Cell *13*, 828–842.

Bardet, P.-L., Guirao, B., Paoletti, C., Serman, F., Léopold, V., Bosveld, F., Goya, Y., Mirouse, V., Graner, F., and Bellaïche, Y. (2013). PTEN controls junction lengthening and stability during cell rearrangement in epithelial tissue. Developmental Cell *25*, 534–546.

Barrett, K., Leptin, M., and Settleman, J. (1997). The Rho GTPase and a Putative RhoGEF Mediate a Signaling Pathway for the Cell Shape Changes in Drosophila Gastrulation. Cell *91*, 905–915.

Bement, W.M., Leda, M., Moe, A.M., Kita, A.M., Larson, M.E., Golding, A.E., Pfeuti, C., Su, K.-C., Miller, A.L., Goryachev, A.B., et al. (2015). Activator-inhibitor coupling between Rho signalling and actin assembly makes the cell cortex an excitable medium. Nat. Cell Biol. *17*, 1471–1483.

Biro, M., Romeo, Y., Kroschwald, S., Bovellan, M., Boden, A., Tcherkezian, J., Roux, P.P., Charras, G., and Paluch, E.K. (2013). Cell cortex composition and homeostasis

resolved by integrating proteomics and quantitative imaging. Cytoskeleton *70*, 741–754.

Blanchard, G.B., Murugesu, S., Adams, R.J., Martinez-Arias, A., and Gorfinkiel, N. (2010). Cytoskeletal dynamics and supracellular organisation of cell shape fluctuations during dorsal closure. Development *137*, 2743–2752.

Bond, M., and Somlyo, A.V. (1982). Dense bodies and actin polarity in vertebrate smooth muscle. The Journal of Cell Biology *95*, 403–413.

Booth, A.J.R., Blanchard, G.B., Adams, R.J., and Röper, K. (2014). A dynamic microtubule cytoskeleton directs medial actomyosin function during tube formation. Developmental Cell *29*, 562–576.

Bovellan, M., Romeo, Y., Biro, M., Boden, A., Chugh, P., Yonis, A., Vaghela, M., Fritzsche, M., Moulding, D., Thorogate, R., et al. (2014). Cellular control of cortical actin nucleation. Curr. Biol. *24*, 1628–1635.

Brozovich, F.V., Nicholson, C.J., Degen, C.V., Gao, Y.Z., Aggarwal, M., and Morgan, K.G. (2016). Mechanisms of Vascular Smooth Muscle Contraction and the Basis for Pharmacologic Treatment of Smooth Muscle Disorders. Pharmacol. Rev. *68*, 476–532.

Buckley, C.D., Tan, J., Anderson, K.L., Hanein, D., Volkmann, N., Weis, W.I., Nelson, W.J., and Dunn, A.R. (2014). The minimal cadherin-catenin complex binds to actin filaments under force. Science *346*, 1254211–1254211.

Bulgakova, N.A., Grigoriev, I., Yap, A.S., Akhmanova, A., and Brown, N.H. (2013). Dynamic microtubules produce an asymmetric E-cadherin–Bazooka complex to maintain segment boundaries. The Journal of Cell Biology *201*, 887–901.

Caldwell, J.E., Heiss, S.G., Mermall, V., and Cooper, J.A. (1989). Effects of CapZ, an actin-capping protein of muscle, on the polymerization of actin. Biochemistry *28*.

Campàs, O., Mammoto, T., Hasso, S., Sperling, R.A., O'Connell, D., Bischof, A.G., Maas, R., Weitz, D.A., Mahadevan, L., and Ingber, D.E. (2014). Quantifying cell-generated mechanical forces within living embryonic tissues. Nat. Methods *11*, 183–189.

Carreno, S., Kouranti, I., Glusman, E.S., Fuller, M.T., Echard, A., and Payre, F. (2008). Moesin and its activating kinase Slik are required for cortical stability and microtubule organization in mitotic cells. The Journal of Cell Biology *180*, 739–746.

Charras, G.T., Coughlin, M., Mitchison, T.J., and Mahadevan, L. (2008). Life and Times of a Cellular Bleb. Biophys. J. *94*, 1836–1853.

Charras, G.T., Hu, C.-K., Coughlin, M., and Mitchison, T.J. (2006). Reassembly of contractile actin cortex in cell blebs. The Journal of Cell Biology *175*, 477–490.

Chen, X.-Q., Tan, I., Ng, C.H., Hall, C., Lim, L., and Leung, T. (2002). Characterization

of RhoA-binding kinase ROKalpha implication of the pleckstrin homology domain in ROKalpha function using region-specific antibodies. J. Biol. Chem. *277*, 12680–12688.

Chou, T.B., Noll, E., and Perrimon, N. (1993). Autosomal P[ovoD1] dominant female-sterile insertions in Drosophila and their use in generating germ-line chimeras. Development *119*, 1359–1369.

Christodoulou, N., and Skourides, P.A. (2015). Cell-Autonomous Ca(2+) Flashes Elicit Pulsed Contractions of an Apical Actin Network to Drive Apical Constriction during Neural Tube Closure. Cell Reports *13*, 2189–2202.

Clark, K.A., McElhinny, A.S., Beckerle, M.C., and Gregorio, C.C. (2002). Striated muscle cytoarchitecture: an intricate web of form and function. Annu. Rev. Cell Dev. Biol. *18*, 637–706.

Clay, M.R., and Halloran, M.C. (2013). Rho activation is apically restricted by Arhgap1 in neural crest cells and drives epithelial-to-mesenchymal transition. Development *140*, 3198–3209.

Collinet, C., Rauzi, M., Lenne, P.-F., and Lecuit, T. (2015). Local and tissue-scale forces drive oriented junction growth during tissue extension. Nat. Cell Biol. *17*, 1247–1258.

Copp, A.J., Stanier, P., and Greene, N.D. (2013). Neural tube defects: recent advances, unsolved questions, and controversies. The Lancet Neurology *12*, 799–810.

Costa, M., Wilson, E.T., and Wieschaus, E. (1994). A putative cell signal encoded by the folded gastrulation gene coordinates cell shape changes during Drosophila gastrulation. Cell *76*, 1075–1089.

Costes, S.V., Daelemans, D., Cho, E.H., Dobbin, Z., Pavlakis, G., and Lockett, S. (2004). Automatic and quantitative measurement of protein-protein colocalization in live cells. Biophys. J. *86*, 3993–4003.

Cox Paulson, E., Cannataro, V., Gallagher, T., Hoffman, C., Mantione, G., Mcintosh, M., Silva, M., Vissichelli, N., Walker, R., Simske, J., et al. (2014). The minus-end actin capping protein, UNC-94/tropomodulin, regulates development of the Caenorhabditis elegans intestine. Developmental Dynamics *243*, 753–764.

Cox-Paulson, E.A., Walck-Shannon, E., Lynch, A.M., Yamashiro, S., Zaidel-Bar, R., Eno, C.C., Ono, S., and Hardin, J. (2012). Tropomodulin Protects α-Catenin-Dependent Junctional-Actin Networks under Stress during Epithelial Morphogenesis. Current Biology *22*, 1500–1505.

Cunningham, C.C., Gorlin, J.B., Kwiatkowski, D.J., Hartwig, J.H., Janmey, P.A., Byers, H.R., and Stossel, T.P. (1992). Actin-binding protein requirement for cortical stability and efficient locomotion. Science *255*, 325–327.

Dai, J., and Sheetz, M.P. (1999). Membrane Tether Formation from Blebbing Cells.

Biophys. J. *77*, 3363–3370.

David, D.J.V., Tishkina, A., and Harris, T.J.C. (2010). The PAR complex regulates pulsed actomyosin contractions during amnioserosa apical constriction in Drosophila. Development *137*, 1645–1655.

David, D.J.V., Wang, Q., Feng, J.J., and Harris, T.J.C. (2013). Bazooka inhibits aPKC to limit antagonism of actomyosin networks during amnioserosa apical constriction. Development *140*, 4719–4729.

Dawes-Hoang, R.E., Parmar, K.M., Christiansen, A.E., Phelps, C.B., Brand, A.H., and Wieschaus, E.F. (2005). folded gastrulation, cell shape change and the control of myosin localization. Development *132*, 4165–4178.

Desai, R., Sarpal, R., Ishiyama, N., Pellikka, M., Ikura, M., and Tepass, U. (2013). Monomeric [alpha]-catenin links cadherin to the actin cytoskeleton. Nat. Cell Biol. *15*, 261–273.

Dubreuil, R.R., Frankel, J., Wang, P., Howrylak, J., Kappil, M., and Grushko, T.A. (1998). Mutations of alpha spectrin and labial block cuprophilic cell differentiation and acid secretion in the middle midgut of Drosophila larvae. Developmental Biology *194*, 1–11.

Edwards, M., Zwolak, A., Schafer, D.A., Sept, D., Dominguez, R., and Cooper, J.A. (2014). Capping protein regulators fine-tune actin assembly dynamics. Nat. Rev. Mol. Cell Biol. *15*, 677–689.

Ennomani, H., Letort, G., Guérin, C., Martiel, J.-L., Cao, W., Nedelec, F., La Cruz, De, E.M., Théry, M., and Blanchoin, L. (2016). Architecture and Connectivity Govern Actin Network Contractility. Current Biology *26*, 616–626.

Eto, M., Ohmori, T., Suzuki, M., Furuya, K., and Morita, F. (1995). A Novel Protein Phosphatase-1 Inhibitory Protein Potentiated by Protein Kinase C. Isolation from Porcine Aorta Media and Characterization. J Biochem *118*, 1104–1107.

Fay, F.S., Fujiwara, K., Rees, D.D., and Fogarty, K.E. (1983). Distribution of alpha-actinin in single isolated smooth muscle cells. The Journal of Cell Biology *96*, 783–795.

Fernandez-Gonzalez, R., and Zallen, J.A. (2011). Oscillatory behaviors and hierarchical assembly of contractile structures in intercalating cells. Phys Biol *8*, 045005.

Fievet, B.T., Gautreau, A., Roy, C., Del Maestro, L., Mangeat, P., Louvard, D., and Arpin, M. (2004). Phosphoinositide binding and phosphorylation act sequentially in the activation mechanism of ezrin. The Journal of Cell Biology *164*, 653–659.

Fischer, R.S., and Fowler, V.M. (2003). Tropomodulins: life at the slow end. Trends in Cell Biology *13*, 593–601.

Flanagan, L.A., Chou, J., Falet, H., Neujahr, R., Hartwig, J.H., and Stossel, T.P. (2001). Filamin A, the Arp2/3 complex, and the morphology and function of cortical actin filaments in human melanoma cells. The Journal of Cell Biology *155*, 511–517.

Fosgerau, K., and Hoffmann, T. (2015). Peptide therapeutics: current status and future directions. Drug Discovery Today *20*, 122–128.

Fowler, V.M., Sussmann, M.A., Miller, P.G., Flucher, B.E., and Daniels, M.P. (1993). Tropomodulin is associated with the free (pointed) ends of the thin filaments in rat skeletal muscle. The Journal of Cell Biology *120*, 411–420.

Fox, D.T., and Peifer, M. (2007). Abelson kinase (Abl) and RhoGEF2 regulate actin organization during cell constriction in Drosophila. Development *134*, 567–578.

Fritzsche, M., Erlenkämper, C., Moeendarbary, E., Charras, G., and Kruse, K. (2016). Actin kinetics shapes cortical network structure and mechanics. Sci Adv *2*, e1501337–e1501337.

Fukata, Y., Kaibuchi, K., and Amano, M. (2001). Rho–Rho-kinase pathway in smooth muscle contraction and cytoskeletal reorganization of non-muscle cells. Trends in Pharmacological Sciences *22*, 32–39.

Gardel, M.L., Sabass, B., Ji, L., Danuser, G., Schwarz, U.S., and Waterman, C.M. (2008). Traction stress in focal adhesions correlates biphasically with actin retrograde flow speed. The Journal of Cell Biology *183*, 999–1005.

Gelbart, M.A., He, B., Martin, A.C., Thiberge, S.Y., Wieschaus, E.F., and Kaschube, M. (2012). Volume conservation principle involved in cell lengthening and nucleus movement during tissue morphogenesis. Proc. Natl. Acad. Sci. U.S.a. *109*, 19298–19303.

Gokhin, D.S., Ochala, J., Domenighetti, A.A., and Fowler, V.M. (2015). Tropomodulin 1 directly controls thin filament length in both wild-type and tropomodulin 4-deficient skeletal muscle. Development *142*, 4351–4362.

Goll, D.E., Dayton, W.R., Singh, I., and Robson, R.M. (1991). Studies of the alpha-actinin/actin interaction in the Z-disk by using calpain. J. Biol. Chem. *266*, 8501–8510.

Goode, B.L., and Eck, M.J. (2007). Mechanism and function of formins in the control of actin assembly. Annu. Rev. Biochem. *76*, 593–627.

Gorfinkiel, N. (2016). From actomyosin oscillations to tissue-level deformations. Developmental Dynamics *245*, 268–275.

Hashimoto, Y., and Soderling, T.R. (1990). Phosphorylation of smooth muscle myosin light chain kinase by Ca2+/calmodulin-dependent protein kinase II: Comparative study of the phosphorylation sites. Archives of Biochemistry and Biophysics *278*, 41–45.

He, B., Doubrovinski, K., Polyakov, O., and Wieschaus, E. (2014). Apical constriction drives tissue-scale hydrodynamic flow to mediate cell elongation. Nature *508*, 392–396.

He, L., Wang, X., Tang, H.L., and Montell, D.J. (2010). Tissue elongation requires oscillating contractions of a basal actomyosin network. Nat. Cell Biol. *12*, 1133–1142.

Herrera, A.M., McParland, B.E., Bienkowska, A., Tait, R., Paré, P.D., and Seow, C.Y. (2005). `Sarcomeres' of smooth muscle: functional characteristics and ultrastructural evidence. J. Cell. Sci. *118*, 2381–2392.

Hildebrand, J.D., and Soriano, P. (1999). Shroom, a PDZ domain-containing actin-binding protein, is required for neural tube morphogenesis in mice. Cell *99*, 485–497.

Hirokawa, N., T C Keller, 3., Chasan, R., and Mooseker, M.S. (1983). Mechanism of brush border contractility studied by the quick-freeze, deep-etch method. The Journal of Cell Biology *96*, 1325–1336.

Homem, C.C.F., and Peifer, M. (2008). Diaphanous regulates myosin and adherens junctions to control cell contractility and protrusive behavior during morphogenesis. Development *135*, 1005–1018.

Horowitz, A., Menice, C.B., Laporte, R., and Morgan, K.G. (1996). Mechanisms of smooth muscle contraction. Physiological Reviews *76*, 967–1003.

Hu, R.J., Moorthy, S., and Bennett, V. (1995). Expression of functional domains of beta G-spectrin disrupts epithelial morphology in cultured cells. The Journal of Cell Biology *128*, 1069–1080.

Huxley, A.F., and Niedergerke, R. (1954). Structural changes in muscle during contraction; interference microscopy of living muscle fibres. Nature *173*, 971–973.

Huxley, H., and Hanson, J. (1954). Changes in the Cross-Striations of Muscle during Contraction and Stretch and their Structural Interpretation. Nature *173*, 973–976.

Isenberg, G., Aebi, U., and Pollard, T.D. (1980). An actin-binding protein from Acanthamoeba regulates actin filament polymerization and interactions. Nature *288*, 455–459.

Ito, M., Nakano, T., Erdödi, F., and Hartshorne, D.J. (2004). Myosin phosphatase: Structure, regulation and function. Mol Cell Biochem *259*, 197–209.

Janody, F., and Treisman, J.E. (2006). Actin capping protein α maintains vestigial-expressing cells within the Drosophila wing disc epithelium. Development *133*, 3349–3357.

Jezowska, B., Fernández, B.G., Amândio, A.R., Duarte, P., Mendes, C., Brás-Pereira, C., and Janody, F. (2011). A dual function of Drosophila capping protein on DE-cadherin maintains epithelial integrity and prevents JNK-mediated apoptosis.

Developmental Biology *360*, 143–159.

Jodoin, J.N., Coravos, J.S., Chanet, S., Vasquez, C.G., Tworoger, M., Kingston, E.R., Perkins, L.A., Perrimon, N., and Martin, A.C. (2015). Stable Force Balance between Epithelial Cells Arises from F-Actin Turnover. Developmental Cell *35*, 685–697.

Kaiser, H.W., O'Keefe, E., and Bennett, V. (1989). Adducin: Ca++-dependent association with sites of cell-cell contact. The Journal of Cell Biology *109*, 557–569.

Kamisoyama, H., Araki, Y., and Ikebe, M. (1994). Mutagenesis of the phosphorylation site (serine 19) of smooth muscle myosin regulatory light chain and its effects on the properties of myosin. Biochemistry *33*, 840–847.

Karagiosis, S.A., and Ready, D.F. (2004). Moesin contributes an essential structural role in Drosophila photoreceptor morphogenesis. Development *131*, 725–732.

Kargacin, G.J., Cooke, P.H., Abramson, S.B., and Fay, F.S. (1989). Periodic organization of the contractile apparatus in smooth muscle revealed by the motion of dense bodies in single cells. The Journal of Cell Biology *108*, 1465–1475.

Kasza, K.E., and Zallen, J.A. (2011). Dynamics and regulation of contractile actin–myosin networks in morphogenesis. Curr. Opin. Cell Biol. *23*, 30–38.

Katoh, K., Kano, Y., Amano, M., Onishi, H., Kaibuchi, K., and Fujiwara, K. (2001). Rho-kinase--mediated contraction of isolated stress fibers. The Journal of Cell Biology *153*, 569–584.

Katz, A.M. (2010). Physiology of the Heart (Philadelphia: Lippincott Williams & Wilkins).

Kim, H.Y., and Davidson, L.A. (2011). Punctuated actin contractions during convergent extension and their permissive regulation by the non-canonical Wnt-signaling pathway. J. Cell. Sci. *124*, 635–646.

Kimura, K., Ito, M., Amano, M., Chihara, K., Fukata, Y., Nakafuku, M., Yamamori, B., Feng, J., Nakano, T., Okawa, K., et al. (1996). Regulation of myosin phosphatase by Rho and Rho-associated kinase (Rho-kinase). Science *273*, 245–248.

Knipe, R.S., Tager, A.M., and Liao, J.K. (2015). The Rho kinases: critical mediators of multiple profibrotic processes and rational targets for new therapies for pulmonary fibrosis. Pharmacol. Rev. *67*, 103–117.

Knudsen, K.A., Soler, A.P., Johnson, K.R., and Wheelock, M.J. (1995). Interaction of alpha-actinin with the cadherin/catenin cell-cell adhesion complex via alpha-catenin. The Journal of Cell Biology *130*, 67–77.

Kobielak, A., Pasolli, H.A., and Fuchs, E. (2003). Mammalian formin-1 participates in adherens junctions and polymerization of linear actin cables. Nat. Cell Biol. *6*, 21–30.

Koride, S., He, L., Xiong, L.-P., Lan, G., Montell, D.J., and Sun, S.X. (2014). Mechanochemical regulation of oscillatory follicle cell dynamics in the developing Drosophila egg chamber. Mol. Biol. Cell *25*, 3709–3716.

Kovacs, E.M., Goodwin, M., Ali, R.G., Paterson, A.D., and Yap, A.S. (2002). Cadherin-directed actin assembly: E-cadherin physically associates with the Arp2/3 complex to direct actin assembly in nascent adhesive contacts. Current Biology *12*, 379–382.

Kovacs, E.M., Verma, S., Ali, R.G., Ratheesh, A., Hamilton, N.A., Akhmanova, A., and Yap, A.S. (2011). N-WASP regulates the epithelial junctional actin cytoskeleton through a non-canonical post-nucleation pathway. Nat. Cell Biol. *13*, 934–943.

Kölsch, V., Seher, T., Fernandez-Ballester, G.J., Serrano, L., and Leptin, M. (2007). Control of Drosophila gastrulation by apical localization of adherens junctions and RhoGEF2. Science *315*, 384–386.

Köster, D.V., Husain, K., Iljazi, E., Bhat, A., Bieling, P., Mullins, R.D., Rao, M., and Mayor, S. (2016). Actomyosin dynamics drive local membrane component organization in an in vitro active composite layer. Proc. Natl. Acad. Sci. U.S.a. *113*, E1645–E1654.

Kuhlman, P.A., Hughes, C.A., Bennett, V., and Fowler, V.M. (1996). A new function for adducin. Calcium/calmodulin-regulated capping of the barbed ends of actin filaments. J. Biol. Chem. *271*, 7986–7991.

Kunda, P., Pelling, A.E., Liu, T., and Baum, B. (2008). Moesin Controls Cortical Rigidity, Cell Rounding, and Spindle Morphogenesis during Mitosis. Current Biology *18*, 91–101.

Kunda, P., Rodrigues, N.T.L., Moeendarbary, E., Liu, T., Ivetic, A., Charras, G., and Baum, B. (2012). PP1-Mediated Moesin Dephosphorylation Couples Polar Relaxation to Mitotic Exit. Current Biology *22*, 231–236.

Lan, B., Deng, L., Donovan, G.M., Chin, L.Y.M., Syyong, H.T., Wang, L., Zhang, J., Pascoe, C.D., Norris, B.A., Liu, J.C.-Y., et al. (2015). Force maintenance and myosin filament assembly regulated by Rho-kinase in airway smooth muscle. *308*, L1–L10.

Lecuit, T., Lenne, P.-F., and Munro, E. (2011). Force Generation, Transmission, and Integration during Cell and Tissue Morphogenesis. Annu. Rev. Cell Dev. Biol. *27*, 157–184.

Lee, J.K., Brandin, E., Branton, D., and Goldstein, L.S. (1997). alpha-Spectrin is required for ovarian follicle monolayer integrity in Drosophila melanogaster. Development *124*, 353–362.

Lee, J.K., Coyne, R.S., Dubreuil, R.R., Goldstein, L.S., and Branton, D. (1993). Cell shape and interaction defects in alpha-spectrin mutants of Drosophila melanogaster. The Journal of Cell Biology *123*, 1797–1809.

Lee, J.-Y., and Harland, R.M. (2007). Actomyosin contractility and microtubules drive

apical constriction in Xenopus bottle cells. Developmental Biology *311*, 40–52.

Lee, S.-K., and Thomas, G.H. (2011). Rac1 modulation of the apical domain is negatively regulated by β (Heavy)-spectrin. Mech. Dev. *128*, 116–128.

Leerberg, J.M., Gomez, G.A., Verma, S., Moussa, E.J., Wu, S.K., Priya, R., Hoffman, B.D., Grashoff, C., Schwartz, M.A., and Yap, A.S. (2014). Tension-sensitive actin assembly supports contractility at the epithelial zonula adherens. Curr. Biol. *24*, 1689–1699.

Lehman, W. (2016). Thin Filament Structure and the Steric Blocking Model. Compr Physiol *6*, 1043–1069.

Leptin, M. (1991). twist and snail as positive and negative regulators during Drosophila mesoderm development. Genes Dev. *5*, 1568–1576.

Leptin, M., and Grunewald, B. (1990). Cell shape changes during gastrulation in Drosophila. Development *110*, 73–84.

Li, X., Matsuoka, Y., and Bennett, V. (1998). Adducin preferentially recruits spectrin to the fast growing ends of actin filaments in a complex requiring the MARCKS-related domain and a newly defined oligomerization domain. J. Biol. Chem. *273*, 19329–19338.

Lieber, R.L. (2002). Skeletal Muscle Structure, Function, and Plasticity (Philadelphia: Lippincott Williams & Wilkins).

Liem, R.K.H. (2016). Cytoskeletal Integrators: The Spectrin Superfamily. Cold Spring Harb Perspect Biol *8*, a018259.

Littlefield, R., Almenar-Queralt, A., Fowler, V.M., and Fowler, V.M. (2001). Actin dynamics at pointed ends regulates thin filament length in striated muscle. Nat. Cell Biol. *3*, 544–551.

Luo, W., Lieu, Z.Z., Manser, E., Bershadsky, A.D., and Sheetz, M.P. (2016). Formin DAAM1 Organizes Actin Filaments in the Cytoplasmic Nodal Actin Network. PLoS ONE *11*, e0163915.

Luther, P.K. (2009). The vertebrate muscle Z-disc: sarcomere anchor for structure and signalling. J. Muscle Res. Cell. Motil. *30*, 171–185.

Machnicka, B., Grochowalska, R., Bogusławska, D.M., Sikorski, A.F., and Lecomte, M.C. (2012). Spectrin-based skeleton as an actor in cell signaling. Cell. Mol. Life Sci. *69*, 191–201.

Maître, J.-L., Niwayama, R., Turlier, H., Nedelec, F., and Hiiragi, T. (2015). Pulsatile cell-autonomous contractility drives compaction in the mouse embryo. Nat. Cell Biol. *17*, 849–855.

Mak, M., Zaman, M.H., Kamm, R.D., and Kim, T. (2016). Interplay of active processes modulates tension and drives phase transition in self-renewing, motor-driven cytoskeletal networks. Nature Communications *7*, 10323.

Manders, E., Verbeek, F.J., and Aten, J.A. (1993). Measurement of co-localization of objects in dual-colour confocal images. Journal of Microscopy *169*, 375–382.

Manning, A.J., Peters, K.A., Peifer, M., and Rogers, S.L. (2013). Regulation of epithelial morphogenesis by the G protein-coupled receptor mist and its ligand fog. Sci Signal *6*, ra98–ra98.

Mardahl-Dumesnil, M., and Fowler, V.M. (2001). Thin filaments elongate from their pointed ends during myofibril assembly in Drosophila indirect flight muscle. The Journal of Cell Biology *155*, 1043–1053.

Martin, A.C., Gelbart, M., Fernandez-Gonzalez, R., Kaschube, M., and Wieschaus, E.F. (2010). Integration of contractile forces during tissue invagination. The Journal of Cell Biology *188*, 735–749.

Martin, A.C., and Goldstein, B. (2014). Apical constriction: themes and variations on a cellular mechanism driving morphogenesis. Development *141*, 1987–1998.

Martin, A.C., Kaschube, M., and Wieschaus, E.F. (2009). Pulsed contractions of an actin-myosin network drive apical constriction. Nature *457*, 495–499.

Mason, F.M., Tworoger, M., and Martin, A.C. (2013). Apical domain polarization localizes actin-myosin activity to drive ratchet-like apical constriction. Nat. Cell Biol. *15*, 926–936.

Mason, F.M., Xie, S., Vasquez, C.G., Tworoger, M., and Martin, A.C. (2016). RhoA GTPase inhibition organizes contraction during epithelial morphogenesis. The Journal of Cell Biology *214*, 603–617.

McKeown, C., Praitis, V., and Austin, J. (1998). sma-1 encodes a betaH-spectrin homolog required for Caenorhabditis elegans morphogenesis. Development *125*, 2087–2098.

Médina, E., Williams, J., Klipfell, E., Zarnescu, D., Thomas, G., and Le Bivic, A. (2002). Crumbs interacts with moesin and beta(Heavy)-spectrin in the apical membrane skeleton of Drosophila. The Journal of Cell Biology *158*, 941–951.

Miller, A.L., and Bement, W.M. (2009). Regulation of cytokinesis by Rho GTPase flux. Nat. Cell Biol. *11*, 71–77.

Mitra, S.K., Hanson, D.A., and Schlaepfer, D.D. (2005). Focal adhesion kinase: in command and control of cell motility. Nat. Rev. Mol. Cell Biol. *6*, 56–68.

Mizuno, T., Amano, M., Kaibuchi, K., and Nishida, Y. (1999). Identification and

characterization of Drosophila homolog of Rho-kinase. Gene *238*, 437–444.

Mohan, S., Rizaldy, R., Das, D., Bauer, R.J., Heroux, A., Trakselis, M.A., Hildebrand, J.D., and Vandemark, A.P. (2012). Structure of Shroom domain 2 reveals a three-segmented coiled-coil required for dimerization, Rock binding, and apical constriction. Mol. Biol. Cell *23*, 2131–2142.

Morgan-Fisher, M., Wewer, U.M., and Yoneda, A. (2013). Regulation of ROCK activity in cancer. J. Histochem. Cytochem. *61*, 185–198.

Muliyil, S., and Narasimha, M. (2014). Mitochondrial ROS regulates cytoskeletal and mitochondrial remodeling to tune cell and tissue dynamics in a model for wound healing. Developmental Cell *28*, 239–252.

Munjal, A., Philippe, J.-M., Munro, E., and Lecuit, T. (2015). A self-organized biomechanical network drives shape changes during tissue morphogenesis. Nature *524*, 351–355.

Munro, E., Nance, J., and Priess, J.R. (2004). Cortical flows powered by asymmetrical contraction transport PAR proteins to establish and maintain anterior-posterior polarity in the early C. elegans embryo. Developmental Cell *7*, 413–424.

Murakami, N., Chauhan, V.P., and Elzinga, M. (1998). Two nonmuscle myosin II heavy chain isoforms expressed in rabbit brains: filament forming properties, the effects of phosphorylation by protein kinase C and casein kinase II, and location of the phosphorylation sites. Biochemistry *37*, 1989–2003.

Murrell, M.P., and Gardel, M.L. (2012). F-actin buckling coordinates contractility and severing in a biomimetic actomyosin cortex. Proc. Natl. Acad. Sci. U.S.a. *109*, 20820–20825.

Murrell, M., Murrell, M., Oakes, P.W., Lenz, M., and Gardel, M.L. (2015). Forcing cells into shape: the mechanics of actomyosin contractility. Nat. Rev. Mol. Cell Biol. *16*, 486–498.

Nagafuchi, A. (2001). Molecular architecture of adherens junctions. Curr. Opin. Cell Biol. *13*, 600–603.

Naydenov, N.G., and Ivanov, A.I. (2010). Adducins regulate remodeling of apical junctions in human epithelial cells. Mol. Biol. Cell *21*, 3506–3517.

Neisch, A.L., and Fehon, R.G. (2011). Ezrin, Radixin and Moesin: key regulators of membrane-cortex interactions and signaling. Curr. Opin. Cell Biol. *23*, 377–382.

Neisch, A.L., Formstecher, E., and Fehon, R.G. (2013). Conundrum, an ARHGAP18 orthologue, regulates RhoA and proliferation through interactions with Moesin. Mol. Biol. Cell *24*, 1420–1433.

Newell-Litwa, K.A., Newell-Litwa, K.A., Badoual, M., Badoual, M., Asmussen, H., Asmussen, H., Patel, H., Patel, H., Whitmore, L., Whitmore, L., et al. (2015). ROCK1 and 2 differentially regulate actomyosin organization to drive cell and synaptic polarity. The Journal of Cell Biology *210*, 225–242.

Ng, B.F., Selvaraj, G.K., Santa-Cruz Mateos, C., Grosheva, I., Alvarez-Garcia, I., Martín-Bermudo, M.D., and Palacios, I.M. (2016). α-Spectrin and integrins act together to regulate actomyosin and columnarization, and to maintain a monolayered follicular epithelium. Development *143*, 1388–1399.

Nishimura, T., and Takeichi, M. (2008). Shroom3-mediated recruitment of Rho kinases to the apical cell junctions regulates epithelial and neuroepithelial planar remodeling. Development *135*, 1493–1502.

Norman, K.R., and Moerman, D.G. (2002). α spectrin is essential for morphogenesis and body wall muscle formation in Caenorhabditis elegans. The Journal of Cell Biology *157*, 665–677.

Papa, I., Astier, C., Kwiatek, O., Raynaud, F., Bonnal, C., Lebart, M.-C., Roustan, C., and Benyamin, Y. (1999). Alpha actinin–CapZ, an anchoring complex for thin filaments in Z-line. J Muscle Res Cell Motil *20*, 187–197.

Pappas, C.T., Bhattacharya, N., and Cooper, J.A. (2008). Pappas: Nebulin interacts with CapZ and regulates... - Google Scholar (Molecular biology of …).

Pfister, K., Shook, D.R., Chang, C., Keller, R., and Skoglund, P. (2016). Molecular model for force production and transmission during vertebrate gastrulation. Development *143*, 715–727.

Phng, L.-K., Gebala, V., Bentley, K., Philippides, A., Wacker, A., Mathivet, T., Sauteur, L., Stanchi, F., Belting, H.-G., Affolter, M., et al. (2015). Formin-mediated actin polymerization at endothelial junctions is required for vessel lumen formation and stabilization. Developmental Cell *32*, 123–132.

Piekny, A.J., and Mains, P.E. (2002). Rho-binding kinase (LET-502) and myosin phosphatase (MEL-11) regulate cytokinesis in the early Caenorhabditis elegans embryo. J. Cell. Sci. *115*, 2271–2282.

Polesello, C., and Payre, F. (2004). Small is beautiful: what flies tell us about ERM protein function in development. Trends in Cell Biology *14*, 294–302.

Polesello, C., Delon, I., Valenti, P., Ferrer, P., and Payre, F. (2002). Dmoesin controls actin-based cell shape and polarity during Drosophila melanogaster oogenesis. Nat. Cell Biol. *4*, 782–789.

Pollard, T.D., and Cooper, J.A. (1984). Quantitative analysis of the effect of Acanthamoeba profilin on actin filament nucleation and elongation. Biochemistry *23*, 6631–6641.

Polyakov, O., He, B., Swan, M., Shaevitz, J.W., Kaschube, M., and Wieschaus, E. (2014). Passive mechanical forces control cell-shape change during Drosophila ventral furrow formation. Biophys. J. *107*, 998–1010.

Pradhan, D., Lombardo, C.R., Roe, S., Rimm, D.L., and Morrow, J.S. (2001). alpha - Catenin binds directly to spectrin and facilitates spectrin-membrane assembly in vivo. J. Biol. Chem. *276*, 4175–4181.

Praitis, V., Ciccone, E., and Austin, J. (2005). SMA-1 spectrin has essential roles in epithelial cell sheet morphogenesis in C. elegans. Developmental Biology *283*, 157–170.

Priya, R., Gomez, G.A., Budnar, S., Verma, S., Cox, H.L., Hamilton, N.A., and Yap, A.S. (2015). Feedback regulation through myosin II confers robustness on RhoA signalling at E-cadherin junctions. Nat. Cell Biol. *17*, 1282–1293.

Rajfur, Z., Roy, P., Otey, C., Romer, L., and Jacobson, K. (2002). Dissecting the link between stress fibres and focal adhesions by CALI with EGFP fusion proteins. Nat. Cell Biol. *4*, 286–293.

Rao, J.N., Madasu, Y., and Dominguez, R. (2014). Mechanism of actin filament pointed-end capping by tropomodulin. Science *345*, 463–467.

Rao, M.V., and Zaidel-Bar, R. (2016). Formin-mediated actin polymerization at cell-cell junctions stabilizes E-cadherin and maintains monolayer integrity during wound repair. Mol. Biol. Cell *27*, 2844–2856.

Ratheesh, A., Gomez, G.A., Priya, R., Verma, S., Kovacs, E.M., Jiang, K., Brown, N.H., Akhmanova, A., Stehbens, S.J., and Yap, A.S. (2012). Centralspindlin and [alpha]-catenin regulate Rho signalling at the epithelial zonula adherens. Nat. Cell Biol. *14*, 818–828.

Rauzi, M., Krzic, U., Saunders, T.E., Krajnc, M., Ziherl, P., Hufnagel, L., and Leptin, M. (2015). Embryo-scale tissue mechanics during Drosophila gastrulation movements. Nature Communications *6*, 8677.

Rauzi, M., Lenne, P.-F., and Lecuit, T. (2010). Planar polarized actomyosin contractile flows control epithelial junction remodelling. Nature *468*, 1110–1114.

Reyes, C.C., Jin, M., Breznau, E.B., Espino, R., Delgado-Gonzalo, R., Goryachev, A.B., and Miller, A.L. (2014). Anillin Regulates Cell-Cell Junction Integrity by Organizing Junctional Accumulation of Rho-GTP and Actomyosin. Current Biology *24*, 1263–1270.

Reymann, A.-C., Boujemaa-Paterski, R., Martiel, J.-L., Guérin, C., Cao, W., Chin, H.F., La Cruz, De, E.M., Théry, M., and Blanchoin, L. (2012). Actin Network Architecture Can Determine Myosin Motor Activity. Science *336*, 1310–1314.

Riddick, N., Ohtani, K.-I., and Surks, H.K. (2008). Targeting by myosin phosphatase-

RhoA interacting protein mediates RhoA/ROCK regulation of myosin phosphatase. J. Cell. Biochem. *103*, 1158–1170.

Ridley, A.J., and Hall, A. (1992). The small GTP-binding protein rho regulates the assembly of focal adhesions and actin stress fibers in response to growth factors. Cell *70*, 389–399.

Ridley, A.J. (2015). Rho GTPase signalling in cell migration. Curr. Opin. Cell Biol. *36*, 103–112.

Riento, K., and Ridley, A.J. (2003). ROCKs: multifunctional kinases in cell behaviour. Nat. Rev. Mol. Cell Biol. *4*, 446–456.

Rogers, S.L., Wiedemann, U., Häcker, U., Turck, C., and Vale, R.D. (2004). Drosophila RhoGEF2 Associates with Microtubule Plus Ends in an EB1-Dependent Manner. Current Biology *14*, 1827–1833.

Roh-Johnson, M., Shemer, G., Higgins, C.D., McClellan, J.H., Werts, A.D., Tulu, U.S., Gao, L., Betzig, E., Kiehart, D.P., and Goldstein, B. (2012). Triggering a cell shape change by exploiting preexisting actomyosin contractions. Science *335*, 1232–1235.

Roubinet, C., Decelle, B., Chicanne, G., Dorn, J.F., Payrastre, B., Payre, F., and Carreno, S. (2011). Molecular networks linked by Moesin drive remodeling of the cell cortex during mitosis. The Journal of Cell Biology *195*, 99–112.

Röper, K. (2012). Anisotropy of Crumbs and aPKC drives myosin cable assembly during tube formation. Developmental Cell *23*, 939–953.

Sabino, D., Gogendeau, D., Gambarotto, D., Nano, M., Pennetier, C., Dingli, F., Arras, G., Loew, D., and Basto, R. (2015). Moesin Is a Major Regulator of Centrosome Behavior in Epithelial Cells with Extra Centrosomes. Current Biology *25*, 879–889.

Salbreux, G., Charras, G., and Paluch, E. (2012). Actin cortex mechanics and cellular morphogenesis. Trends in Cell Biology *22*, 536–545.

Saravanan, S., Meghana, C., and Narasimha, M. (2013). Local, cell-nonautonomous feedback regulation of myosin dynamics patterns transitions in cell behavior: a role for tension and geometry? Mol. Biol. Cell *24*, 2350–2361.

Sawyer, J.K., Choi, W., Jung, K.-C., He, L., Harris, N.J., and Peifer, M. (2011). A contractile actomyosin network linked to adherens junctions by Canoe/afadin helps drive convergent extension. Mol. Biol. Cell *22*, 2491–2508.

Saxena, A., Denholm, B., Bunt, S., Bischoff, M., VijayRaghavan, K., and Skaer, H. (2014). Epidermal growth factor signalling controls myosin II planar polarity to orchestrate convergent extension movements during Drosophila tubulogenesis. PLoS Biol. *12*, e1002013.

Schafer, D.A., Mooseker, M.S., and Cooper, J.A. (1992). Localization of capping protein in chicken epithelial cells by immunofluorescence and biochemical fractionation. The Journal of Cell Biology *118*, 335–346.

Schofield, A.V., and Bernard, O. (2013). Rho-associated coiled-coil kinase (ROCK) signaling and disease. Crit. Rev. Biochem. Mol. Biol. *48*, 301–316.

Schutt, C.E., Myslik, J.C., Rozycki, M.D., Goonesekere, N.C., and Lindberg, U. (1993). The structure of crystalline profilin-beta-actin. Nature *365*, 810–816.

Sedzinski, J., Biro, M., Oswald, A., Tinevez, J.-Y., Salbreux, G., and Paluch, E. (2011). Polar actomyosin contractility destabilizes the position of the cytokinetic furrow. Nature *476*, 462–466.

Sellers, J.R. (1991). Regulation of cytoplasmic and smooth muscle myosin. Curr. Opin. Cell Biol. *3*, 98–104.

Shekhar, S., Kerleau, M., Kühn, S., Pernier, J., Romet-Lemonne, G., Jégou, A., and Carlier, M.-F. (2015). Formin and capping protein together embrace the actin filament in a ménage à trois. Nature Communications *6*, 8730.

Sherrard, K.M., and Fehon, R.G. (2015). The transmembrane protein Crumbs displays complex dynamics during follicular morphogenesis and is regulated competitively by Moesin and aPKC. Development *142*, 1869–1878.

Shibuya, M., Suzuki, Y., Sugita, K., Saito, I., Sasaki, T., Takakura, K., Nagata, I., Kikuchi, H., Takemae, T., Hidaka, H., et al. (1992). Effect of AT877 on cerebral vasospasm after aneurysmal subarachnoid hemorrhage. Journal of Neurosurgery *76*, 571–577.

Shimokawa, H., Sunamura, S., and Satoh, K. (2016). RhoA/Rho-Kinase in the Cardiovascular System. Circ. Res. *118*, 352–366.

Silva, M.S.E., Depken, M., Stuhrmann, B., Korsten, M., MacKintosh, F.C., and Koenderink, G.H. (2011). Active multistage coarsening of actin networks driven by myosin motors. Pnas *108*, 9408–9413.

Simoes, S.D.M., Mainieri, A., and Zallen, J.A. (2014). Rho GTPase and Shroom direct planar polarized actomyosin contractility during convergent extension. The Journal of Cell Biology *204*, 575–589.

Simões, S. de M., Blankenship, J.T., Weitz, O., Farrell, D.L., Tamada, M., Fernandez-Gonzalez, R., and Zallen, J.A. (2010). Rho-Kinase Directs Bazooka/Par-3 Planar Polarity during Drosophila Axis Elongation. Developmental Cell *19*, 377–388.

Skoglund, P., Rolo, A., Chen, X., Gumbiner, B.M., and Keller, R. (2008). Convergence and extension at gastrulation require a myosin IIB-dependent cortical actin network. Development *135*, 2435–2444.

Sokolow, A., Toyama, Y., Kiehart, D.P., and Edwards, G.S. (2012). Cell ingression and apical shape oscillations during dorsal closure in Drosophila. Biophys. J. *102*, 969–979.

Solon, J., Kaya-Çopur, A., Colombelli, J., and Brunner, D. (2009). Pulsed Forces Timed by a Ratchet-like Mechanism Drive Directed Tissue Movement during Dorsal Closure. Cell *137*, 1331–1342.

Somlyo, A.P., and Somlyo, A.V. (2000). Signal transduction by G-proteins, Rho-kinase and protein phosphatase to smooth muscle and non-muscle myosin II. J. Physiol. (Lond.) *522*, 177–185.

Somlyo, A.P., and Somlyo, A.V. (2003). Ca2+ Sensitivity of Smooth Muscle and Nonmuscle Myosin II: Modulated by G Proteins, Kinases, and Myosin Phosphatase. Physiological Reviews *83*, 1325–1358.

Speck, O., Hughes, S.C., Noren, N.K., Kulikauskas, R.M., and Fehon, R.G. (2003). Moesin functions antagonistically to the Rho pathway to maintain epithelial integrity. Nature *421*, 83–87.

Spindler, V., Schlegel, N., and Waschke, J. (2010). Role of GTPases in control of microvascular permeability. Cardiovascular Research *87*, cvq086–cvq253.

Spudich, J.A., and Watt, S. (1971). The regulation of rabbit skeletal muscle contraction. I. Biochemical studies of the interaction of the tropomyosin-troponin complex with actin and the proteolytic fragments of myosin. J. Biol. Chem. *246*, 4866–4871.

Stachowiak, M.R., McCall, P.M., Thoresen, T., Balcioglu, H.E., Kasiewicz, L., Gardel, M.L., and O'Shaughnessy, B. (2012). Self-organization of myosin II in reconstituted actomyosin bundles. Biophys. J. *103*, 1265–1274.

Surks, H.K., Richards, C.T., and Mendelsohn, M.E. (2003). Myosin phosphatase-Rho interacting protein. A new member of the myosin phosphatase complex that directly binds RhoA. J. Biol. Chem. *278*, 51484–51493.

Surks, H.K., Riddick, N., and Ohtani, K.-I. (2005). M-RIP targets myosin phosphatase to stress fibers to regulate myosin light chain phosphorylation in vascular smooth muscle cells. J. Biol. Chem. *280*, 42543–42551.

Suzuki, Y., Shibuya, M., Satoh, S.-I., Sugimoto, Y., and Takakura, K. (2007). A postmarketing surveillance study of fasudil treatment after aneurysmal subarachnoid hemorrhage. Surgical Neurology *68*, 126–131.

Svitkina, T.M., Verkhovsky, A.B., McQuade, K.M., and Borisy, G.G. (1997). Analysis of the actin-myosin II system in fish epidermal keratocytes: mechanism of cell body translocation. The Journal of Cell Biology *139*, 397–415.

Sweeton, D., Parks, S., Costa, M., and Wieschaus, E. (1991). Gastrulation in Drosophila: the formation of the ventral furrow and posterior midgut invaginations.

Development *112*, 775–789.

Symons, M.H., and Mitchison, T.J. (1991). Control of actin polymerization in live and permeabilized fibroblasts. The Journal of Cell Biology *114*, 503–513.

Tan, T.H., Garbi, M.M., Abu-Shah, E., Li, J., Sharma, A., MacKintosh, F.C., Keren, K., Schmidt, C.F., and Fakhri, N. (2016). Self-organization of stress patterns drives state transitions in actin cortices. arXiv.

Tang, V.W., and Brieher, W.M. (2012). α-Actinin-4/FSGS1 is required for Arp2/3-dependent actin assembly at the adherens junction. The Journal of Cell Biology *196*, 115–130.

Thievessen, I., Thompson, P.M., Berlemont, S., Plevock, K.M., Plotnikov, S.V., Zemljic-Harpf, A., Ross, R.S., Davidson, M.W., Danuser, G., Campbell, S.L., et al. (2013). Vinculin-actin interaction couples actin retrograde flow to focal adhesions, but is dispensable for focal adhesion growth. The Journal of Cell Biology *202*, 163–177.

Thomas, G.H., and Kiehart, D.P. (1994). Beta heavy-spectrin has a restricted tissue and subcellular distribution during Drosophila embryogenesis. Development *120*, 2039–2050.

Thomas, G.H., Zarnescu, D.C., Juedes, A.E., Bales, M.A., Londergan, A., Korte, C.C., and Kiehart, D.P. (1998). Drosophila betaHeavy-spectrin is essential for development and contributes to specific cell fates in the eye. Development *125*, 2125–2134.

Tkachenko, E., Sabouri-Ghomi, M., Pertz, O., Kim, C., Gutierrez, E., Machacek, M., Groisman, A., Danuser, G., and Ginsberg, M.H. (2011). Protein kinase A governs a RhoA-RhoGDI protrusion-retraction pacemaker in migrating cells. Nat. Cell Biol. *13*, 660–667.

Totsukawa, G., Wu, Y., Sasaki, Y., Hartshorne, D.J., Yamakita, Y., Yamashiro, S., and Matsumura, F. (2004). Distinct roles of MLCK and ROCK in the regulation of membrane protrusions and focal adhesion dynamics during cell migration of fibroblasts. The Journal of Cell Biology *164*, 427–439.

Truebestein, L., Elsner, D.J., Fuchs, E., and Leonard, T.A. (2015). A molecular ruler regulates cytoskeletal remodelling by the Rho kinases. Nature Communications *6*, 10029.

Tsai, F.-C., and Meyer, T. (2012). Ca2+ pulses control local cycles of lamellipodia retraction and adhesion along the front of migrating cells. Curr. Biol. *22*, 837–842.

Tsukita, S., Tsukita, S., Tsukita, S., and Ishikawa, H. (1983). Association of actin and 10 nm filaments with the dense body in smooth muscle cells of the chicken gizzard. Cell Tissue Res. *229*, 233–242.

Uehata, M., Narumiya, S., Ishizaki, T., Satoh, H., Ono, T., Kawahara, T., Morishita, T.,

Tamakawa, H., Yamagami, K., Inui, J., et al. (1997). Calcium sensitization of smooth muscle mediated by a Rho-associated protein kinase in hypertension. Nature *389*, 990–994.

Valencia-Expósito, A., Grosheva, I., Míguez, D.G., González-Reyes, A., and Martín-Bermudo, M.D. (2016). Myosin light-chain phosphatase regulates basal actomyosin oscillations during morphogenesis. Nature Communications *7*, 10746.

van Nieuw Amerongen, G.P., Draijer, R., Vermeer, M.A., and van Hinsbergh, V.W.M. (1998). Transient and Prolonged Increase in Endothelial Permeability Induced by Histamine and Thrombin Role of Protein Kinases, Calcium, and RhoA. Circ. Res. *83*, 1115–1123.

van Nieuw Amerongen, G.P., van Delft, S., Vermeer, M.A., Collard, J.G., and van Hinsbergh, V.W.M. (2000). Activation of RhoA by Thrombin in Endothelial Hyperpermeability Role of Rho Kinase and Protein Tyrosine Kinases. Circ. Res. *87*, 335–340.

Vasquez, C.G., Heissler, S.M., Billington, N., Sellers, J.R., and Martin, A.C. (2016). Drosophila non-muscle myosin II motor activity determines the rate of tissue folding. eLife *5*, 1761.

Vasquez, C.G., Tworoger, M., and Martin, A.C. (2014). Dynamic myosin phosphorylation regulates contractile pulses and tissue integrity during epithelial morphogenesis. The Journal of Cell Biology *206*, 435–450.

Vavylonis, D., Wu, J.-Q., Hao, S., O'Shaughnessy, B., and Pollard, T.D. (2008). Assembly mechanism of the contractile ring for cytokinesis by fission yeast. Science *319*, 97–100.

Verkhovsky, A.B., and Borisy, G.G. (1993). Non-sarcomeric mode of myosin II organization in the fibroblast lamellum. The Journal of Cell Biology *123*, 637–652.

Verkhovsky, A.B., Svitkina, T.M., and Borisy, G.G. (1995). Myosin II filament assemblies in the active lamella of fibroblasts: their morphogenesis and role in the formation of actin filament bundles. The Journal of Cell Biology *131*, 989–1002.

Verma, S., Han, S.P., Michael, M., Gomez, G.A., Yang, Z., Teasdale, R.D., Ratheesh, A., Kovacs, E.M., Ali, R.G., and Yap, A.S. (2012). A WAVE2-Arp2/3 actin nucleator apparatus supports junctional tension at the epithelial zonula adherens. Mol. Biol. Cell *23*, 4601–4610.

Vicente-Manzanares, M., Ma, X., Adelstein, R.S., and Horwitz, A.R. (2009). Non-muscle myosin II takes centre stage in cell adhesion and migration. Nat. Rev. Mol. Cell Biol. *10*, 778–790.

Vignaud, T., Blanchoin, L., and Théry, M. (2012). Directed cytoskeleton self-organization. Trends in Cell Biology *22*, 671–682.

Wallingford, J.B., Niswander, L.A., Shaw, G.M., and Finnell, R.H. (2013). The Continuing Challenge of Understanding, Preventing, and Treating Neural Tube Defects. Science *339*, 1222002–1222002.

Wang, S., Yang, J., Tsai, A., Kuca, T., Sanny, J., Lee, J., Dong, K., Harden, N., and Krieger, C. (2011). Drosophila adducin regulates Dlg phosphorylation and targeting of Dlg to the synapse and epithelial membrane. Developmental Biology *357*, 392–403.

Wear, M.A., Yamashita, A., Kim, K., Maéda, Y., and Cooper, J.A. (2003). How capping protein binds the barbed end of the actin filament. Current Biology *13*, 1531–1537.

Weber, A., Pennise, C.R., Babcock, G.G., and Fowler, V.M. (1994). Tropomodulin caps the pointed ends of actin filaments. The Journal of Cell Biology *127*, 1627–1635.

Weber, K.L., Fischer, R.S., and Fowler, V.M. (2007). Tmod3 regulates polarized epithelial cell morphology. J. Cell. Sci. *120*, 3625–3632.

Winter, C.G., Wang, B., Ballew, A., Royou, A., Karess, R., Axelrod, J.D., and Luo, L. (2001). Drosophila Rho-associated kinase (Drok) links Frizzled-mediated planar cell polarity signaling to the actin cytoskeleton. Cell *105*, 81–91.

Wójciak-Stothard, B., Potempa, S., Eichholtz, T., and Ridley, A.J. (2001). Rho and Rac but not Cdc42 regulate endothelial cell permeability. J. Cell. Sci. *114*, 1343–1355.

Xie, S., and Martin, A.C. (2015). Intracellular signalling and intercellular coupling coordinate heterogeneous contractile events to facilitate tissue folding. Nature Communications *6*, 7161.

Xu, K., Zhong, G., and Zhuang, X. (2013). Actin, spectrin, and associated proteins form a periodic cytoskeletal structure in axons. Science *339*, 452–456.

Yu, J.C., and Fernandez-Gonzalez, R. (2016). Local mechanical forces promote polarized junctional assembly and axis elongation in Drosophila. eLife *5*, 20246.

Yue, L., and Spradling, A.C. (1992). hu-li tai shao, a gene required for ring canal formation during Drosophila oogenesis, encodes a homolog of adducin. Genes Dev. *6*, 2443–2454.

Zanin, E., Desai, A., Poser, I., Toyoda, Y., Andree, C., Moebius, C., Bickle, M., Conradt, B., Piekny, A., and Oegema, K. (2013). A conserved RhoGAP limits M phase contractility and coordinates with microtubule asters to confine RhoA during cytokinesis. Developmental Cell *26*, 496–510.

Zarnescu, D.C., and Thomas, G.H. (1999). Apical Spectrin Is Essential for Epithelial Morphogenesis but Not Apicobasal Polarity in Drosophila. The Journal of Cell Biology *146*, 1075–1086.

Zhang, J., Herrera, A.M., Paré, P.D., and Seow, C.Y. (2010). Dense-body aggregates

as plastic structures supporting tension in smooth muscle cells. Am. J. Physiol. Lung Cell Mol. Physiol. *299*, L631–L638.

Zhou, Y., Huang, X., Hecker, L., Kurundkar, D., Kurundkar, A., Liu, H., Jin, T.-H., Desai, L., Bernard, K., and Thannickal, V.J. (2013). Inhibition of mechanosensitive signaling in myofibroblasts ameliorates experimental pulmonary fibrosis. J. Clin. Invest. *123*, 1096–1108.